General Disclaimer

One or more of the Following Statements may affect this Document

- This document has been reproduced from the best copy furnished by the organizational source. It is being released in the interest of making available as much information as possible.

- This document may contain data, which exceeds the sheet parameters. It was furnished in this condition by the organizational source and is the best copy available.

- This document may contain tone-on-tone or color graphs, charts and/or pictures, which have been reproduced in black and white.

- This document is paginated as submitted by the original source.

- Portions of this document are not fully legible due to the historical nature of some of the material. However, it is the best reproduction available from the original submission.

DEPARTMENT OF MECHANICAL ENGINEERING AND MECHANICS
SCHOOL OF ENGINEERING
OLD DOMINION UNIVERSITY
NORFOLK, VIRGINIA
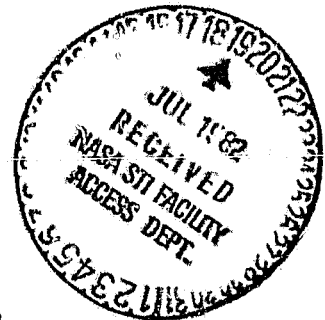
IMPROVED FINITE ELEMENT METHODOLOGY FOR INTEGRATED

THERMAL STRUCTURAL ANALYSIS

By

Pramote Dechaumphai

Earl A. Thornton
Principal Investigator

Progress Report
For the period ending June 30, 1982

Prepared for the
National Aeronautics and Space Administration
Langley Research Center
Hampton, Virginia 23665

June 1982

OLD DOMINION UNIVERSITY RESEARCH FOUNDATION

DEPARTMENT OF MECHANICAL ENGINEERING AND MECHANICS
SCHOOL OF ENGINEERING
OLD DOMINION UNIVERSITY
NORFOLK, VIRGINIA

IMPROVED FINITE ELEMENT METHODOLOGY FOR INTEGRATED

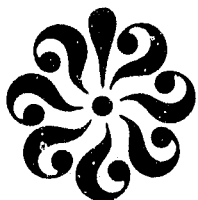THERMAL STRUCTURAL ANALYSIS

By

Pramote Dechaumphai

Earl A. Thornton
Principal Investigator

Progress Report
For the period ending June 30, 1982

June 1982

SUMMARY

An integrated thermal-structural finite element approach for effi-
cient coupling of thermal and structural analysis is presented. New
thermal finite elements which yield exact nodal and element tempera-
tures for one-dimensional linear steady-state heat transfer problems
are developed. A nodeless variable formulation is used to established
improved thermal finite elements for one-dimensional nonlinear transi-
ent and two-dimensional linear transient heat transfer problems. The
thermal finite elements provide detailed temperature distributions
without using additional element nodes and permit a common discretiza-
tion with lower-order congruent structural finite elements. The accu-
racy of the integrated approach is evaluated by comparisons with anal-
ytical solutions and conventional finite element thermal-structural
analyses for a number of academic and more realistic problems. Results
indicate that the approach provides a significant improvement in the
accuracy and efficiency of thermal-stress analysis for structures with
complex temperature distributions.

TABLE OF CONTENTS

LIST OF TABLES

LIST OF FIGURES

LIST OF SYMBOLS

a	Surface absorptivity
A	Cross sectional area
$[B_s]$	Strain-displacement interpolation matrix
$[B_T]$	Temperature gradient interpolation matrix
c	Specific heat
$[C]$	Finite element capacitance matrix
$[C_s]$	Finite element damping matrix
$[D]$	Elasticity matrix
E	Modulus of elasticity
$\{f\}$	Vector of body forces
$\{F\}$	Finite element nodal force vector
$\{F_T\}$	Finite element nodal thermal force vector
$\{g\}$	Vector of surface tractions
h	Convective heat transfer coefficient
$[J]$	Finite element Jacobian matrix
k	Thermal conductivity
$[k]$	Thermal conductivity matrix
$[K]$	Finite element conductance matrix
$[K_s]$	Finite element stiffness matrix
l	length
L	Finite element length
$\dot{m}$	Fluid mass flow rate

$[M]$	Finite element mass matrix
n_x, n_y, n_z	Direction cosines of surface normal vector
$[N]$	Finite element interpolation function matrix
$[N_s]$	Finite element displacement interpolation function matrix
$[N_T]$	Finite element temperature interpolation function matrix
p	Perimeter
p_s	Perimeter for surface emitted energy
p_q	Perimeter for surface incident energy
q_s	Surface heating rate
q_r	Surface incident radiation heating rate
q_x, q_y, q_z	Components of heat flow rate in Cartesian coordinates
Q	Volumetric heat generation rate
$\{Q\}$	Finite element heat load vector
r	Radial coordinate
$\{R\}$	Finite element heat load vector
t	Time
T	Temperature
T_0	Nodeless variable
T_{ref}	Reference temperature for zero stress
T_∞	Convective medium temperature
u, v, w	Displacement components
U	Internal strain energy
V	Potential energy
x, y, z	Cartesian coordinates
$\{\alpha\}$	Vector of thermal expansion coefficients
$\{\delta\}$	Vector of finite element displacements

Chapter 1

INTRODUCTION

The finite element method is one of the most significant developments for solving problems of continuum mechanics. It was first applied by Turner et al. [1]* in 1956 for the analysis of complex aerospace structures. With increasing availability of digital computers, the method has become widespread and well recognized as applicable to a variety of continuum problems. Applications of the method to thermal problems were introduced in the middle of 1960's for the solution of steady-state conduction heat transfer [2]. Thereafter, extensions of the method were made to both transient and nonlinear analyses where nonlinearities may arise from temperature dependent material properties and nonlinear boundary conditions. Important publications of finite element heat transfer analysis appear in references [3-12]. With these developments and considerable effort contributed during the past decade, the method has gradually increased in thermal analysis capability and become a practical technique for analyzing realistic thermal problems.

---

*The numbers in brackets indicate references.

1.1 Current Status of Thermal-Structural Analysis

Thermal stresses induced by aerodynamic heating on advanced space transportation vehicles are an important concern in structural design. Nonuniform heating may have a significant effect on the performance of the structures and efficient techniques for determining thermal stresses are required. Frequently, the thermal analysis of the structure is performed by the finite difference method. Production-type finite difference programs such as MITAS and SINDA have demonstrated excellent capabilities for analyzing complex structures [13]. In structural analysis, however, the finite element method is favorable due to better capabilities in modeling complex structural geometries and handling various types of boundary conditions. To perform coupled thermal-structural analysis with efficiency, a computer program which includes both thermal and structural analysis codes is preferred, and a single numerical method is desirable to eliminate the tedious and perhaps expensive task of transferring data between different analytical models.

Currently, the capabilities and efficiency of the finite element method is analyzing typical heat transfer problems such as combined conduction-forced convection is about the same as using the finite difference method [14]. With the wide acceptance of the finite element method in structures and its rapid growth in thermal analysis, it is particularly well-suited for coupled thermal-structural analysis. At present, several finite element programs which include both thermal and structural analysis capabilities exist; e.g. NASTRAN, ANSYS, ADINA and SPAR are widely used. These programs use

a common data base for transferring temperatures computed from a thermal analysis processor to a structural analysis processor for determining displacements and stresses. With the use of a common finite element discretization, a significant reduction of effort in preparing data is achieved and errors that may occur by manually transferring data between analyses is eliminated.

1.2 Needs for Improving Finite Element Methodology

Although the finite element method offers high potential for coupled thermal-structural analysis, further improvements of the method are needed. Quite often, the finite element thermal model requires a finer discretization than the structural model to compute the temperature distribution accurately. Detailed temperature distributions are necessary for the structural analysis to predict thermal stress distributions including critical stress locations accurately. Improvement of thermal finite elements is, therefore, required so that a common discretization between the two analytical models can be maintained.

Another need for improving the method includes a capability of the thermal analysis to produce thermal loads required for the structural analysis directly. At present, typical thermal-structural finite element programs only transfer nodal temperatures computed from the thermal analysis to the structural analysis. These nodal temperatures are generally inadequate because additional information, such as element temperature distributions and temperature gradients, may be required to compute thermal stress distributions correctly.

These needs are important in improvement of finite element coupled thermal-structural analysis capability. The use of improved thermal finite elements can reduce model size and computational costs especially for analysis of complex aerospace vehicle structures. Improved thermal elements will also have a direct effect in increasing the structural analysis accuracy through improving the accuracy of thermal loads.

To meet these requirements for improved thermal-structural analysis and to demonstrate benefits that can be achieved, this dissertation will develop an approach called integrated finite element thermal-structural analysis. First, basic concepts of the integrated finite element thermal-structural formulation are introduced in Chapter 2. Finite elements which provide exact solutions to one-dimensional linear steady-state thermal-structural problems are developed in Chapter 3. Chapter 4 demonstrates the use of these finite elements for linear transient analysis. Next, in Chapter 5 a generalized approach for improved finite elements is established and its efficiency is demonstrated through thermal-structural analysis with radiation heat transfer. Finally, in Chapter 6 extension of the approach to two dimensions is made with a new two-dimensional finite element. In each chapter, benefits of utilizing the improved finite elements are demonstrated by both academic and realistic thermal-structural problems.

Throughout the development of the improved finite elements, detailed analytical and finite element formulations are presented. Such details are provided in the form of equations, finite element matrices in tables and computer subroutines in appendices.

Chapter 2

AN INTEGRATED THERMAL-STRUCTURAL FINITE
ELEMENT FORMULATION

2.1 Basic Concepts

Before applying the finite element method to thermal-structural
analysis, it is appropriate to establish basic concepts and procedures
of the method. Briefly described, the finite element method is a
numerical analysis technique for obtaining approximate solutions to
problems by idealizing the continuum model as a finite number of
discrete regions called elements. These elements are connected at
points called nodes where normally the dependent variables such as
temperature and displacements are determined. Numerical computations
for each individual element generate element matrices which are then
assembled to form a set of linear algebraic equations (for
steady state problems) to represent the entire problem. These
algebraic equations are solved simultaneously for the unknown
dependent variables. Usually the more elements used, the greater
the accuracy of the results. Accuracy, however, can be affected by
factors such as the type of element selected to represent the con-
tinuum, and the sophistication of element interpolation functions.

2.2 Element Interpolation Functions

The first step after replacing the continuum model by a discrete number of finite elements is to determine a functional relationship between the dependent variable within the element and the nodal variables. The function that represents the variation of a dependent variable is called the interpolation function. In thermal analysis, the element temperature $T(x,y,z,t)$ are generally expressed in the form

$$T(x,y,z,t) = \lfloor N_T(x,y,z) \rfloor \{T(t)\} \tag{2.1}$$

where $\lfloor N_T(x,y,z) \rfloor$ denotes a row matrix of the element temperature interpolation functions, and $\{T(t)\}$ denotes a vector of nodal temperatures. Similarly, in a structural analysis, the element displacements, $\{\delta\}$, are expressed as,

$$\{\delta(x,y,z,t)\} = [N_S(x,y,z)] \{\bar{\delta}(t)\} \tag{2.2}$$

where $[N_S(x,y,z)]$ denotes a matrix of structural displacement inter-polation functions, and $\{\bar{\delta}(t)\}$ denotes a vector of nodal displacements.

Usually, polynomials are selected as element interpolation functions and the degree of the polynomial chosen depends on the number of nodes assigned to the element. Regardless of the algebraic form, these interpolation functions have a value of unity at the node to which it pertains and a value of zero at other nodes. For example, linear temperature variation for a two-node one-dimensional rod

element with nodal temperatures T_1 and T_2 at $x = 0$ (node 1) and $x = L$ (node 2), respectively, can be written in the form

$$T(x,t) = \lfloor 1 - \frac{x}{L} \quad \frac{x}{L} \rfloor \begin{Bmatrix} T_1(t) \\ \\ T_2(t) \end{Bmatrix}$$

By comparing this equation with the general form of the element temperature variation, Eq. (2.1), the element interpolation functions are

$$N_1(x) = 1 - \frac{x}{L} \quad \text{and} \quad N_2(x) = \frac{x}{L}$$

These element interpolation functions, therefore, have the properties of $N_i = 1$ at node i and $N_i = 0$ at the other node.

2.3 Finite Element Thermal Analysis

Once the type of elements and their interpolation functions have been selected, the matrix equations expressing the properties of the individual element are evaluated. In thermal analysis, the method of weighted residuals [15] is frequently employed starting from the governing differential equations. For condution heat transfer in a three-dimensional anisotropic solid Ω bounded by surface Γ (Fig. 1), an energy balance on a small element is given by,

$$- (\frac{\partial q_x}{\partial x} + \frac{\partial q_y}{\partial y} + \frac{\partial q_z}{\partial z}) + Q(x,y,z,t) = \rho c \frac{\partial T}{\partial t}(x,y,z,t) \qquad (2.3)$$

where q_x, q_y, q_z are components of the heat flow rate per unit area, Q is the internal heat generation rate per unit volume, ρ is the
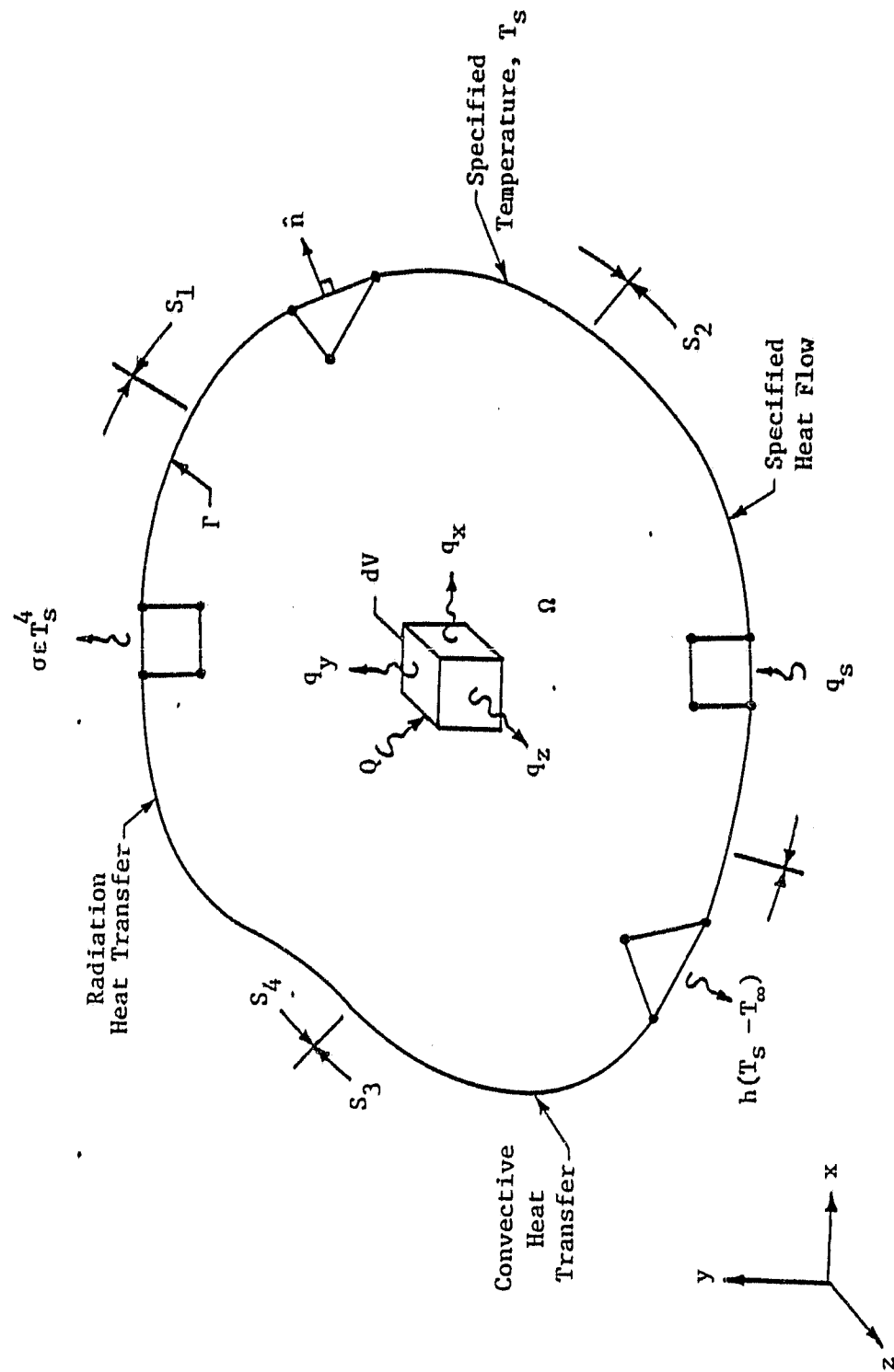
Fig. 1. Three dimensional solution domain for general heat conduction.

density, and c is the specific heat. Using Fourier's Law, the components of heat flow rate for an anisotropic medium can be written in the matrix form.

$$\left\{ \begin{array}{c} q_x \\ q_y \\ q_z \end{array} \right\} = - \left[\begin{array}{ccc} k_{11} & k_{12} & k_{13} \\ k_{21} & k_{22} & k_{23} \\ k_{31} & k_{32} & k_{33} \end{array} \right] \left\{ \begin{array}{c} \partial T/\partial x \\ \partial T/\partial y \\ \partial T/\partial z \end{array} \right\} \qquad (2.4)$$

where k_{ij} is the symmetric conductivity tensor. Figure 1 shows several types of boundary conditions frequently encountered in the analysis. These boundary conditions are (1) specified surface temperatures, (2) surface heating, (3) surface convection, and (4) surface radiation:

$$T = T_s \qquad \text{on} \quad S_1 \qquad (2.5a)$$

$$q_x n_x + q_y n_y + q_z n_z = - q_s \qquad \text{on} \quad S_2 \qquad (2.5b)$$

$$q_x n_x + q_y n_y + q_z n_z = h(T_s - T_\infty) \qquad \text{on} \quad S_3 \qquad (2.5c)$$

$$q_x n_x + q_y n_y + q_z n_z = \sigma \varepsilon T_s^4 - a q_r \qquad \text{on} \quad S_4 \qquad (2.5d)$$

where T_s is the specified surface temperature; n_x, n_y, n_z are the direction cosines of the outward normal to the surface, q_s is the surface heating rate unit area, h is the convection coefficient, T_∞ is the convective medium temperature, σ is the Stefan-Boltzmann constant, ε is the surface emissivity, a is the surface absorptivity, and q_r is the incident radiant heat flow rate per unit area.

To apply the finite element technique, the domain Ω is first discretized into a number of elements. For an element with r nodes, the element temperature, Eq. (2.1), can be written in the form

$$T(x,y,z,t) = \sum_{i=1}^{r} N_i(x,y,z) \, T_i(t) \qquad (2.7a)$$

and the temperature gradients within each element are

$$\frac{\partial T}{\partial x}(x,y,z,t) = \sum_{i=1}^{r} \frac{\partial N_i(x,y,z)}{\partial x} T_i(t) \qquad (2.7b)$$

$$\frac{\partial T}{\partial y}(x,y,z,t) = \sum_{i=1}^{r} \frac{\partial N_i(x,y,z)}{\partial y} T_i(t) \qquad (2.7c)$$

$$\frac{\partial T}{\partial z}(x,y,z,t) = \sum_{i=1}^{r} \frac{\partial N_i(x,y,z)}{\partial z} T_i(t) \qquad (2.7d)$$

These element temperature gradients can be written in the matrix form,

$$\left\{ \begin{array}{c} \dfrac{\partial T}{\partial x}(x,y,z,t) \\[2ex] \dfrac{\partial T}{\partial y}(x,y,z,t) \\[2ex] \dfrac{\partial T}{\partial z}(x,y,z,t) \end{array} \right\} = [B(x,y,z)] \, \{T(t)\} \qquad (2.8)$$

where $[B(x,y,z)]$ is the temperature-gradient interpolation matrix:

$$[B(x,y,z)] = \begin{bmatrix} \dfrac{\partial N_1}{\partial x} & \dfrac{\partial N_2}{\partial x} & \cdots\cdots & \dfrac{\partial N_r}{\partial x} \\[2mm] \dfrac{\partial N_1}{\partial y} & \dfrac{\partial N_2}{\partial y} & \cdots\cdots & \dfrac{\partial N_r}{\partial y} \\[2mm] \dfrac{\partial N_1}{\partial z} & \dfrac{\partial N_2}{\partial z} & \cdots\cdots & \dfrac{\partial N_r}{\partial z} \end{bmatrix} \qquad (2.9)$$

and, therefore, the components of heat flow rate, Eq. (2.4), become

$$\begin{Bmatrix} q_x \\ q_y \\ q_z \end{Bmatrix} = -[k][B]\{T\} \qquad (2.10)$$

where [k] denotes the thermal conductivity matrix.

In the derivation of the element equations, the method of weighted residuals is applied to the energy equation, Eq. (2.3), for each individual element (e). This method requires

$$\int_{\Omega(e)} \left(\frac{\partial q_x}{\partial x} + \frac{\partial q_y}{\partial y} + \frac{\partial q_z}{\partial z} - Q + \rho c \frac{\partial T}{\partial t} \right) N_i d\Omega = 0 \qquad (2.11)$$

$$i = 1,2 \ldots r$$

After the integrations are performed on the first three terms by using Gauss's Theorem, a surface integral of the heat flow across the element boundary, $\Gamma^{(e)}$, is introduced, and the above equations become

$$\left(\int_{\Gamma(e)} (\vec{q} \cdot \hat{n}) N_i \, d\Gamma - \int_{\Omega(e)} \left\lfloor \frac{\partial N_i}{\partial x} \quad \frac{\partial N_i}{\partial y} \quad \frac{\partial N_i}{\partial z} \right\rfloor \begin{Bmatrix} q_x \\ q_y \\ q_z \end{Bmatrix} d\Omega \right)$$

$$-\int_{\Omega(e)} QN_i \, d\Omega + \int_{\Omega(e)} \rho c \frac{\partial T}{\partial t} N_i \, d\Omega = 0 \tag{2.12}$$

where $\vec{q}$ is the vector of conduction heat flux across the element boundary and $\hat{n}$ is a unit vector normal to the boundary. The boundary conditions as shown in Eqs. (2.5a – 2.5d) are then imposed,

$$\left(\int_{S_1} (\vec{q} \cdot \hat{n}) N_i \, d\Gamma - \int_{S_2} q_s N_i \, d\Gamma + \int_{S_3} h(T - T_\infty) N_i \, d\Gamma \right.$$

$$+ \int_{S_4} (\sigma \epsilon T^4 - a q_r) \, d\Gamma - \int_{\Omega(e)} \left\lfloor \frac{\partial N_i}{\partial x} \quad \frac{\partial N_i}{\partial y} \quad \frac{\partial N_i}{\partial z} \right\rfloor \left\{ \begin{array}{c} q_x \\ q_y \\ q_z \end{array} \right\} \, d\Omega \left. \right)$$

$$- \int_{\Omega(e)} QN_i \, d\Omega + \int_{\Omega(e)} \rho c \frac{\partial T}{\partial t} N_i \, d\Omega = 0 \tag{2.13}$$

By substituting the vector of heat flow rate, Eq. (2.10), the above element equations finally result in the matrix form,

$$[C]\{\dot{T}\} + [[K_c] + [K_h] + [K_r]]\{T\}$$

$$= \{R_c\} + \{R_Q\} + \{R_q\} + \{R_h\} + \{R_r\} \tag{2.14}$$

where $[C]$ is the element capacitance matrix; $[K_c]$, $[K_h]$ and $[K_r]$ are element conductance matrices corresponding to conduction, convection and radiation, respectively. These matrices are expressed as follows:

$$[C] = \int_{\Omega(e)} \rho c \, \{N_T\} \lfloor N_T \rfloor \, d\Omega \tag{2.15a}$$

$$[K_c] = \int_{\Omega(e)} [B_T]^T [k] [B_T] \, d\Omega \tag{2.15b}$$

$$[K_h] = \int_{S_3} h \, \{N_T\} \lfloor N_T \rfloor \, d\Gamma \tag{2.15c}$$

$$[K_r]\{T\} = \int_{S_4} \sigma \varepsilon T^4 \, \{N_T\} \, d\Gamma \tag{2.15d}$$

The right-hand side of the discretized equation (2.14) contains heat load vectors due to specified nodal temperatures, internal heat generation, specified surface heating, surface convection and surface radiation. These vectors are defined by

$$\{R_c\} = -\int_{S_1} (\vec{q} \cdot \hat{n}) \, \{N_T\} \, d\Gamma \tag{2.16a}$$

$$\{R_Q\} = \int_{\Omega(e)} Q \, \{N_T\} \, d\Omega \tag{2.16b}$$

$$\{R_q\} = \int_{S_2} q_s \, \{N_T\} \, d\Gamma \tag{2.16c}$$

$$\{R_h\} = \int_{S_3} h \, T_\infty \, \{N_T\} \, d\Gamma \tag{2.16d}$$

$$\{R_r\} = \int_{S_4} a q_r \, \{N_T\} \, d\Gamma \tag{2.16e}$$

where $\vec{q}$ is the vector of conduction heat flux across boundary that is required to maintain the specified nodal temperatures.

2.4 Finite Element Structural Analysis

In a finite element structural analysis, element matrices may
be derived by the method of weighted residuals, or by a variational
method such as the principle of minimum potential energy [17-19].
For simplicity in establishing these element matrices and understand-
ing general derivations, the last approach is presented herein.
The basic idea of this approach is to derive the static equilibrium
equations and then include dynamic effects through the use of
D'Alembert's principle.

Consider an elastic body in a three-dimensional state of stress.
The internal strain energy of an element (e) can be written in a
form,

$$U = \frac{1}{2} \int_{\Omega(e)} \lfloor \varepsilon - \varepsilon_0 \rfloor \{\sigma\} \, d\Omega \qquad (2.17)$$

where $\Omega^{(e)}$ is the element volume, $\{\sigma\}$ denotes a vector of stress
components; $\lfloor \varepsilon \rfloor$ and $\lfloor \varepsilon_0 \rfloor$ denote row matrices of total strain and
initial strain components, respectively. Using the stress-strain
relations,

$$\{\sigma\} = [D] \{\varepsilon - \varepsilon_0\} \qquad (2.18)$$

where [D] is the elasticity matrix, the internal strain energy
becomes

$$U = \frac{1}{2} \int_{\Omega(e)} \lfloor \varepsilon - \varepsilon_0 \rfloor [D] \{\varepsilon - \varepsilon_0\} \, d\Omega$$

or

$$U = \frac{1}{2} \int_{\Omega^{(e)}} \lfloor \varepsilon \rfloor [D] \{\varepsilon\} \, d\Omega - \int_{\Omega^{(e)}} \lfloor \varepsilon \rfloor [D] \{\varepsilon_0\} \, d\Omega$$

$$+ \frac{1}{2} \int_{\Omega^{(e)}} \lfloor \varepsilon_0 \rfloor [D] \{\varepsilon_0\} \, d\Omega \qquad (2.19)$$

For each element, the potential energy of the external forces may result from body forces and boundary surface tractions. The potential energy due to body forces can be written in a form,

$$V_B = - \int_{\Omega^{(e)}} \lfloor \delta \rfloor \{f\} \, d\Omega \qquad (2.20)$$

where $\{f\}$ denotes a vector of body force components. Similarly, the potential energy due to surface tractions is,

$$V_S = - \int_{\Gamma^{(e)}} \lfloor \delta \rfloor \{g\} \, d\Gamma \qquad (2.21)$$

where $\{g\}$ denotes a vector of surface traction components, and $\Gamma^{(e)}$ denotes the element boundary. The total element potential energy, π_e, the sum of the internal strain energy and the potential energy of the external forces is,

$$\pi_e = \frac{1}{2} \int_{\Omega^{(e)}} \lfloor \varepsilon \rfloor [D] \{\varepsilon\} \, d\Omega - \int_{\Omega^{(e)}} \lfloor \varepsilon \rfloor [D] \{\varepsilon_0\} \, d\Omega$$

$$+ \frac{1}{2} \int_{\Omega^{(e)}} \lfloor \varepsilon_0 \rfloor [D] \{\varepsilon_0\} \, d\Omega - \int_{\Omega^{(e)}} \lfloor \delta \rfloor \{f\} \, d\Omega$$

$$- \int_{\Gamma^{(e)}} \lfloor \delta \rfloor \{g\} \, d\Gamma \qquad (2.22)$$

For a three-dimensional finite element with r nodes, the displacement field can be expressed as

$$\{\delta\} = \begin{Bmatrix} u(x,y,z,t) \\ \\ v(x,y,z,t) \\ \\ \\ w(x,y,z,t) \end{Bmatrix} = \begin{Bmatrix} \sum_{i=1}^{r} N_i(x,y,z)\, u_i(t) \\ \\ \sum_{i=1}^{r} N_i(x,y,z)\, v_i(t) \\ \\ \sum_{i=1}^{r} N_i(x,y,z)\, w_i(t) \end{Bmatrix} = [N_S]\{\bar{\delta}\} \qquad (2.23)$$

where u, v, w are components of displacement in the three coordinate directions. The vector of strain components can be computed from

$$\{\varepsilon\} = \begin{Bmatrix} \varepsilon_x \\ \varepsilon_y \\ \varepsilon_z \\ \gamma_{xy} \\ \gamma_{yz} \\ \gamma_{xz} \end{Bmatrix} = \begin{Bmatrix} \dfrac{\partial u}{\partial x} \\ \dfrac{\partial v}{\partial y} \\ \dfrac{\partial w}{\partial z} \\ \dfrac{\partial u}{\partial y} + \dfrac{\partial v}{\partial x} \\ \dfrac{\partial v}{\partial z} + \dfrac{\partial w}{\partial y} \\ \dfrac{\partial u}{\partial z} + \dfrac{\partial w}{\partial x} \end{Bmatrix} = [B_S]\{\bar{\delta}\} \qquad (2.24)$$

where $[B_S]$ is the strain-displacement interpolation matrix. By substituting the element displacement vector, Eq. (2.23), and the vector of strain components, Eq. (2.24) into Eq. (2.22), the total element potential energy is expressed in terms of the nodal displacement vector $\{\bar{\delta}\}$ as

$$\pi_e = \frac{1}{2} \lfloor \bar{\delta} \rfloor \int_{\Omega(e)} [B_s]^T [D] [B_s] \, d\Omega \{\bar{\delta}\} - \{\delta\} \int_{\Omega(e)} [B_s]^T [D] \{\varepsilon_0\} \, d\Omega$$

$$+ \frac{1}{2} \int_{\Omega(e)} \lfloor \varepsilon_0 \rfloor [D] \{\varepsilon_0\} \, d\Omega - \{\bar{\delta}\} \int_{\Omega(e)} [N_s]^T \{f\} \, d\Omega$$

$$- \{\bar{\delta}\} \int_{\Gamma(e)} [N_s]^T \{g\} \, d\Gamma \tag{2.25}$$

The principle of minimum potential energy requires,

$$\frac{\partial \pi_e}{\partial \{\bar{\delta}\}} = 0$$

which yields the element equilibrium equations,

$$[K_s] \{\bar{\delta}\} = \{F_c\} + \{F_B\} + \{F_s\} + \{F_T\} \tag{2.26}$$

where $[K_s]$ is the element stiffness matrix defined by

$$[K_s] = \int_{\Omega(e)} [B_s]^T [D] [B_s] \, d\Omega \tag{2.27a}$$

The right hand side of the equilibrium equations contains force vectors due to concentrated forces, body forces, surface tractions and initial strain, respectively. The nodal force vectors due to body forces and surface tractions are

$$\{F_B\} = \int_{\Omega(e)} [N_s]^T \{f\} \, d\Omega \tag{2.27b}$$

$$\{F_s\} = \int_{\Gamma(e)} [N_s]^T \{g\} \, d\Gamma \tag{2.27c}$$

For initial strains from thermal effects, the corresponding nodal vector $\{F_T\}$ is due to the change of temperature from a reference temperature of the zero-stress state and may be written as

$$\{F_T\} = \int_{\Omega}(e) \; [B_s]^T \; [D] \; \{\alpha\} \; (T - T_{ref}) \; d\Omega \qquad (2.27d)$$

where $\{\alpha\}$ is a vector of thermal expansion coefficients, T is the element temperature distribution, and T_{ref} is the reference temperature for zero stress.

For elastic bodies subjected to dynamic loads, the effects of inertia and damping forces must be taken into account. Using D'Alembert's principle, the inertia force can be treated as a body force given by

$$\{f\} = - \rho \{\ddot{\delta}\} \qquad (2.28a)$$

where ρ is the mass per unit volume. By using element displacement variations, Eq. (2.23), this inertia force is expressed in terms of nodal displacements as

$$\{f\} = - \rho \; [N_s] \; \{\ddot{\bar{\delta}}\} \qquad (2.28b)$$

Similarly, the damping force which is usually assumed to be proportional to the velocity can be expressed in the form,

$$\{f\} = - \mu \; [N_s] \; \{\dot{\bar{\delta}}\} \qquad (2.28c)$$

where μ is a damping coefficient. By substituting these inertia and damping forces, Eqs. (2.28b - 2.28c), into Eq. (2.27b), the equivalent nodal body forces shown in Eq. (2.27b) become

$$\{F_B\} = \int_{\Omega(e)} [N_s]^T \{f\} \, d\Omega - \int_{\Omega(e)} [N_s]^T \rho [N_s] \, d\Omega \{\ddot{\bar{\delta}}\}$$

$$- \int_{\Omega(e)} [N_s]^T \mu [N_s] \, d\Omega \{\dot{\bar{\delta}}\} \qquad (2.29)$$

Finally, by using the static equilibrium equations, Eq. (2.26), with the above equivalent nodal body force, the basic equations of structural dynamics can be written in the form,

$$[M] \{\ddot{\bar{\delta}}\} + [C_s] \{\dot{\bar{\delta}}\} + [K_s] \{\bar{\delta}\} = \{F_c\} + \{F_B\} + \{F_s\} + \{F_T\} \qquad (2.30)$$

where [M] and [C$_s$] are the element mass and damping matrices, respectively, and defined by

$$[M] = \int_{\Omega(e)} [N_s]^T \rho [N_s] \, d\Omega \qquad (2.31a)$$

$$[C_s] = \int_{\Omega(e)} [N_s]^T \mu [N_s] \, d\Omega \qquad (2.31b)$$

In a general formulation of transient thermal-stress problem, the heat conduction equation (2.3) contains a mechanical coupling term in addition [16]. This coupling term represents the mechanical energy associated with deformation of the continuum and in some highly specialized problems (see Ref. 16) can affect the temperature solution. In most of engineering applications, fortunately, this term is insignificant and is usually disregarded in the heat conduction equation. This simplification permits transient thermal solutions and dynamic structural responses to be computed independently.

For a structural analysis where the inertia and damping effects are negligible, the static structural response, Eq. (2.26), can be

computed at selected times corresponding to the transient thermal solutions. Such a sequence of computations, widely used in thermal-structural applications, is called a quasi-static analysis. Results of temperatures directly enter the structural analysis through the computation of the thermal nodal force vector, Eq. (2.27d). Temperatures also have an indirect effect on the analysis through the structural material properties, since the elasticity matrix $[D]$ and the thermal expansion coefficient vector $\{\alpha\}$ are, in general, temperature dependent. Temperature dependent properties may result in a variation of the structural element stiffness matrix, Eq. (2.27a), throughout the transient response.

2.5 Integrated Approach

The representation of the element temperature distribution in the computation of structural nodal forces is an important step in the coupled thermal-structural finite element analysis. In typical production-type finite element programs, element nodal temperatures are the only information transferred from the thermal analysis to the structural analysis. This general procedure is shown schematically in Fig. 2(a) and herein is called the conventional finite element approach. Since the conventional thermal analysis only provides nodal temperatures, an approximate temperature distribution is assumed in the structural analysis which results in a reduction in accuracy of displacements and thermal stresses.

To improve the capabilities and efficiency of the finite element method, an approach called integrated thermal-structural analysis is developed as illustrated by Fig. 2(b). The goals of

CONVENTIONAL

THERMAL → DATA {T} ONLY → DATA PROCESSING → STRUCTURAL

- THERMAL AND STRUCTURAL ELEMENTS SIMILAR

- NODAL TEMPERATURES {T} TRANSFERRED

- THERMAL FORCES BASED ONLY ON NODAL {T}

(a) Conventional analysis

INTEGRATED

THERMAL → DATA → STRUCTURAL

COULD BE
$T(x)$
$\dfrac{\partial T}{\partial x}$
$\int T dx$

- IMPROVED THERMAL ELEMENTS – FORMULATION FUNCTION OF HEATING

- COMPATIBLE THERMAL DATA TRANSFER AS REQUIRED BY STRUCTURAL ELEMENT

- THERMAL FORCES BASED ON ACTUAL TEMPERATURE DISTRIBUTIONS

(b) Integrated analysis

Fig. 2. Conventional versus integrated thermal and structural analysis.

the integrated approach are to: (1) provide thermal elements which predict detailed temperature variations accurately, (2) maintain the same discretization for both thermal and structural models with fully compatible thermal and structural elements, and (3) provide accurate thermal loads to the structural analysis to improve the accuracy of displacements and stresses.

These goals of the integrated approach require developing new thermal finite elements that can provide higher accuracy and efficiency than conventional finite elements. The basic restriction on these new thermal elements is the required compatability with the structural elements to preserve a common discretization. Detailed temperature distributions resulting from the improved thermal finite elements can provide accurate thermal loads required for the structural analysis by rigorously evaluating the thermal load integral, Eq. (2.27d).

Chapter 3

EXACT FINITE ELEMENTS FOR ONE-DIMENSIONAL
LINEAR THERMAL-STRUCTURAL PROBLEMS

In general, polynomials are selected as element interpolation functions to describe variations of the dependent variable within elements. In one-dimensional analysis, the simplest polynomial which provides a linear variation within an element is of the first order,

$$\phi = C_1 + C_2 x \tag{3.1}$$

where ϕ denotes the dependent variable such as temperature or displacement; C_1 and C_2 denote constants, and x is the coordinate of a point within the element. A finite element with two nodes is formulated by imposing the conditions at nodes,

$$\phi(x=0) = \phi_1 \qquad \phi(x=L) = \phi_2 \tag{3.2}$$

where L is the element length; ϕ_1 and ϕ_2 are nodal values at node 1 and 2, respectively. The dependent variable, therefore, can be written in terms of nodal values as

$$\phi = \left(1 - \frac{x}{L}\right) \phi_1 + \left(\frac{x}{L}\right) \phi_2$$

or in the matrix form,

$$\phi = \lfloor (1 - \tfrac{x}{L}) \quad (\tfrac{x}{L}) \rfloor \begin{Bmatrix} \phi_1 \\ \phi_2 \end{Bmatrix}$$

$$= \lfloor N_1 \quad N_2 \rfloor \begin{Bmatrix} \phi_1 \\ \phi_2 \end{Bmatrix}$$

$$= \lfloor N \rfloor \{\phi\} \tag{3.3}$$

where $\lfloor N \rfloor$ is the row matrix of element interpolation functions. The type of finite element where the dependent variable is assumed to vary linearly between the two element nodes is often used in one-dimensional problems and is called a conventional finite element herein. With the linear approximation, a large number of elements are required to represent a sharply varying dependent variable. In some special cases, however, conventional finite elements can provide exact solutions when the solutions to problems are in the form of a linear variation. For example, a linear temperature variation is the exact solution of one-dimensional steady-state heat conduction in a slab; therefore, the use of the conventional finite element leads to an exact solution. Further observation [20] has shown that, under some conditions, exact nodal values are obtained through the use of this element type. Temperatures for steady-state heat conduction with internal heat generation in a slab and deformations of a bar loaded by its own weight are examples of this case. In the past, the capability of conventional finite elements to provide exact solutions has been regarded as a property of the particular equation being solved and not applicable to general problems.

In this chapter, finite elements that provide exact solutions to one-dimensional linear steady-state thermal-structural problems are given. The fundamental approach in developing exact finite elements is based on the use of exact solutions to one-dimensional problems governed by linear ordinary differential equations. A general formulation of the exact finite element is first derived and applications are made to various thermal-structural problems. Benefits of utilizing the exact finite elements are demonstrated by comparison with results from conventional finite elements and exact solutions.

3.1 Exact Element Formulation

In this section, a general derivation of exact finite elements is given. Exact finite elements for various thermal and structural problems are derived and described in detail in the subsequent sections. Consider an ordinary, linear, nonhomogeneous differential equation,

$$a_n \frac{d^n \phi}{dx^n} + a_{n-1} \frac{d^{n-1} \phi}{dx^{n-1}} + \cdots\cdots\cdots + a_1 \frac{d\phi}{dx} + a_0 \phi = r(x) \qquad (3.4)$$

where x is the independent variable, $\phi(x)$ is the dependent variable, a_i, $i = 0$, n are constant coefficients, and $r(x)$ is the forcing function. A general solution to the above differential equation has the form

$$\phi(x) = \sum_{i=1}^{n} C_i f_i(x) + g(x) \qquad (3.5)$$

where C_i are arbitrary constants, $f_i(x)$ are typical functions in the homogeneous solution and $g(x)$ is a particular solution. For example, a typical one-dimensional steady-state thermal analysis is governed by second order differential equation of the form of Eq. (3.4) and has a general solution

$$\phi(x) = C_1 \, f_1(x) + C_2 \, f_2(x) + g(x) \tag{3.6}$$

By comparing this general solution with the solution in the form of polynomials used to describe a linear variation of dependent variable in the conventional finite element, Eq. (3.1), basic differences between these two solutions are noted: (1) the function $f_i(x)$ in the general solution to a given differential equation can be forms other than the polynomials, and (2) the general solution contains a particular solution $g(x)$ which is known in general and depends on forcing function $r(x)$ on the right hand side of the differential equation (3.4).

3.1.1 Exact Element Interpolation Functions and Nodeless Parameters

Once a general solution to a given differential is obtained, exact element interpolation functions can be derived. For a typical finite element with n degrees of freedom, n boundary conditions are required. With the general solution shown in equation (3.5), the required boundary conditions are

$$\phi(x_i) = \phi_i \qquad i = 1, 2, \ldots, n \tag{3.7}$$

where x_i is the nodal coordinate and ϕ_i is the element nodal

unknown at node i. After applying the boundary conditions, the exact element variation of $\phi(x)$ has the form,

$$\phi(x) = G(x) + \sum_{i=1}^{n} N_i \phi_i$$

where $N_i(x)$ is the element interpolation function corresponding to node i. The function $G(x)$ is a known function associated with the particular solution. In general, this function can be expressed as a product of a spatial function $N_0(x)$ and a scalar term ϕ_0 which contains a physical forcing parameter such as body force, surface heating, etc.;

$$G(x) = N_0(x)\ \phi_0$$

and, therefore, the exact element $\phi(x)$ variation becomes,

$$\phi(x) = N_0(x)\ \phi_0 + \sum_{i=1}^{n} N_i \phi_i \qquad (3.8a)$$

or in the matrix form

$$\phi(x) = \lfloor N_0\ N_1\ N_2\ \cdots\ N_n \rfloor \left\{ \begin{array}{c} \phi_0 \\ \hline \phi_1 \\ \phi_2 \\ \vdots \\ \phi_n \end{array} \right\} = \lfloor N_0\ N \rfloor \left\{ \frac{\phi_0}{\phi} \right\} \qquad (3.8b)$$

Note that the element interpolation function $N_i(x_i)$ has a value of unity at node i to satisfy the boundary conditions, Eq. (3.7), thus the spatial function $N_0(x)$ must vanish at nodes. Since the

term ϕ_0 is a known quantity and neither relates to the element nodal coordinates nor is identified with the element nodes, it is called a nodeless parameter. Likewise, the corresponding spatial function $\overset{\circ}{N_0}(x)$ is called a nodeless interpolation function. Comparison between element variations of a typical nodeless parameter finite element, Eq. (3.8), and the conventional linear finite element, Eq. (3.3), is shown in Fig. 3.

3.1.2 Exact Element Matrices

After exact element interpolation functions are obtained, the corresponding element matrices can be formulated. For the governing ordinary differential equation, Eq. (3.4), typical element matrices can be derived (see section 2.2) and element equations can be written in the form,

$$
\begin{bmatrix}
K_{00} & \vdots & K_{01} & K_{02} & \cdots\cdots & K_{0n} \\
\hdashline
K_{10} & \vdots & K_{11} & K_{12} & & K_{1n} \\
K_{20} & \vdots & K_{21} & K_{22} & & K_{2n} \\
\vdots & \vdots & & & \ddots & \\
K_{n0} & \vdots & K_{n1} & K_{n2} & & K_{nn}
\end{bmatrix}
\begin{Bmatrix}
\phi_0 \\
\hdashline
\phi_1 \\
\phi_2 \\
\vdots \\
\phi_n
\end{Bmatrix}
=
\begin{Bmatrix}
F_0 \\
\hdashline
F_1 \\
F_2 \\
\vdots \\
F_n
\end{Bmatrix}
\tag{3.9}
$$

where K_{ij}, $i, j = 0, n$ are typical terms in the element stiffness matrix; F_i, $i = 0, n$ are typical terms in the element load vector, ϕ_i, $i = 1, n$ are the element nodal unknowns, and ϕ_0 is the element nodeless parameter. Since the element nodeless parameter is known, the above element equations reduce to
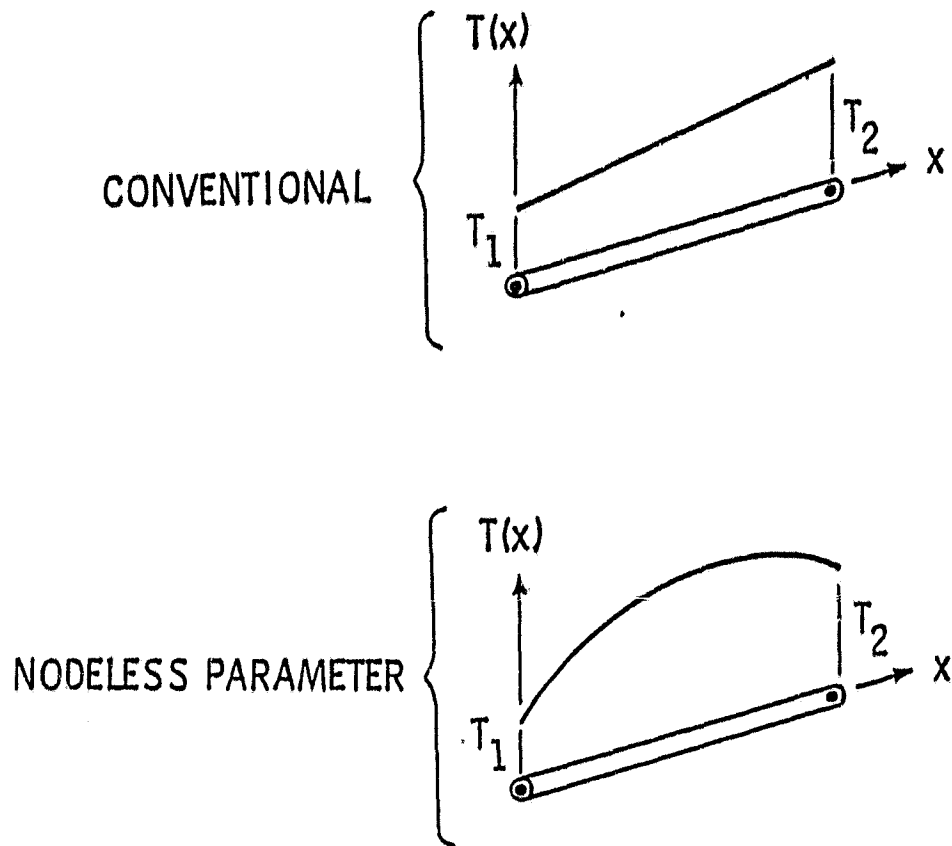
Fig. 3. Comparison of conventional and nodeless parameter elements.

$$
\begin{bmatrix}
K_{11} & K_{12} & \cdots\cdots & K_{1n} \\
K_{21} & K_{22} & & K_{2n} \\
\vdots & & \ddots\ddots & \\
K_{n1} & K_{n2} & & K_{nn}
\end{bmatrix}
\begin{Bmatrix}
\phi_1 \\ \phi_2 \\ \vdots \\ \vdots \\ \phi_n
\end{Bmatrix}
=
\begin{Bmatrix}
F_1 \\ F_2 \\ \vdots \\ \vdots \\ F_n
\end{Bmatrix}
- \phi_0
\begin{Bmatrix}
K_{10} \\ K_{20} \\ \vdots \\ \vdots \\ K_{n0}
\end{Bmatrix}
\tag{3.10}
$$

3.2 Exact Finite Elements in Thermal Problems

In one-dimensional linear steady-state thermal problems, typical governing differential equations can be derived from a heat balance on a small segment in the form, .

$$
\frac{d}{dx}\left(a_2(x)\,\frac{dT}{dx}\right) + a_1(x)\,\frac{dT}{dx} + a_0(x)\,T = r(x)
\tag{3.11}
$$

where T denotes the temperature, x denotes a typical one-dimensional space coordinate in cartesian, cylindrical or spherical coordinates; a_i, $i = 0, 1, 2$ are variable coefficients, and $r(x)$ is a function associated with a heat load for a given problem. A general solution to the above differential equation has the form,

$$
T(x) = C_1\,f_1(x) + C_2\,f_2(x) + g(x)
\tag{3.12}
$$

where $f_1(x)$ and $f_2(x)$ are linearly independent solutions of the homogeneous equation, C_1 and C_2 are constants of integration, and $g(x)$ is a particular solution. Since the particular solution $g(x)$ is known, the above general solution has two unknowns to be determined. A finite element with two nodes, therefore, can be formulated using the conditions,

$$T(x_1) = T_1 \qquad (3.13a)$$

$$T(x_2) = T_2 \qquad (3.13b)$$

where x_i, $i = 1, 2$ are nodal coordinates and T_i, $i = 1, 2$ are the nodal temperatures. Imposing these conditions on the general solution yields two equations for evaluating C_1 and C_2,

$$T(x_1) = T_1 = C_1 f_1(x_1) + C_2 f_2(x_1) + g(x_1)$$

$$T(x_2) = T_2 = C_1 f_1(x_2) + C_2 f_2(x_2) + g(x_2)$$

or in matrix form

$$\begin{bmatrix} f_1(x_1) & f_2(x_1) \\ f_1(x_2) & f_2(x_2) \end{bmatrix} \begin{Bmatrix} C_1 \\ C_2 \end{Bmatrix} = \begin{Bmatrix} T_1 - g(x_1) \\ T_2 - g(x_2) \end{Bmatrix}$$

After C_1 and C_2 are determined and substituted into the general solution, Eq. (3.12), the exact element temperature variation can be written as

$$T(x) = N_0(x) T_0 + N_1(x) T_1 + N_2(x) T_2 \qquad (3.14a)$$

or in the matrix form,

$$T(x) = \lfloor N_0 \quad N_1 \quad N_2 \rfloor \begin{Bmatrix} T_0 \\ T_1 \\ T_2 \end{Bmatrix} \qquad (3.14b)$$

where $N_0(x)$ is the nodeless interpolation function and T_0 is the

nodeless parameter; $N_1(x)$ and $N_2(x)$ are element interpolation functions corresponding to node 1 and 2, respectively. These element interpolation functions including the nodeless parameter are known functions defined by

$$N_1(x) = \frac{f_1(x)\ f_2(x_2) - f_1(x_2)\ f_2(x)}{W} \tag{3.15a}$$

$$N_2(x) = \frac{f_1(x_1)\ f_2(x) - f_1(x)\ f_2(x_1)}{W} \tag{3.15b}$$

$$N_0(x)\ T_0 = g(x) + \frac{f_2(x_1)\ g(x_2) - f_2(x_2)\ g(x_1)}{W}\ f_1(x)$$

$$+ \frac{f_1(x_2)\ g(x_1) - f_1(x_1)\ g(x_2)}{W}\ f_2(x) \tag{3.15c}$$

where $W = f_1(x_1)\ f_2(x_2) - f_1(x_2)\ f_2(x_1)$.

Using the exact element interpolation functions shown in Eq. (3.14), and the governing differential equation, Eq. (3.11), element matrices can be derived through the use of the method of weighted residuals;

$$\int_{x_1}^{x_2} [\frac{d}{dx} (a_2 \frac{dT}{dx}) + a_1 \frac{dT}{dx} + a_0 T - r]\ N_i\ dx = 0 \qquad i=0,1,2 \tag{3.16}$$

Performing an integration by parts on the first term and substituting for element temperature in terms of the interpolation functions, Eq. (3.14), yields element equations in the form,

$$[[K_c] + [K_v] + [K_h]] \begin{Bmatrix} T_0 \\ T_1 \\ T_2 \end{Bmatrix} = \{Q_c\} + \{Q\} \tag{3.17}$$

where $[K_c]$, $[K_v]$, and $[K_h]$ are the element conductance matrices associated with the second, the first, and the zero-order derivative term on the left hand side of the governing differential equation (3.11), respectively; $\{Q_c\}$ is the element vector of conduction heat flux across element boundary, and $\{Q\}$ is the element load vector from the heat load $r(x)$ in the governing differential equation. These matrices are defined as follows:

$$[K_c] = \int_{x_1}^{x_2} - a_2 \left\{\frac{dN}{dx}\right\} \left\lfloor \frac{dN}{dx} \right\rfloor dx \tag{3.18a}$$

$$[K_v] = \int_{x_1}^{x_2} a_1 \{N\} \left\lfloor \frac{dN}{dx} \right\rfloor dx \tag{3.18b}$$

$$[K_h] = \int_{x_1}^{x_2} a_0 \{N\} \lfloor N \rfloor dx \tag{3.18c}$$

$$\{Q_c\} = \left\{ [- a_2 \frac{dT}{dx} N] \Big|_{x_1}^{x_2} \right\} \tag{3.18d}$$

$$\{Q\} = \int_{x_1}^{x_2} r\{N\} \, dx \qquad (3.18e)$$

Depending on the complexity of element interpolation functions, the element matrices may be evaluated in closed form or they may require numerical integration. However, after the element matrices are computed, typical element equations can be written in the form,

$$\begin{bmatrix} K_{00} & K_{01} & K_{02} \\ K_{10} & K_{11} & K_{12} \\ K_{20} & K_{21} & K_{22} \end{bmatrix} \begin{Bmatrix} T_0 \\ T_1 \\ T_2 \end{Bmatrix} = \{Q_c\} + \begin{Bmatrix} Q_0 \\ Q_1 \\ Q_2 \end{Bmatrix} \qquad (3.19)$$

Since the nodeless parameter is known, the first equation is uncoupled from the nodal unknowns in the second and third equations. Thus, the exact element matrices have the same size as of the conventional linear finite element and element equations can be written as

$$\begin{bmatrix} K_{11} & K_{12} \\ K_{21} & K_{22} \end{bmatrix} \begin{Bmatrix} T_1 \\ T_2 \end{Bmatrix} = \{Q_c\} + \begin{Bmatrix} Q_1 \\ Q_2 \end{Bmatrix} - T_0 \begin{Bmatrix} K_{10} \\ K_{20} \end{Bmatrix} \qquad (3.20)$$

Note that, in general, the above conductance matrix is an asymmetric matrix. This asymmetry is caused by the conductance matrix $[K_v]$ shown in Eq. (3.18b) associated with the first-order derivative in the governing differential equation, Eq. (3.11). To obtain a symmetrical conductance matrix, the first-order derivative

is eliminated by casting the governing differential equation in self-adjoint form,

$$\frac{d}{dx}\left[P(x)\frac{dT}{dx}\right] + Q(x)\ T = R(x) \tag{3.21}$$

where

$$P(x) = \exp\left(\int\left[(a_1 + \frac{da_2}{dx})\ /\ a_2\right]\ dx\right) \tag{3.22a}$$

$$Q(x) = \frac{a_0 P}{a_2} \tag{3.22b}$$

$$R(x) = \frac{rP}{a_2} \tag{3.22c}$$

Element matrices can then be derived using the method of weighted residuals in the same manner as previously described. In this case, element equations have the form,

$$[[\bar{K}_c] + [\bar{K}_h]]\begin{Bmatrix} T_0 \\ T_1 \\ T_2 \end{Bmatrix} = \{\bar{Q}_c\} + \{\bar{Q}\} \tag{3.23}$$

where the conductance matrices and heat load vectors are defined by

$$[\bar{K}_c] = \int_{x_1}^{x_2} -\ P\ \{\frac{dN}{dx}\}\ \lfloor\frac{dN}{dx}\rfloor\ dx \tag{3.24a}$$

$$[\bar{K}_h] = \int_{x_1}^{x_2} Q \{N\} \lfloor N \rfloor \, dx \tag{3.24b}$$

$$\{\bar{Q}_c\} = \left\{ -P \frac{dT}{dx} N \bigg|_{x_1}^{x_2} \right\} \tag{3.24c}$$

$$\{\bar{Q}\} = \int_{x_1}^{x_2} R \{N\} \, dx \tag{3.24d}$$

Similarly, element equations for the two nodal unknowns are

$$\begin{bmatrix} \bar{K}_{11} & \bar{K}_{12} \\ \bar{K}_{12} & \bar{K}_{22} \end{bmatrix} \begin{Bmatrix} T_1 \\ T_2 \end{Bmatrix} = \{\bar{Q}_c\} + \begin{Bmatrix} \bar{Q}_1 \\ \bar{Q}_2 \end{Bmatrix} - T_0 \begin{Bmatrix} \bar{K}_{10} \\ \bar{K}_{20} \end{Bmatrix} \tag{3.25}$$

where $\bar{K}_{ij}$, $i,j = 0,1,2$ is the summation of the corresponding coefficients in the conductance matrices $[\bar{K}_c]$ and $[\bar{K}_h]$;

$$\bar{K}_{ij} = \int_{x_1}^{x_2} -P \frac{dN_i}{dx} \frac{dN_j}{dx} \, dx + \int_{x_1}^{x_2} Q N_i N_j \, dx \tag{3.26}$$

$$i,j = 0,1,2$$

An additional advantage of using the self-adjoint differential equation is that the coefficients $\bar{K}_{10}$ and $\bar{K}_{20}$ shown on the right hand side of Eq. (3.25) are identically zero. This result can be proved by observing that the element interpolation function N_i,

$i = 1, 2$ are the solution of the homogeneous differential equation, Eq. (3.21), because N_i is a linear combination of the homogeneous solutions $f_1(x)$ and $f_2(x)$ as shown in Eqs. (3.15a-b), i.e.

$$\frac{d}{dx} \left[P \frac{dN_i}{dx} \right] + Q N_i = 0 \qquad i = 1, 2$$

Multiplying this equation by the nodeless parameter interpolation function N_0 and performing integration by parts on the first term yields

$$P \frac{dN_i}{dx} N_0 \Big|_{x_1}^{x_2} + \int_{x_1}^{x_2} - P \frac{dN_i}{dx} \frac{dN_0}{dx} dx + \int_{x_1}^{x_2} Q N_i N_0 dx = 0$$

Then since the nodeless interpolation function N_0 vanishes at nodes, i.e. at the coordinates x_1 and x_2, the above equations yield

$$\bar{K}_{i0} = 0 \qquad i = 1, 2$$

and the element equations, Eq. (3.25), become

$$\begin{bmatrix} \bar{K}_{11} & \bar{K}_{12} \\ \bar{K}_{12} & \bar{K}_{22} \end{bmatrix} \begin{Bmatrix} T_1 \\ T_2 \end{Bmatrix} = \{\bar{Q}_c\} + \begin{Bmatrix} \bar{Q}_1 \\ \bar{Q}_2 \end{Bmatrix} \qquad (3.27)$$

After element nodal temperatures are computed, exact temperatures within an element can be obtained using the exact element temperature variation, Eq. (3.14).

To demonstrate the exact finite element formulation previously derived, exact finite elements for eight heat transfer cases in several solids of different shapes and a flow passage (Fig. 4) are presented. In the first seven cases, heat transfer may consist of: (1) pure conduction, (2) conduction with internal heat generation, (3) conduction with surface heating, and (4) conduction with surface convection. Case eight is a one-dimensional flow where heat transfer may consist of fluid conduction and mass transport convection with surface heating or surface convection. For these cases, the boundary conditions considered are:

$$T = \text{Constant} \tag{3.28a}$$

or

$$- k \frac{dT}{dx} = q \tag{3.28b}$$

or

$$- k \frac{dT}{dx} = h(T - T_\infty) \tag{3.28c}$$

where k is the material thermal conductivity, q is the specified surface heating rate per unit area, h is the convection coefficient, and T_∞ is the convection medium temperature. In each case, the derivation of exact finite elements for appropriate heat transfer cases are given for clarity. Governing differential equations and the corresponding nodeless parameters, exact element interpolation functions, and element matrices for all cases are shown in Tables 1 and 2 and Appendices A and B.

3.2.1 Rod and Slab

A rod element with arbitrary cross-sectional area A, circumfer... .ial perimeter p and length L as shown in (Fig. 4, Case 1)
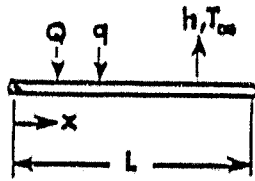
Case 1, ROD
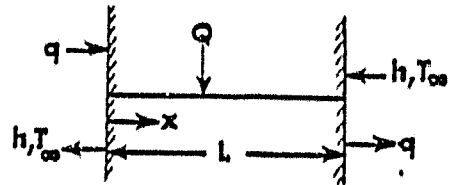
Case 2, SLAB
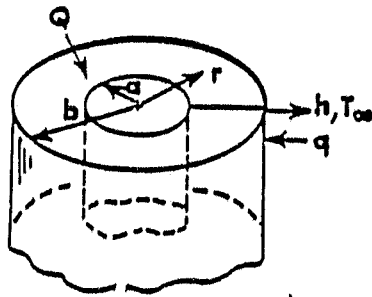
Case 3, HOLLOW CYLINDER
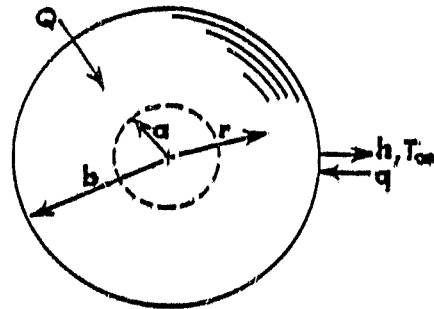
Case 4, HOLLOW SPHERE
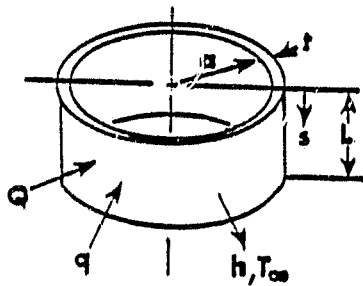
Case 5, CYLINDRICAL SHELL
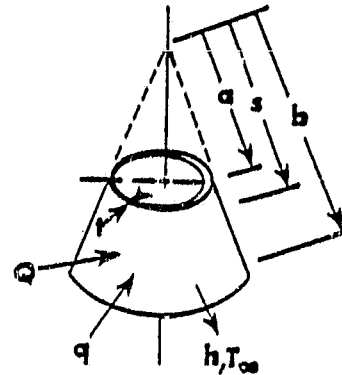
Case 6, CONICAL SHELL
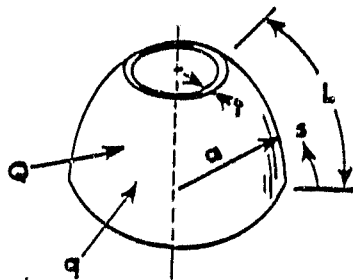
Case 7, SPHERICAL SHELL
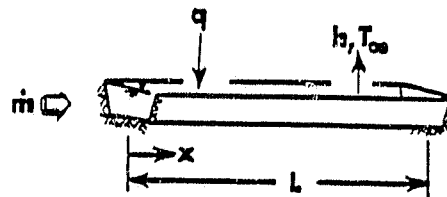
Case 8, FLOW PASSAGE

Fig. 4. Exact finite elements for one-dimensional conduction
and convection cases.

Table II

Governing Self-Adjoint Differential Equations

Case	Conduction (a)	Convection (b)	Heat Loads		
			Convection (b)	Source (c)	Surface Flux (d)
1	$-\dfrac{d}{dx}\left[\dfrac{dT}{dx}\right]$	$\dfrac{hp}{kA} T$	$\dfrac{hp}{kA} T_\infty$	$\dfrac{Q}{k}$	$\dfrac{qp}{kA}$
2	$-\dfrac{d}{dx}\left[\dfrac{dT}{dx}\right]$	—	—	$\dfrac{Q}{k}$	—
3	$-\dfrac{d}{dr}\left[r\dfrac{dT}{dr}\right]$	—	—	$\dfrac{Q}{k} r$	—
4	$-\dfrac{d}{dr}\left[r^2\dfrac{dT}{dr}\right]$	—	—	$\dfrac{Q}{k} r^2$	—
5	$-\dfrac{d}{ds}\left[\dfrac{dT}{ds}\right]$	$\dfrac{h}{kt} T$	$\dfrac{h}{kt} T_\infty$	$\dfrac{Q}{k}$	$\dfrac{q}{kt}$
6.	$-\dfrac{d}{ds}\left[s\dfrac{dT}{ds}\right]$	$\dfrac{h}{kt} sT$	$\dfrac{h}{kt} sT_\infty$	$\dfrac{Q}{k} s$	$\dfrac{q}{kt} s$
7	$-\dfrac{d}{ds}\left[\cos\dfrac{s}{a}\dfrac{dT}{ds}\right]$	—	—	$\dfrac{Q}{k}\cos\dfrac{s}{a}$	$\dfrac{q}{kt}\cos\dfrac{s}{a}$
8	$-\dfrac{d}{dx}\left[P\dfrac{dT}{dx}\right]$*	$\dfrac{hp}{kA} P T$	$\dfrac{hp}{kA} P T_\infty$	—	$\dfrac{qp}{kA} P$

*Combined conduction and mass transport convection where $P = \exp(-\dot{m}cx/kA)$.

Table 2

Nodeless Parameters for Thermal Problems

Case	T_0		
	Convection (b)	Source (c)	Surface Flux (d)
1	T_∞	$\dfrac{QL^2}{2k}$	$\dfrac{qpL^2}{2kA}$
2	---	$\dfrac{QL^2}{2k}$	---
3	---	$\dfrac{Qb^2}{4kw}$	---
4	---	$\dfrac{Q}{6k}$	---
5	T_∞	$\dfrac{QL^2}{2k}$	$\dfrac{qL^2}{2kt}$
6	T_∞	$\dfrac{Qb^2}{4kw}$	$\dfrac{qb^2}{4ktw}$
7	---	$\dfrac{Qa^2}{k}$	$\dfrac{Qa^2}{kt}$
8	T_∞	---	$\dfrac{qpL}{\dot{m}c}$

where $w = \ln(b/a)$.

is subjected to internal heat generation, surface heating, and surface convection. Governing differential equations for each heat transfer case in self-adjoint form are shown in Table 1. For example, the governing differential equation for the case of conduction with surface convection is

$$-\frac{d}{dx}\left(kA\frac{dT}{dx}\right) + hpT = hpT_\infty \tag{3.29}$$

where k is the material thermal conductivity, h is the convection coefficient, and T_∞ is the convective medium temperature. A general solution to the above differential equation is

$$T(x) = C_1 \sinh mx + C_2 \cosh mx + T_\infty$$

where $m = \sqrt{hp/kA}$, and C_1 and C_2 are unknown constants. Applying the boundary conditions at the nodes,

$$T(x=0) = T_1 \qquad \text{and} \qquad T(x=L) = T_2$$

the two unknown constants are evaluated and the above solution becomes

$$T(x) = \left(1 - \frac{\sinh m(L-x)}{\sinh mL} - \frac{\sinh mx}{\sinh mL}\right) T_\infty$$

$$+ \left(\frac{\sinh m(L-x)}{\sinh mL}\right) T_1 + \left(\frac{\sinh mx}{\sinh mL}\right) T_2 \tag{3.30}$$

This exact element temperature variation can be written in the form of Eq. (3.14) where the element interpoation functions and the nodeless parameter are:

$$N_0(x) = (1 - \frac{\sinh m(L-x)}{\sinh mL} - \frac{\sinh mx}{\sinh mL}); \quad T_0 = T_\infty$$

$$(3.31)$$

$$N_1(x) = \frac{\sinh m(L-x)}{\sinh mL}; \quad N_2(x) = \frac{\sinh mx}{\sinh mL}$$

As described in the previous section, element equations for a typical self-adjoint differential equation have the form of Eq. (3.23), and using the definitions of the element matrices shown in Eq. (3.24), the element matrices for this problem are:

$$[\bar{K}_c] = \int_0^L kA \{\frac{dN}{dx}\} \lfloor\frac{dN}{dx}\rfloor dx \qquad (3.32a)$$

$$[\bar{K}_h] = \int_0^L hp \{N\} \lfloor N\rfloor dx \qquad (3.32b)$$

$$\{\bar{Q}\} = \int_0^L hpT_\infty \{N\} dx \qquad (3.32c)$$

where $[\bar{K}_c]$ and $[\bar{K}_h]$ are conductance matrices corresponding to conduction and convection, respectively, and $\{\bar{Q}\}$ is the load vector due to surface convection. With the exact interpolation functions shown in Eq. (3.31), the above element matrices can be evaluated in closed form. Exact nodal temperatures and element temperature variation can then be computed using Eqs. (3.27) and (3.30), respectively.

For the cases where the rod is subjected to an internal heat generation or specified surface heating, exact element interpolation functions and element matrices can be derived in the same manner as

described above. It should be noted that only the conductance matrix
associated with conduction and heat load vectors corresponding to
internal heat generation or surface heating exist in the two cases.
The exact conductance matrix and heat load vectors are found to be
identical to those from the conventional linear element. Therefore,
exact nodal temperatures can also be obtained through the use of
the conventional linear finite element in such cases. However, since
the linear temperature variation is not an exact solution to these
problems, the conventional linear finite element can not provide the
exact temperature distribution within the element.

The derivation of exact finite elements for one-dimensional heat
transfer in a slab follows the derivation for the exact rod element.
A slab with thickness L subjected to an internal heat generation
(Fig. 4, Case 2) where both sides of slab may be subjected to a
specified surface heating or surface convection. In Table 1, the
governing differential equations are shown only for the case of pure
conduction and conduction with internal heat generation because the
effects of surface heating and surface convection enter the problem
through the boundary conditions. For example, a governing differen-
tial equation describing heat conduction in a slab with specified
temperature T_1 at x = 0 (node 1) and surface convection at x = L
(node 2) is

$$-\frac{d}{dx}\left[k\frac{dT}{dx}\right] = 0 \quad . \tag{3.33}$$

where k denotes the material thermal conductivity. After solving
for the general solution to the governing differential equation above

and applying nodal temperatures as boundary conditions at $x = 0$ and $x = L$, the exact element temperature variation is (see Appendix A)

$$T(x) = (1 - \frac{x}{L})\, T_1 + (\frac{x}{L})\, T_2 = \lfloor N_1(x) \quad N_2(x) \rfloor \begin{Bmatrix} T_1 \\ T_2 \end{Bmatrix} \qquad (3.34)$$

With the corresponding element conductance matrix shown in Appendix B, exact element equations for this problem are

$$\frac{k}{L} \begin{bmatrix} 1 & -1 \\ -1 & 1 \end{bmatrix} \begin{Bmatrix} T_1 \\ T_2 \end{Bmatrix} = \begin{Bmatrix} Q_{c_1} \\ Q_{c_2} \end{Bmatrix} = \begin{Bmatrix} -k\,\frac{dT}{dx}\,(x=0) \\ k\,\frac{dT}{dx}\,(x=L) \end{Bmatrix}$$

since at $x = L$ (node 2) the boundary condition is

$$-k\,\frac{dT}{dx}\,(x=L) = h(T_2 - T_\infty)$$

where h is the convection coefficient and T_∞ is the surrounding medium temperature, therefore, the above element equations become

$$\begin{bmatrix} \frac{k}{L} & -\frac{k}{L} \\ -\frac{k}{L} & \frac{k}{L}+h \end{bmatrix} \begin{Bmatrix} T_1 \\ T_2 \end{Bmatrix} = \begin{Bmatrix} -k\,\frac{dT(x=0)}{dx} \\ h\,T_\infty \end{Bmatrix} \qquad (3.35)$$

the exact nodal unknown T_2 can then be computed and the exact element tempterature distribution is obtained using equation (3.34).

The same procedure can be applied for the case when the slab is subjected to surface heating. In this case, the boundary condition is

$$- k \frac{dT}{dx} = q$$

where   q   denotes the specified surface heating. When the slab

consists several layers with different thermal conductivities, an

exact element can be used to represent each layer. If the slab is

subjected to surface heating or surface convection in addition, the

above procedure applies for the elements located at the outer

surfaces.

3.2.2 Hollow Cylinder and Sphere

A thermal model of a hollow cylinder with radial heat conduction

subjected to an internal heat generation is shown in Fig. 4, Case 3.

Specified heating or surface convection are considered through the

boundary conditions at the inner and outer surfaces of radii   a   and

b,   respectively. Governing differential equations corresponding to

each heat transfer case are provided in Table 1. For example, the

governing differential equation for the case of pure conduction is

$$k \frac{d}{dr} \left[r \frac{dT}{dr} \right] = 0 \tag{3.36}$$

where   k   is the material thermal conductivity, and   r   is the radial

coordinate. A general solution to the above differential equation is

$$T(r) = C_1 + C_2 \ln r$$

Nodal temperatures are imposed on the element boundary conditions,

$$T(r = a) = T_1 \quad \text{and} \quad T(r = b) = T_2$$

and the exact element variation is obtained as (see Appendix A),

$$T(r) = \left\lfloor \frac{\ln(b/r)}{w} \quad \frac{\ln(r/a)}{w} \right\rfloor \left\{ \begin{matrix} T_1 \\ T_2 \end{matrix} \right\} \qquad (3.37)$$

where $w = \ln(b/a)$. Note that the exact element variation for this case is completely different from the linear element variation, therefore, the conventional linear finite element can not provide exact element or nodal temperatures. Applying the method of weighted residuals to the governing differential equation, element equations are

$$[\bar{K}_c] \{T\} = \{\bar{Q}_c\} \qquad (3.38a)$$

where

$$[\bar{K}_c] = \int_a^b k\{\frac{dN}{dr}\} \lfloor \frac{dN}{dr} \rfloor \ r \ dr \qquad (3.38b)$$

$$\{\bar{Q}_c\} = \left\{ kr \ \frac{dT}{dr} \ N \ \Big|_a^b \right\} \qquad (3.38c)$$

Using the exact element interpolation functions shown in Eq. (3.37), element equations for this case are

$$\frac{k}{w} \begin{bmatrix} 1 & -1 \\ -1 & 1 \end{bmatrix} \left\{ \begin{matrix} T_1 \\ T_2 \end{matrix} \right\} = \left\{ \begin{matrix} -ka \ \frac{dT}{dr} \\ kb \ \frac{dT}{dr} \end{matrix} \right\} \qquad (3.39)$$

When the cylinder is subjected to surface heating or surface convection, the same procedure previously described for the slab can be used. For example, in case of convection heat transfer on the outer surface, the boundary condition is

$$r = b; \qquad -k \frac{dT}{dr} = h(T_2 - T_\infty)$$

where h is the convection coefficient and T_∞ is the surrounding medium temperature. Thus, the element equations, Eq. (3.39), become

$$\begin{bmatrix} \dfrac{k}{w} & -\dfrac{k}{w} \\[2ex] -\dfrac{k}{w} & \dfrac{k}{w} + hb \end{bmatrix} \begin{Bmatrix} T_1 \\[2ex] T_2 \end{Bmatrix} = \begin{Bmatrix} -ka \dfrac{dT}{dr} \\[2ex] hb\,T_\infty \end{Bmatrix} \qquad (3.40)$$

Exact finite elements can be formulated for conduction heat transfer in the radial direction of a hollow sphere with internal heat generation. A thermal model of a hollow sphere with inner and outer surface radii a and b, respectively, is illustrated in Fig. 4, Case 4. The hollow sphere may be subjected to surface heating or surface convection on both inner and outer surfaces. For heat conduction with internal heat generation, the governing differential equation is (see Table 1)

$$- k \frac{d}{dr} [r^2 \frac{dT}{dr}] = Qr^2 \qquad (3.41)$$

where k is the material thermal conductivity, Q is the heat generation rate per unit volume, and r is the independent variable representing the radial coordinate. A general solution to this differential equation is

$$T(r) = \frac{C_1}{r} + C_2 - \frac{Qr^2}{6k}$$

Due to the presence of the particular solution in the above general solution, a nodeless parameter exists, and the exact element variation is written in the form

$$T(r) = N_0(r) \; T_0 + N_1(r) \; T_1 + N_2(r) \; T_2 \qquad (3.42a)$$

where the element interpolation functions including the nodeless parameter are:

$$N_0(r) = \frac{1}{r}(r-a)(b-r)(r+a+b); \qquad T_0 = \frac{Q}{6k}$$

$$N_1(r) = \frac{a(b-r)}{r(b-a)} \qquad N_2(r) = \frac{b(r-a)}{r(b-a)} \qquad (3.42b)$$

Element matrices can be derived using the method of weighted residuals and element equations are resulted in the form

$$[\bar{K}_c] \; \{T\} = \{\bar{Q}_c\} + \{\bar{Q}\} \qquad (3.43a)$$

where these element matrices are defined by:

$$[\bar{K}_c] = \int_a^b k \; \{\frac{dN}{dr}\} \; \lfloor\frac{dN}{dr}\rfloor \; r^2 \; dr \qquad (3.43b)$$

$$\{\bar{Q}_c\} = \left\{ k \; r^2 \; \frac{dT}{dr} \; N \; \Big|_a^b \right\} \qquad (3.43c)$$

$${\bar{Q}} = \int_a^b Q\{N\}\, r^2\, dr \qquad\qquad (3.43d)$$

If surface heating and surface convection are applied on the inner and outer surface, the same procedure described for the cylinder is required.

3.2.3 Thin Shells

Three thermal models of thin shells of revolution with cylindrical, conical and spherical shapes are presented (see Fig. 4). These shells may be subjected to thermal loads such as surface heating, surface convection, and internal heat generation as shown in Fig. 4, Cases 5-7. In Case 5, a cylindrical shell of radius a, thickness t and meridional coordinate s is considered. Governing differential equations corresponding to different thermal loads are shown in Table 1. These governing differential equations are in the same form as for the rod element (Case 1). Therefore, the exact rod element interpolation functions and element matrices previously derived can be modified and used for the exact cylindrical shell element.

A truncated conical shell element with thickness t is shown in Fig. 4, Case 6. Governing differential equations corresponding to internal heat generation and surface heating are given in Table 1. These differential equations are in the same form as for the hollow cylinder (Case 3) with surface heating, and therefore, element interpolation functions and element matrices are similars. For the case of the shell subjected to surface convection, a form of

nonhomogeneous modified Bessel's differential equation results,

$$\frac{d^2T}{ds^2} + \frac{1}{s}\frac{dT}{ds} - \frac{h}{kt}\,T = -\frac{h}{kt}\,T_\infty \qquad (3.44)$$

A general solution to the above differential equation includes
modified Bessel functions of the first and second kind of order zero.
A nodeless parameter also exists in this case due to the nonhomo-
geneous differential equation. Applying nodal temperatures as the
boundary conditions at $s = a$ and $s = b$, exact element interpola-
tion functions are obtained as shown in Appendix A.

Fig. 4, Case 7 shows a truncated spherical shell with radius
a and thickness t. The spherical shell may be subjected to
internal heat generation or surface heating. Governing differential
equations corresponding to these thermal loads are in the form of
Legendre's differential equation of order zero. For example, the
governing differential equation for the case of uniform surface
heating q is

$$(1 - \eta^2)\,\frac{d^2T}{d\eta^2} - 2\eta\,\frac{dT}{d\eta} = -\frac{qa^2}{kt} \qquad (3.45)$$

where $\eta = \sin(s/a)$. A general solution to the above differential
equation is

$$T = \frac{C_1}{2}\ln\left[\frac{1+\eta}{1-\eta}\right] + C_2 + \frac{qa^2}{2kt}\ln[1-\eta^2] \qquad (3.46)$$

where C_1 and C_2 are unknown constants. By imposing nodal
temperatures as element boundary conditions at $s = 0$ and $s = L$,

exact element interpolation functions are obtained as shown in Appendix A.

Due to the complexity of the exact element interpolation functions that arise from the truncated conical shell with surface convection and the truncated spherical shell, the corresponding element matrices in closed form are not provided. The element matrices, if desired, can be obtained using the element matrix formulation shown in Equations (3.14a-d) and performing the integrations numerically.

3.2.4 Flow Passage

A thermal model of fluid flow in a passage with conduction and mass transport convection is illustrated in Fig. 4, Case 8. The fluid may be heated by surface heating, or surface convection. Governing differential equations corresponding to these heat transfer cases are given in Table 1. For simplicity, consider the case without heat loads where the governing homogeneous differential equation is given by

$$- \frac{d}{dx} \left[kA \frac{dT}{dx} \right] + \dot{m}c \frac{dT}{dx} = 0 \tag{3.47}$$

where k is the fluid thermal conductivity, A is the flow cross-sectional area, $\dot{m}$ is the fluid mass flow rate, and c is the fluid specific heat. A general solution to this differential equation is

$$T(x) = C_1 + C_2 \exp(2\alpha x)$$

where C_1 and C_2 are arbitrary constants and $\alpha = \dot{m}c/2kA$. An exact finite element with length L and nodal temperatures T_1 and

T_2 at $x = 0$ and $x = L$, respectively, can be formulated. The exact element temperature variation is

$$T(x) = \lfloor 1 - \frac{1 - e^{2\alpha x}}{1 - e^{2\alpha L}} \quad \frac{1 - e^{2\alpha x}}{1 - e^{2\alpha L}} \rfloor \left\{ \begin{array}{c} T_1 \\ \\ T_2 \end{array} \right\} \tag{3.48a}$$

As previously described, the appearance of the first-order derivative term in the governing differential equation results in an unsymmetrical conductance matrix (see Eq. (3.18b)). In this case, the corresponding element conductance matrices are

$$[K_c] = kA\alpha \frac{(e^{2\alpha L} + 1)}{(e^{2\alpha L} - 1)} \begin{bmatrix} 1 & -1 \\ -1 & 1 \end{bmatrix} \tag{3.48b}$$

$$[K_v] = \frac{\dot{m}c}{2} \begin{bmatrix} -1 & 1 \\ -1 & 1 \end{bmatrix} \tag{3.48c}$$

where $[K_c]$ and $[K_v]$ denote conductance matrices representing fluid conduction and mass transport fluid convection, respectively.

It has been shown that if the conventional finite element with an optimum upwind weighting function is used, exact temperatures at nodes can also be obtained [21]. With upwind weighting functions the element temperature variation is expressed as,

$$T(x) = \lfloor 1 - \frac{x}{L} + F(x) \quad \frac{x}{L} - F(x) \rfloor \left\{ \begin{array}{c} T_1 \\ \\ T_2 \end{array} \right\} \tag{3.49a}$$

where $F(x)$ is the optimum upwind weighting function defined by

$$F(x) = [\coth (2\alpha L) - \frac{1}{\alpha L}] \; [3(\frac{x^2}{L^2} - \frac{x}{L})]$$

With these element interpolation functions, element conductance matrices corresponding to the fluid conduction and mass transport convection are

$$[K_c]_{\text{upwind}} = \frac{kA}{L} \begin{bmatrix} 1 & -1 \\ -1 & 1 \end{bmatrix} \tag{3.49b}$$

$$[K_v]_{\text{upwind}} = \frac{\dot{m}c}{2} \begin{bmatrix} -1 & 1 \\ -1 & 1 \end{bmatrix} + \frac{\dot{m}c}{2} (\coth (\alpha L) - \frac{1}{\alpha L}) \begin{bmatrix} 1 & -1 \\ -1 & 1 \end{bmatrix} \tag{3.49c}$$

It can be shown that the combination of these element conductance matrices are identical to those obtained from the exact finite element, Eqs. (3.48b-c). Therefore, the conventional finite element with the optimum upwind weighting function provide exact nodal temperatures. However, since the upwind element temperature variation differs from the exact element temperature variation shown in Eq. (3.48a), the finite element with the optimum upwind weighting function does not provide the exact temperature variation within an element.

3.3 Exact Finite Elements in Thermal-Structural Problems

With the general exact finite element formulation described in section 3.1, exact structural finite elements can be developed for problems governed by ordinary differential equations. For example, exact finite elements for a rod loaded by its own weight

or a beam with a distributed load can be formulated. However, for the purpose of demonstrating benefits on exact finite elements in coupled thermal-structural problems, exact structural finite elements subjected to thermal loads are considered herein.

3.3.1 Truss

Typical thermal and structural models for truss elements are shown in Fig. 5. For a steady-state analysis, exact thermal finite elements for internal heat generation, surface convection and specified surface heating are presented in section 3.2. In this section the exact element temperatures are used in the development of truss elements for computations of displacements and thermal stresses.

For a truss element subjected to a temperature change, thermal strain is introduced in the stress-strain relation;

$$\sigma_x = E \left[\frac{du(x)}{dx} - \alpha \left(T(x) - T_{ref} \right) \right] \tag{3.50}$$

where σ_x is the axial stress, E is the modulus of elasticity, u is the axial displacement which varies with the axial coordinate x, α is the coefficient of thermal expansion, $T(x)$ is the temperature, and T_{ref} is the reference temperature for zero stress. The rod equilibrium equation with an assumption of negligible body force is

$$\frac{d\sigma_x}{dx} = 0 \tag{3.51}$$

which when combined with the stress-strain relation, Eq. (3.50), and
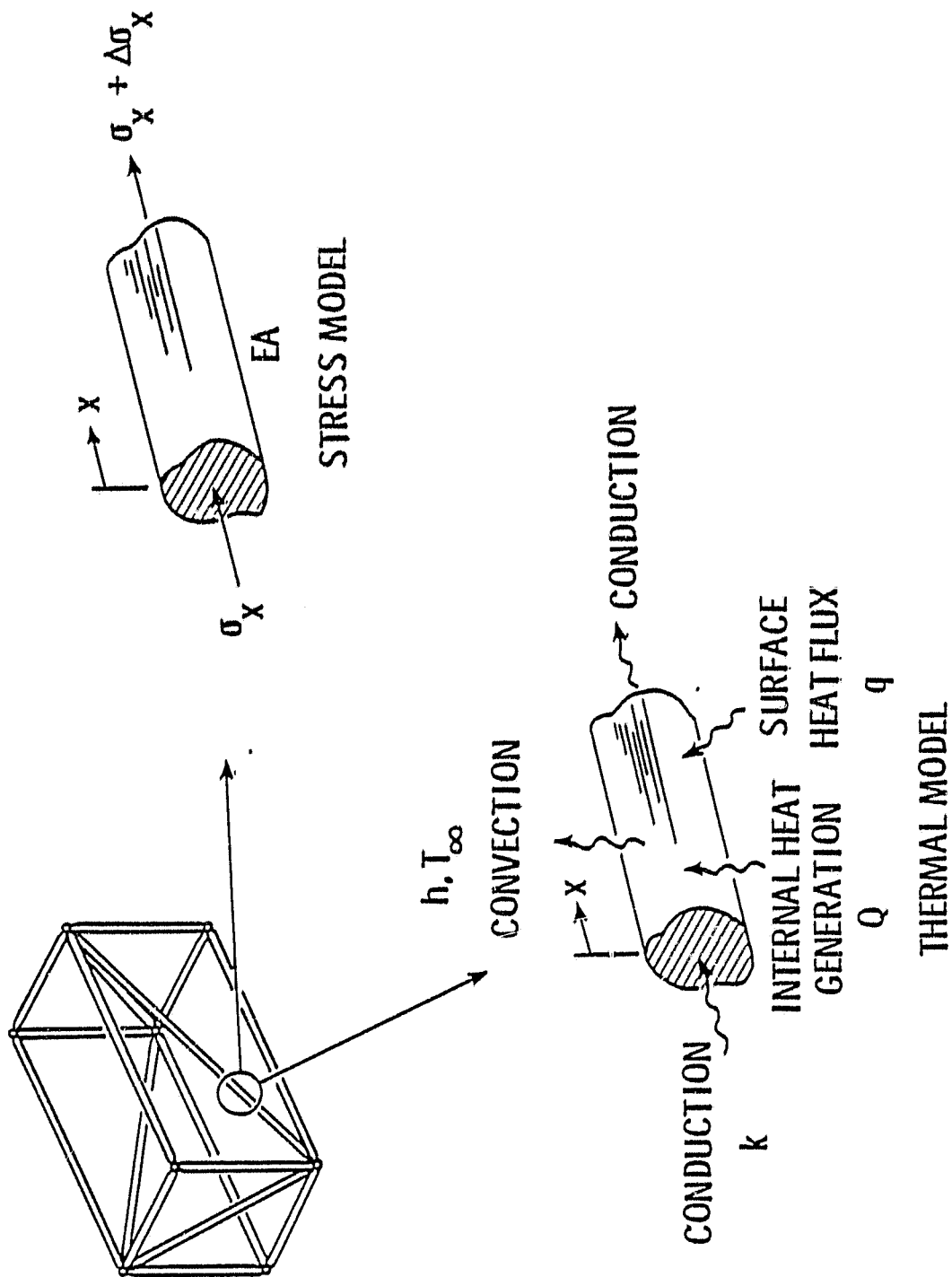
Fig. 5.   Thermal and stress models of rod element.

multiplied through by the truss cross-sectional area A, yields the governing differential equation,

$$EA \frac{d^2u}{dx^2} = \alpha EA \frac{dT}{dx} \qquad (3.52)$$

Since the temperature T is known from the thermal analysis, a general solution to the above differential equation can be obtained. An exact finite element can be formulated by applying the nodal displacements u_1 and u_2 as the boundary conditions at $x = 0$ and $x = L$, respectively. In this case, the exact element displacement variation is

$$u(x) = (\alpha \int_0^x T \, dx - \alpha \frac{x}{L} \int_0^L T \, dx) + (1 - \frac{x}{L}) u_1 + (\frac{x}{L}) u_2 \qquad (3.53)$$

or in the matrix form

$$u(x) = \lfloor N_0(x) \quad N_1(x) \quad N_2(x) \rfloor \begin{Bmatrix} u_0 \\ u_1 \\ u_2 \end{Bmatrix} = \lfloor N_s \rfloor \{u\} \qquad (3.54a)$$

where $N_0(x)$ is the element nodeless interpolation function; N_i, $i = 1, 2$ are typical element interpolation functions, u_0 is the nodeless parameter, and u_i, $i = 1, 2$ are the element nodal displacements. The element interpolation functions are

$$N_0(x) = \alpha \int_0^x T \, dx - \alpha \frac{x}{L} \int_0^L T \, dx \qquad (3.54b)$$

$$N_1(x) = 1 - \frac{x}{L} \qquad N_2(x) = \frac{x}{L} \qquad\qquad (3.54c)$$

where, for convenience, the nodeless parameter u_0 is taken as unity in this case. Note that the element nodeless interpolation function, $N_0(x)$, vanishes at nodes and depends on the integrals of element temperature variation obtained from the thermal analysis.

To derive exact element matrices, the method of weighted residuals is applied to the equilibrium equation (3.51). After performing an integration by parts and using the stress-strain relation, Eq. (3.50), element equations and element matrices are obtained. These element equations are in the same form as those obtained from the variational principle described in section 2.3 and can be expressed as

$$[K_s] \{u\} = \{F_T\} \qquad\qquad (3.55)$$

where $[K_s]$ is the structural element stiffness matrix, $\{u\}$ is the vector of nodal displacements, and $\{F_T\}$ is the equivalent nodal thermal load vector. The element matrices are defined by (see Eqs. (2.27a) and (2.27d))

$$[K_s] = AE \int_0^L \{\frac{dN_s}{dx}\} \lfloor\frac{dN_s}{dx}\rfloor \, dx \qquad\qquad (3.56a)$$

$$\{F_T\} = AE\alpha \int_0^L \{\frac{dN_s}{dx}\} \, (T - T_{ref}) \, dx \qquad\qquad (3.56b)$$

Using the exact displacement interpolation functions, Eq. (3.54a), the element stiffness matrix above is a three by three matrix which contains coefficients K_{ij}, $i,j = 0,1,2$. Since the governing differential equation, Eq. (3.52), can be cast in the self-adjoint form (see section 3.2), this element stiffness matrix is symmetric and K_{0i}, $i = 1,2$ are zero. Both the element stiffness matrix and the equivalent nodal thermal load vector can be evaluated in closed form as,

$$[K_s] = \frac{AE}{L} \begin{bmatrix} 1 & -1 \\ -1 & 1 \end{bmatrix} \tag{3.57a}$$

$$\{F_T\} = F_T \begin{Bmatrix} -1 \\ 1 \end{Bmatrix} \tag{3.57b}$$

where

$$F_T = AE\alpha \int_0^L (T - T_{ref})\, dx \tag{3.57c}$$

Once exact nodal displacements are determined, exact displacement variation within an element can be computed from Eq. (3.53). Exact element stress can also be obtained by substituting element displacement variation, Eq. (3.53), into the stress-strain relation, Eq. (3.50). In this case, the exact element stress in terms of nodal displacements is

$$\sigma_x = E \left[\frac{u_2 - u_1}{L} - \frac{\alpha}{L} \int_0^L (T - T_{ref}) \, dx \right] \qquad (3.58)$$

Using the exact element temperature variations obtained from the thermal analysis (cases 1a-1d), both element nodeless interpolation functions $N_0(x)$, Eq. (3.54b), and the equivalent nodal thermal load F_T, Eq. (3.57c), can be evaluated in closed form as shown in Table 3 and Appendix B, respectively.

3.3.2 Hollow Cylinder

For a hollow cylinder where the temperature T varies only in the radial direction (Fig. 6), the only non-zero displacement is $u(r)$ and all shearing stresses are zero. The radial stress σ_r and circumferential stress σ_θ satisfy the equilibrium equation [22]

$$\frac{d\sigma_r}{dr} + \frac{\sigma_r - \sigma_\theta}{r} = 0 \qquad (3.59)$$

The stress-strain relations are

$$\varepsilon_r = \frac{1}{E} \left[\sigma_r - \nu(\sigma_\theta + \sigma_z) \right] + \alpha(T - T_{ref}) \qquad (3.60a)$$

$$\varepsilon_\theta = \frac{1}{E} \left[\sigma_\theta - \nu(\sigma_r + \sigma_z) \right] + \alpha(T - T_{ref}) \qquad (3.60b)$$

$$\varepsilon_z = \frac{1}{E} \left[\sigma_z - \nu(\sigma_r + \sigma_\theta) \right] + \alpha(T - T_{ref}) \qquad (3.60c)$$

where ν is Poisson's ratio; ε_r, ε_θ and ε_z are the radial, circumferential and longitudinal strain, respectively.

Table 3

Truss Element Displacement Interpolation Functions, $N_s(X)$*

Case	$N_0(X)$
1(a)	$\dfrac{\alpha(T_2-T_1)L}{2}(X^2-X) + \dfrac{\alpha T_0 L}{6}(-X + 3X^2 - 2X^3)$
1(b)	$\alpha\{\dfrac{T_2-T_1\ \cosh mL + T_0(\cosh mL-1)}{m\ \sinh mL}[(\cosh mLX - 1)$ $- X(\cosh mL -1)] + \dfrac{T_1-T_0}{m}(\sinh mLX - X \sinh mL)\}$
1(c)	$\dfrac{\alpha(T_2-T_1)L}{2}(X^2-X) + \dfrac{\alpha T_0 L}{6}(-X + 3X^2 - 2X^3)$
1(d)	$\dfrac{\alpha(T_2-T_1)L}{2}(X^2-X) + \dfrac{\alpha T_0 L}{6}(-X + 3X^2 - 2X^3)$

*For all cases: $N_1(X) = 1-X$, $N_2(X) = X$ where $X = x/L$.
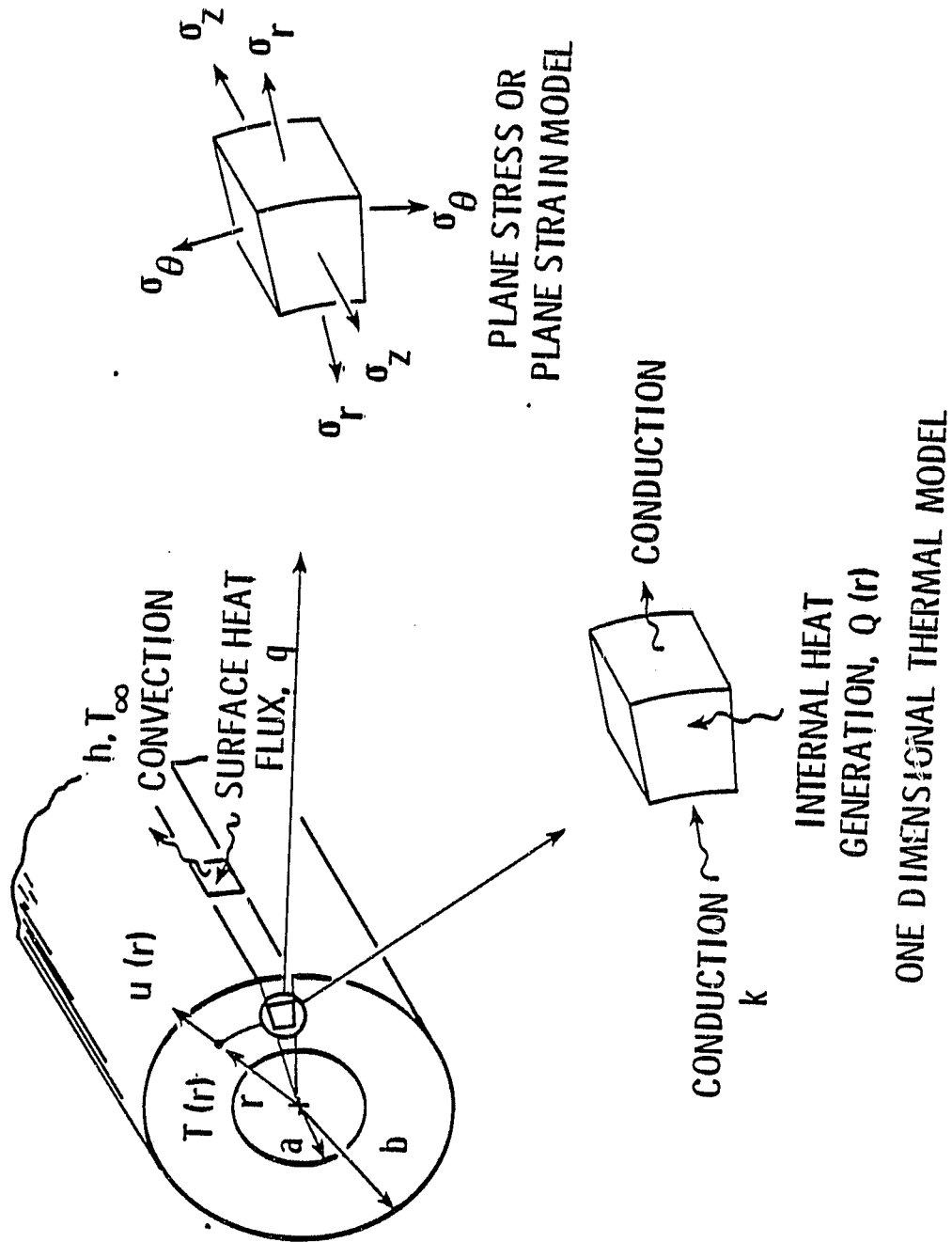
Fig. 6. Thermal and stress models of axisymmetric element.

For the case of a thin hollow cylinder, the assumption of plane stress ($\sigma_z = 0$) is used. Substituting the stress-strain relations, Eqs. (3.60a-b), into the equilibrium Eq. (3.59) and using the strain-displacement relations.

$$\varepsilon_r = \frac{du}{dr} \, , \quad \text{and} \quad \varepsilon_\theta = \frac{u}{r} \tag{3.61}$$

where u denotes the radial displacement, the governing differential equation for the case of plane stress is

$$\frac{d}{dr} \left[\frac{1}{r} \frac{d(ru)}{dr} \right] = (1 + \nu) \, \alpha \, \frac{dT}{dr} \tag{3.62}$$

A general solution to this differential equation is given by

$$u(r) = (1 + \nu) \, \frac{\alpha}{r} \int_0^r (T - T_{ref}) \, r \, dr + C_1 \, r + \frac{C_2}{r} \tag{3.63}$$

Since the radial temperature variation T is known from the thermal analysis (see section 3.2.2), the exact axisymmetric element displacement variation can be derived by applying the nodal displacements u_1 and u_2 as the boundary conditions at $r = a$ and $r = b$, respectively. The exact element displacement variation is

$$u(r) = (1 + \nu) \, \frac{\alpha}{r} \int_a^r (T - T_{ref}) \, r \, dr$$

$$- (1 + \nu) \, \frac{\alpha}{r} \, \frac{(r^2 - a^2)}{(b^2 - a^2)} \int_a^b (T - T_{ref}) \, r \, dr$$

$$+ \; [\; \frac{a}{r} \frac{(b^2 - r^2)}{(b^2 - a^2)}]\; u_1 \; + \; [\; \frac{b}{r} \frac{(r^2 - a^2)}{(b^2 - a^2)}]\; u_2 \qquad (3.64)$$

or in the matrix form

$$u(r) = \lfloor N_0(r) \quad N_1(r) \quad N_2(r) \rfloor \left\{ \begin{array}{c} u_0 \\ u_1 \\ u_2 \end{array} \right\} = \lfloor N_s \rfloor \{u\} \qquad (3.65a)$$

where $N_0(r)$ is the element nodeless interpolation function; N_i, i = 1,2, are typical element interpolation functions, u_0 is the nodeless parameter, and u_i, i = 1,2 are the element nodal displacements. The element interpolation functions are

$$N_0(r) = (1 + \nu) \frac{\alpha}{r} \int_a^r (T - T_{ref}) \; r \; dr$$

$$- (1 + \nu) \frac{\alpha}{r} \frac{(r^2 - a^2)}{(b^2 - a^2)} \int_a^b (T - T_{ref}) \; r \; dr \qquad (3.65b)$$

$$N_1(r) = [\frac{a}{r} \frac{(b^2 - r^2)}{(b^2 - a^2)}] \quad \text{and} \quad N_2(r) = [\frac{b}{r} \frac{(r^2 - a^2)}{(b^2 - a^2)}] \qquad (3.65c)$$

Like for the exact truss element, the nodeless parameter u_0 is taken as unity, and the element nodeless parameter $N_0(r)$ vanishes at nodes. Element matrices can be derived by following the same procedure described for the truss element. In this case, the element stiffness matrix and the equivalent nodal thermal load vector are

$$[K_S] = \int_a^b [B_S]^T [D] [B_S] \, r \, dr \tag{3.66a}$$

$$\{F_T\} = \int_a^b [B_S]^T [D] \{\alpha\} (T - T_{ref}) \, r \, dr \tag{3.66b}$$

where $[B_S]$ is the strain-displacement matrix obtained from Eq. (3.61),

$$\begin{Bmatrix} \varepsilon_r \\ \\ \varepsilon_\theta \end{Bmatrix} = \begin{Bmatrix} \dfrac{du}{dr} \\ \\ \dfrac{u}{r} \end{Bmatrix} = \begin{bmatrix} \dfrac{dN_1}{dr} & \dfrac{dN_2}{dr} \\ \\ \dfrac{N_1}{r} & \dfrac{N_2}{r} \end{bmatrix} \begin{Bmatrix} u_1 \\ \\ u_2 \end{Bmatrix} = [B_S] \{u\} \tag{3.67a}$$

$[D]$ is the elasticity matrix (plane stress),

$$[D] = \frac{E}{1 - \nu^2} \begin{bmatrix} 1 & \nu \\ \nu & 1 \end{bmatrix} \tag{3.67b}$$

and $\{\alpha\}$ is the vector of coefficients of thermal expansion,

$$\{\alpha\} = \alpha \begin{Bmatrix} 1 \\ 1 \end{Bmatrix} \tag{3.67c}$$

Using the exact element interpolation functions, Eq. (3.65), the element stiffness matrix and equivalent nodal load vectors corresponding to the heat transfer cases (see section 3.2.2) can be derived in closed form. Due to complexity of the element interpolation

functions, a computer-based symbolic manipulation language MACSYMA was used to perform the algebra and calculus required for these element matrix derivations. Results of these element matrices and exact element interpolation functions are shown in Appendix B and Table 4, respectively.

Once nodal displacements are computed, exact thermal stresses in both radial and circumferential directions can be determined. Using the stress-strain relations, Eq. (3.60), and the strain-displacement equations in the form of Eq. (3.67a), the element stresses can be written in terms of nodal displacements as

$$\begin{Bmatrix} \sigma_r \\ \sigma_\theta \end{Bmatrix} = [D] \left\{ [B_s] \{u\} - (1 + \nu)\, \alpha\, (T - T_{ref}) \begin{Bmatrix} 1 \\ 1 \end{Bmatrix} \right\} \tag{3.68}$$

For the plane strain case $(\varepsilon_z = 0)$, all equations formulated for the case of plane stress above may be used by replacing $E.(1-\nu^2)$ for E, $\nu/(1-\nu)$ for ν, and $(1+\nu)\alpha$ for α. In addition, the longitudinal stress exists in this case and can be computed from the last equation of the stress-strain relations, Eq. (3.60c),

$$\sigma_z = \nu(\sigma_r + \sigma_\theta) - \alpha E\,(T - T_{ref}) \tag{3.69}$$

3.4 Applications

To demonstrate the capabilities of the exact thermal and structural finite elements developed in sections 3.2 - 3.3, the finite element thermal analysis program TAP2 [23] and the finite structual

Table 4

Axisymmetric Element Displacement Interpolation Functions

$$N_0(r) = \frac{(1+\nu)}{2rw} \{(T_1 + \frac{a^2}{b^2} wT_0) \ [r^2 \ln(\frac{b}{r}) - \frac{(b^2-r^2)a^2 w}{(b^2-a^2)}]$$

$$+ (T_2 + wT_0) \ [r^2 \ln(\frac{r}{a}) - \frac{(r^2-a^2)b^2 w}{(b^2-a^2)}]$$

$$+ w^2 T_0 \ [\frac{(b^2-r^2)(r^2-a^2)}{2b^2}]\}$$

$$N_1(r) = \frac{a(b^2-r^2)}{r(b^2-a^2)}$$

$$N_2(r) = \frac{b(r^2-a^2)}{r(b^2-a^2)}$$

analysis program STAP [24] are used. Elements discussed in this
chapter were added to these programs. Conventional finite elements are
also available in these programs, so comparisons between exact finite
elements and conventional finite elements could be made.

3.4.1 Coffee Spoon Problem

The exact rod element for conduction and convection described
in section 3.2.1 is used for one-dimensional heat transfer in a
coffee spoon [25], Fig. 7. The lower-half of the spoon submerged in
coffee is convectively heated by the coffee at 339 K, and·the upper-
half is convectively cooled by the atmosphere at a temperature of
283 K. The ends of the one-dimensional spoon model are assumed to
have negligible heat transfer.

Three finite element models are used to represent the spoon:
(1) two exact finite elements, (2) two linear conventional finite
elements, and (3) ten linear conventional finite elements. Tempera-
ture variations computed by these three finite element models are
compared in Fig. 7. The figure shows that two conventional finite
elements predict nodal temperatures with fair accuracy but are unable
to provide details of the nonuniform temperature distribution includ-
ing the zero temperature gradients at both ends of the spoon. The
temperature variation obtained from ten conventional finite elements
is in excellent agreement with the result from two exact finite
elements. It should be noted, however, that an approximate solution
results from the use of conventional finite elements since the exact
solution to the problem is in terms of hyperbolic functions, which
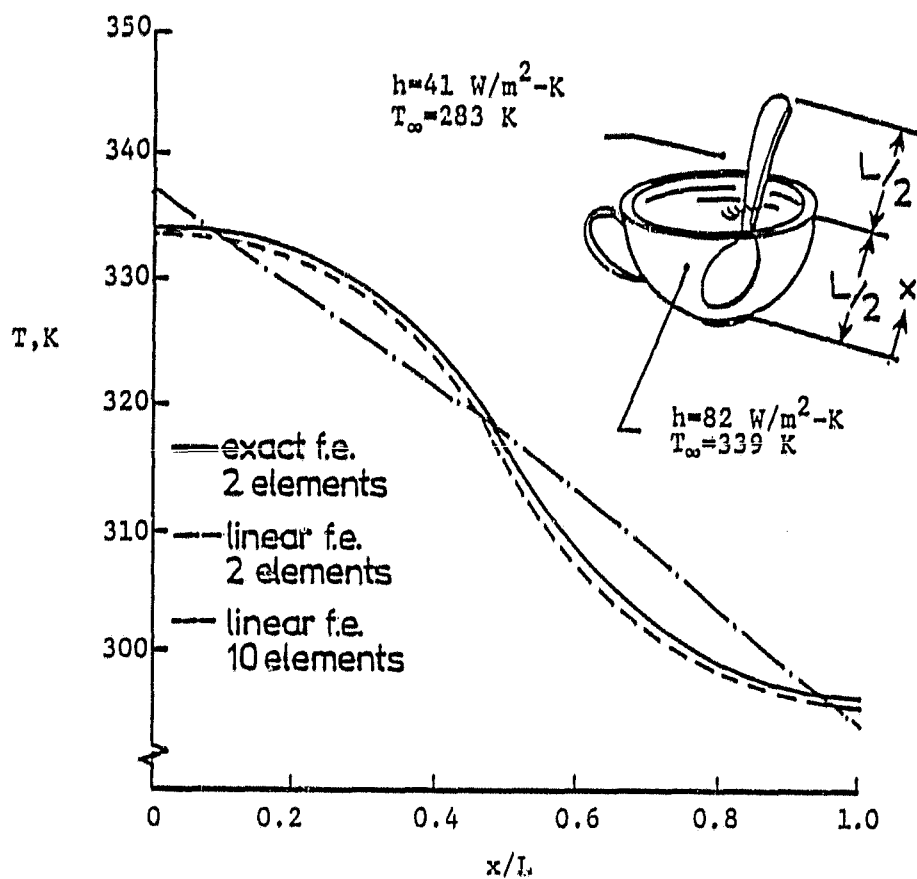were used in the exact element interpolation function (Appendix A,
Case 1b).

Fig. 7. Conventional and exact finite element solutions
for coffee spoon with conduction and convection.

3.4.2 Thermal Stresses in Hypersonic Wing

A 136 member truss model of a hypersonic wing [26], Fig. 8, was chosen to illustrate the use of exact truss finite elements. The wing is assumed to have varying convective heat along the leading edge, top and bottom surfaces and is convectively cooled internally. Temperatures along the wing root are specified. Two finite element thermal models are used to represent the wing truss. The first model consists of 136 exact condution-convection rod elements (see section 3.2.1) with one element per truss member. The second model is identical to the first model, but linear conventional finite elements are used. Fig. 9 shows a comparison of temperature distributions along the bottom members of the center rib of the wing truss. Results show that the exact finite element model provides a realistic temperature distribution which is characterized by higher temperatures near the center of each truss member and lower temperatures at the nodes. The conventional finite element model underestimates the actual temperatures and is not capable of capturing the highly nonlinear temperature distribution along the rib. Therefore, further mesh refinement of the conventional finite element model is needed if a realistic temperature distribution is to be predicted.

For the structural analysis, both models employ the same discretization as in the thermal analysis. The structural boundary conditions consist of constraining the nodes along the wind root. Truss member temperatures obtained from the exact finite element thermal model are directly transferred to the exact finite element structural model for computations of displacements and thermal stresses (see section 3.3.1). Likewise, displacements and thermal
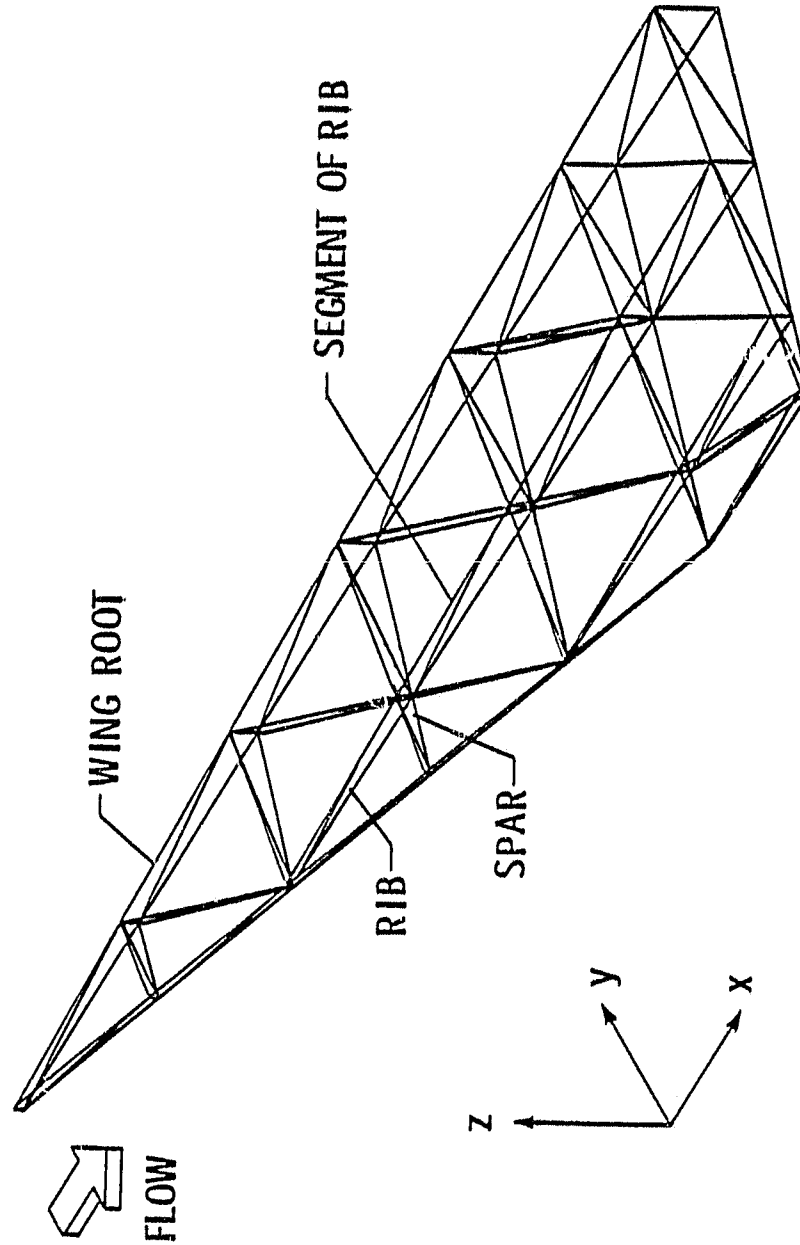
Fig. 8. Thermal structural truss model of a hypersonic wing.
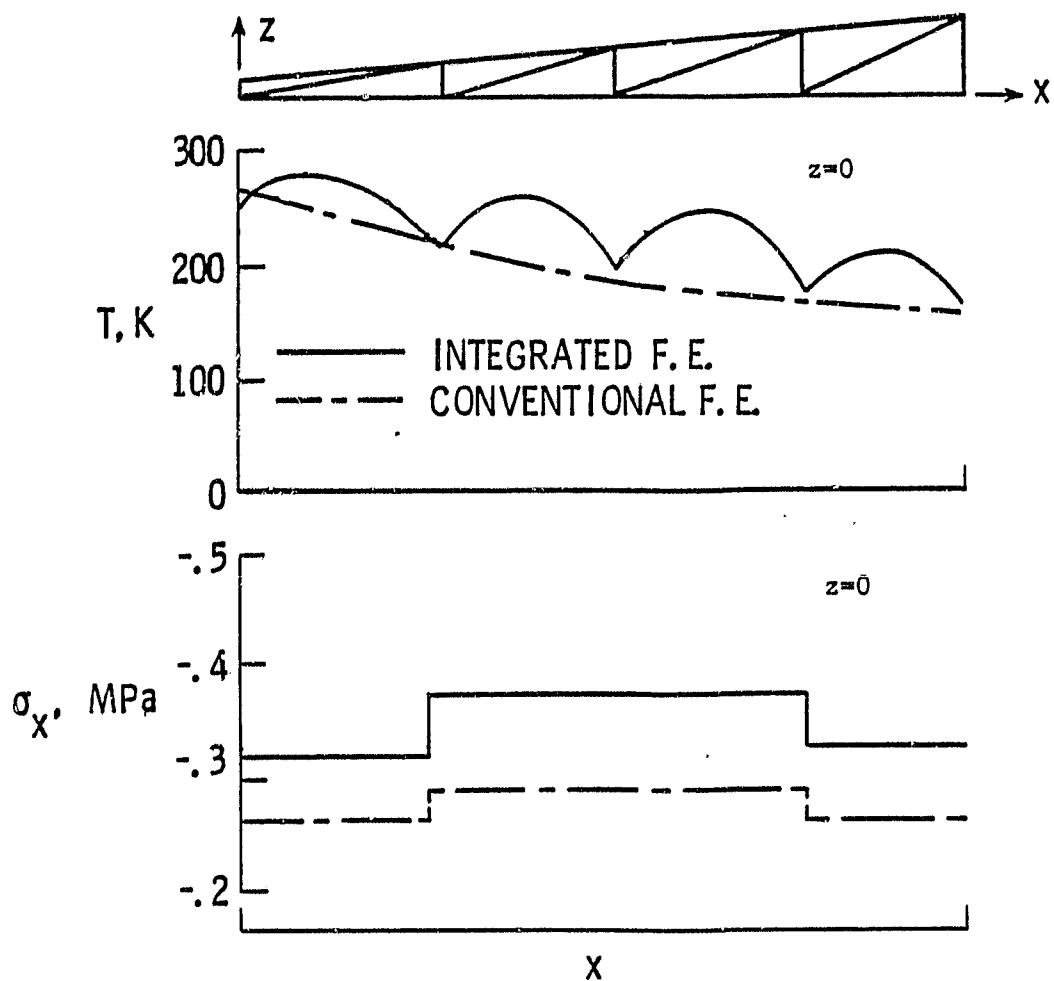
Fig. 9. Comparison of temperature and stress distributions
in wing truss, z=0.

stresses computed from the conventional finite element structural model are based upon linear member temperatures obtained from the conventional finite element thermal model. Comparison of the thermal stress distributions for the two analyses are made as shown in Fig. 9. The figure shows that conventional finite elements under-estimate member stresses with a relatively large error. This error is caused by the use of the inaccurate temperature distribution from the conventional finite element thermal model. Comparative temperature and stress distributions of other wing sections (not shown) have similar trends. The results clearly demonstrate that improved thermal-structural solutions can be obtained through the use of exact finite elements.

Chapter 4

MODIFICATION OF EXACT FINITE ELEMENT FORMULATION FOR
ONE-DIMENSIONAL LINEAR TRANSIENT PROBLEMS

In the preceding chapter, exact thermal finite elements for one-dimensional steady-state heat transfer problems were presented. Steady-state element temperature interpolation functions were formulated in closed form based upon solving ordinary differential equations. In transient analysis, exact element temperature interpolation functions cannot be obtained in closed form since general solutions to typical transient problems are infinite series. However, by modifying the steady-state element temperature interpolation functions for the transient analysis, improved transient temperature solutions can be obtained as described in this chapter.

In steady-state analysis, finite element temperature distributions are a function of only the spatial coordinate, but for transient analysis, the element temperature distribution are a function of both space and time. For example, a one-dimensional transient heat conduction is governed by the partial differential equation,

$$kA \frac{\partial^2 T}{\partial x^2} = \rho c A \frac{\partial T}{\partial t} \qquad (4.1)$$

where k is the material thermal conductivity, ρ is the density, c is the specific heat, A is the conduction area, and T is the

74

temperature which varies with the spatial coordinate x and time t. A two-node linear conventional finite element may be used in the analysis where the element temperature variation T is expressed in the form (Fig. 10(a))

$$T(x,t) = \lfloor 1 - \frac{x}{L} \quad \frac{x}{L} \rfloor \begin{Bmatrix} T_1(t) \\ T_2(t) \end{Bmatrix} = \lfloor N_1(x) \quad N_2(x) \rfloor \begin{Bmatrix} T_1(t) \\ T_2(t) \end{Bmatrix} \quad (4.2)$$

where $N_i(x)$, $i = 1,2$ are the element interpolation functions which are a function of the spatial coordinate x; L is the element length, and $T_i(t)$, $i = 1,2$ are the time-dependent nodal temperatures.

With the heat equation shown in Eq. (4.1), the corresponding element equations and element matrices can be derived as described in section 2.3. Typical element equations have the form

$$[C] \{\dot{T}\} + [K] \{T\} = \{Q\} \quad (4.3)$$

where $\{T\}$ and $\{\dot{T}\}$ denote vectors of nodal temperatures and the time rate of change of nodal temperatures, respectively. The matrix $[K]$ and the vector $\{Q\}$ represent the conductance matrix and the heat load vector, respectively, and have the same meaning as previously described for the steady-state analysis in the preceding chapter. The additional matrix $[C]$ is called the capacitance matrix and defined by (see Eq. (2.15a))

$$[C] = \int_0^L \rho c A \{N_T\} \lfloor N_T \rfloor \, dx \quad (4.4)$$

(a) Conventional F. E.

(b) Nodeless Parameter F. E.

(c) Nodeless Variable F. E.
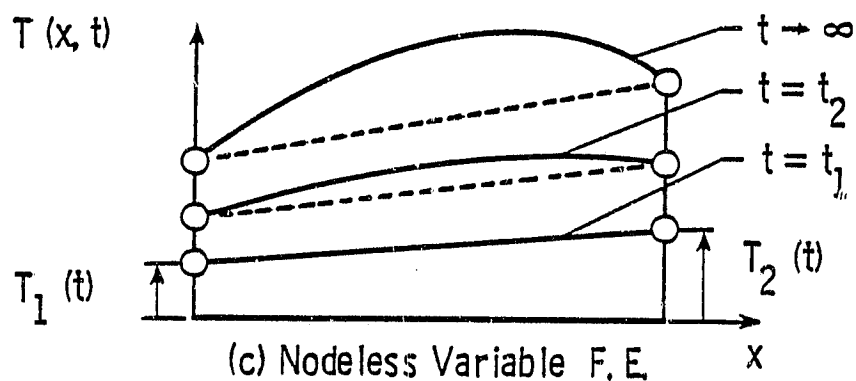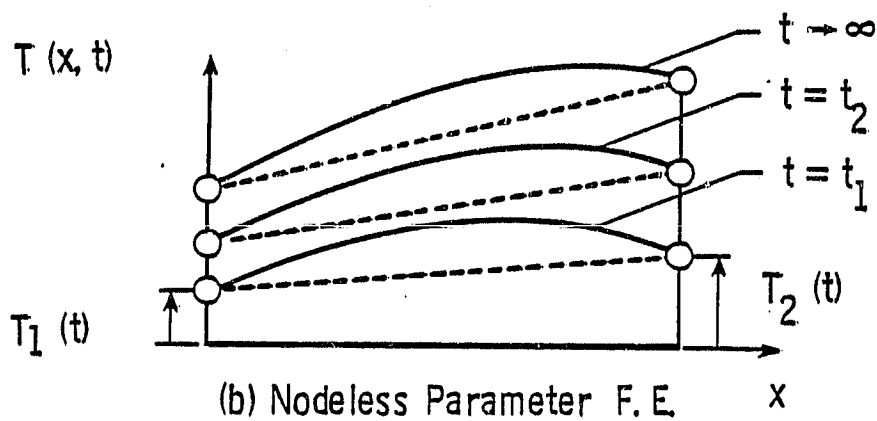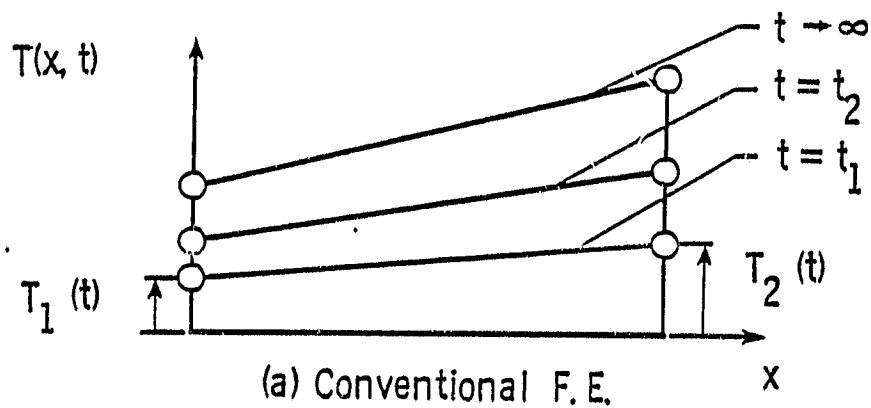
Fig. 10. One-dimensional element interpolation functions.

For the linear interpolation functions shown in Eq. (4.2), the capacitance matrix can be evaluated as

$$[C] = \frac{\rho c A L}{6} \begin{bmatrix} 2 & 1 \\ 1 & 2 \end{bmatrix} \tag{4.5}$$

This form of the capacitance matrix, Eq. (4.5), is called a consistent capacitance matrix because its definition is consistent with the matrix formulation, Eq. (4.4). Quite often, the above capacitance matrix is approximated by lumping the off-diagonal terms with the diagonal terms to give,

$$[C] = \frac{\rho c A L}{2} \begin{bmatrix} 1 & 0 \\ 0 & 1 \end{bmatrix} \tag{4.6}$$

and is called a lumped capacitance matrix. It should be noted that degradation of the solution accuracy may result from the use of the lumped capacitance matrix compared with the consistent capacitance matrix. However, computational advantages (e.g. explicit time integration algorithms) may be achieved using the lumped capacitance matrix whereas the loss of solution accuracy may be insignificant [5].

4.1 The Nodeless Variable

In the preceding chapter, exact finite elements for steady-state analysis are formulated based upon solving ordinary differential equations. Exact element temperature variations after imposing nodal temperatures as boundary conditions are written in the form,

$$T(x) = N_0(x) \, T_0 + N_1(x) \, T_1 + N_2(x) \, T_2 \qquad (4.7)$$

where N_i, $i = 1,2$ are element interpolation functions; T_i, $i = 1,2$ are unknown nodal temperatures, $N_0(x)$ is the element nodeless interpolation function, and T_0 is a known nodeless parameter.

For transient thermal problems, it is not possible to formulate exact element interpolation functions in closed form because general solutions to typical transient problems are infinite series. However, since the transient response may approach exact steady-state solutions as time becomes large, the use of the exact steady-state element temperature variation in the form of Eq. (4.7) may provide better accuracy of solutions than those obtained from the linear conventional element, Eq. (4.2).

To use the steady-state element temperature variation for transient analysis, Eq. (4.7) is written in the form,

$$T(x,t) = N_0(x) \, T_0 + N_1(x) \, T_1(t) + N_2(x) \, T_2(t) \qquad (4.8)$$

where the unknown nodal temperatures T_1 and T_2 become a function of time t. Since the nodeless parameter T_0 is known and independent of time, the product of the nodeless interpolation function and the nodeless parameter, $N_0(x) \, T_0$, retains the same shape throughout the transient response. Characteristics of the element temperature variation expressed by Eq. (4.8) during the response are illustrated in Fig. 10(b).

Equation (4.8) may not be a good representation for a transient thermal response as will be shown by the following argument. As described in section 3.1.1, the nodeless parameter T_0 is a scalar

quantity which contains a physical parameter associated with a given heat load. For example, the nodeless parameter for a slab subjected to a uniform internal heat generation rate Q_1 is given by (see Table 2)

$$T_0 = \frac{Q_1 L^2}{2k}$$

where k is the material thermal conductivity and L is the element length. If a slab is modeled by an exact finite element, the element temperature variation is given by (see Appendix A, Case 2)

$$T = \frac{x}{L}\left(1 - \frac{x}{L}\right)\frac{Q_1 L^2}{2k} + \left(1 - \frac{x}{L}\right)T_1 + \left(\frac{x}{L}\right)T_2$$

where T_1 and T_2 are the element nodal temperatures. If both surfaces of the slab have a specified temperature T_s in addition, the above equation becomes

$$T(x,t=0) = \frac{x}{L}\left(1 - \frac{x}{L}\right)\frac{Q_1 L^2}{2k} + \left(1 - \frac{x}{L}\right)T_s + \left(\frac{x}{L}\right)T_s \qquad (4.9)$$

For the case where the internal heat generation is raised instantaneously from Q_1 to Q_2, the transient temperature variation within the slab should gradually increase and reaches the new steady-state temperature variation

$$T(x,t\rightarrow\infty) = \frac{x}{L}\left(1 - \frac{x}{L}\right)\frac{Q_2 L^2}{2k} + \left(1 - \frac{x}{L}\right)T_s + \left(\frac{x}{L}\right)T_s \qquad (4.10)$$

where the new nodeless parameter is

$$T_0 = \frac{Q_2 L^2}{2k}$$

Since the nodal temperatures at both sides of the slab are fixed, the above two temperature variations, Eqs. (4.9 - 4.10), suggest that the nodeless parameter T_0 should vary with time so the element temperature can change gradually during the transient response. This argument leads to a modification of the element temperature variation employed in the steady-state analysis, Eq. (4.8), to the form

$$T(x,t) = N_0(x) \, T_0(t) + N_1(x) \, T_1(t) + N_2(x) \, T_2(t) \qquad (4.11)$$

where the nodeless parameter becomes an additional time-dependent element unknown and is called a nodeless variable. A typical element temperature variation with the nodeless variable $T_0(t)$ is illustrated in Fig. 10(c).

4.2 Element Equations and Matrices

In this section, element equations and matrices for both the nodeless parameter approach and nodeless variable approach are presented. In the nodeless parameter approach, the element temperature variation shown in Eq. (4.8) can be written in the matrix form

$$T(x,t) = \lfloor N_0(x) \quad N_1(x) \quad N_2(x) \rfloor \left\{ \begin{array}{c} T_0 \\ T_1(t) \\ T_2(t) \end{array} \right\} \qquad (4.12)$$

Using the definition of the element capacitance matrix shown in Eq. (4.4), the capacitance matrix for the given element interpolation functions can be derived. Element equations, Eq. (4.3), can then be written explicitly as

$$
\begin{bmatrix}
C_{00} & C_{01} & C_{02} \\
C_{01} & C_{11} & C_{12} \\
C_{02} & C_{12} & C_{22}
\end{bmatrix}
\begin{Bmatrix}
\partial T_0/\partial t \\
\partial T_1/\partial t \\
\partial T_2/\partial t
\end{Bmatrix}
+
\begin{bmatrix}
K_{00} & 0 & 0 \\
0 & K_{11} & K_{12} \\
0 & K_{12} & K_{22}
\end{bmatrix}
\begin{Bmatrix}
T_0 \\
T_1 \\
T_2
\end{Bmatrix}
=
\begin{Bmatrix}
Q_0 \\
Q_1 \\
Q_2
\end{Bmatrix}
\qquad (4.13)
$$

where C_{ij}, $i,j = 0,1,2$ are typical terms in the capacitance matrix; K_{ij} and Q_i, $i,j = 0,1,2$ are typical terms in the element stiffness matrix and the heat load vector previously described in the steady-state analysis. Since the nodeless parameter T_0 is constant, its time-derivative $\partial T_0/\partial t$ is zero. Therefore, the first equation which involves the nodeless parameter is uncoupled from the nodal unknowns in the second and third equations. Hence, the above equations reduce to

$$
\begin{bmatrix}
C_{11} & C_{12} \\
C_{12} & C_{22}
\end{bmatrix}
\begin{Bmatrix}
\dot{T}_1 \\
\dot{T}_2
\end{Bmatrix}
+
\begin{bmatrix}
K_{11} & K_{12} \\
K_{12} & K_{22}
\end{bmatrix}
\begin{Bmatrix}
T_1 \\
T_2
\end{Bmatrix}
=
\begin{Bmatrix}
Q_1 \\
Q_2
\end{Bmatrix}
\qquad (4.14)
$$

Note that these equations contain two basic element nodal unknowns as for the linear conventional finite element. Once the nodal temperatures at a typical time are computed, element temperature variation can be obtained using Eq. (4.12).

In the nodeless variable approach, the element temperature variation shown in Eq. (4.11) can be written in the matrix form

$$T(x,t) = \lfloor N_0(x) \quad N_1(x) \quad N_2(x) \rfloor \begin{Bmatrix} T_0(t) \\ T_1(t) \\ T_2(t) \end{Bmatrix} \qquad (4.15)$$

where $T_0(t)$ denotes the element nodeless variable which is a function of time as the unknown nodal temperatures $T_1(t)$ and $T_2(t)$. Since the element interpolation functions are identical to those used in the nodeless parameter approach, the element matrices are also identical. Element equations obtained using this approach have the form

$$\begin{bmatrix} C_{00} & C_{01} & C_{02} \\ C_{01} & C_{11} & C_{12} \\ C_{02} & C_{12} & C_{22} \end{bmatrix} \begin{Bmatrix} \dot{T}_0 \\ \dot{T}_1 \\ \dot{T}_2 \end{Bmatrix} + \begin{bmatrix} K_{00} & 0 & 0 \\ 0 & K_{11} & K_{12} \\ 0 & K_{12} & K_{22} \end{bmatrix} \begin{Bmatrix} T_0 \\ T_1 \\ T_2 \end{Bmatrix} = \begin{Bmatrix} Q_0 \\ Q_1 \\ Q_2 \end{Bmatrix} \qquad (4.16)$$

Because the nodeless variable is unknown, the equations are coupled through the capacitance matrix due to the presence of $\dot{T}_0$. Thus typical element equations obtained from the nodeless variable approach contain three unknowns, i.e. one more unknown than the nodeless parameter apporach or the linear conventional finite element.

An advantage of the nodeless parameter and nodeless variable approaches is that both can provide an exact steady-state solution at the initial condition for the transient response. As time becomes large and new steady-state thermal equilibrium is reached, the exact temperature distribution may be predicted by both approaches. It should be noted that with the use of the nodeless variable approach the temperature variation within the nodeless variable element can

vary with time even though the element nodal temperatures are fixed. This feature is characterized by the term $N_0(x) \, T_0(t)$ shown in Eq. (4.11) and is different from the linear conventional finite element where the element temperature distribution is completely controlled by nodal temperatures.

4.2.1 Rod Element

The rod element with heat conduction combined with surface convection, internal heat generation, or surface heating previously considered in Fig. 4, Cases la-d is extended for transient analysis. For each heat transfer case, the governing differential equation for the temperature distribution $T(x,t)$ can be derived using an energy balance on a small segment of the rod. These governing differential equations are:

$$\rho c A \, \frac{\partial T}{\partial t} - k A \, \frac{\partial^2 T}{\partial x^2} = 0 \tag{4.17a}$$

$$\rho c A \, \frac{\partial T}{\partial t} - k A \, \frac{\partial^2 T}{\partial x^2} + h p T = h p T_\infty \tag{4.17b}$$

$$\rho c A \, \frac{\partial T}{\partial t} - k A \, \frac{\partial^2 T}{\partial x^2} = Q A \tag{4.17c}$$

$$\rho c A \, \frac{\partial T}{\partial t} - k A \, \frac{\partial^2 T}{\partial x^2} = q p \tag{4.17d}$$

where A is the element cross-section area, h is the convection coefficient, p is the cross-section perimeter, T_∞ is the surrounding medium temperature, and q is the specified surface heating rate

per unit area. As one example, conduction with internal heat generation where the exact steady-state element temperature variation is (see Appendix A, Case 1(b))

$$T(x,t) = \frac{x}{L} \left(1 - \frac{x}{L}\right) T_0 + \left(1 - \frac{x}{L}\right) T_1 + \left(\frac{x}{L}\right) T_2$$

$$= \lfloor N_0(x) \quad N_1(x) \quad N_2(x) \rfloor \begin{Bmatrix} T_0 \\ T_1 \\ T_2 \end{Bmatrix} \qquad (4.18a)$$

where T_0 is the nodeless parameter given by (see Table 2)

$$T_0 = \frac{QL^2}{2k} \qquad (4.18b)$$

Using the exact element interpolation functions shown in Eq. (4.18a) above, the capacitance matrix is derived using Eq. (4.4). The conductance matrix and heat load vector are derived using Eqs. (2.15b) and (2.16b), respectively. Therefore, the element equations are

$$\rho c A L \begin{bmatrix} \frac{1}{30} & \frac{1}{12} & \frac{1}{12} \\ \frac{1}{12} & \frac{1}{3} & \frac{1}{6} \\ \frac{1}{12} & \frac{1}{6} & \frac{1}{3} \end{bmatrix} \begin{Bmatrix} \dot{T}_0 \\ \dot{T}_1 \\ \dot{T}_2 \end{Bmatrix} + \frac{kA}{L} \begin{bmatrix} \frac{1}{3} & 0 & 0 \\ 0 & 1 & -1 \\ 0 & -1 & 1 \end{bmatrix} \begin{Bmatrix} T_0 \\ T_1 \\ T_2 \end{Bmatrix} = QAL \begin{Bmatrix} \frac{1}{6} \\ \frac{1}{2} \\ \frac{1}{2} \end{Bmatrix} \qquad (4.19)$$

In the nodeless parameter approach, the nodeless parameter T_0 is constant and the above element equations reduce to

$$\rho cAL \begin{bmatrix} \frac{1}{3} & \frac{1}{6} \\[2ex] \frac{1}{6} & \frac{1}{3} \end{bmatrix} \begin{Bmatrix} \dot{T}_1 \\[2ex] \dot{T}_2 \end{Bmatrix} + \frac{kA}{L} \begin{bmatrix} 1 & -1 \\[1ex] -1 & 1 \end{bmatrix} \begin{Bmatrix} T_1 \\[2ex] T_2 \end{Bmatrix} = QAL \begin{Bmatrix} \frac{1}{2} \\[2ex] \frac{1}{2} \end{Bmatrix} \qquad (4.20)$$

with two unknown nodal temperatures $T_1(t)$ and $T_2(t)$. It should be noted that the element equations obtained from using the nodeless parameter approach shown in Eq. (4.20) above are identical to those obtained from the linear conventional finite element for this heat transfer case. Thus, results of nodal temperatures during the transient response are also identical. However, results of element temperatures are different due to the difference of their element interpolation functions, Eqs. (4.2) and (4.18b). As the transient response reaches the steady-state, the nodeless parameter approach provides exact solution for both nodal temperatures and element temperature variations where only exact nodal temperatures are obtained through the use of the linear conventional finite element.

In the nodeless variable apporach, the element equations with two unknowns of nodal temperatures and an unknown of nodeless variable shown in Eq. (4.19) must be solved simultaneously. It can be seen from these equations that as the steady-state thermal equilibrium is reached, the rate of change of nodal temperatures and the nodeless variable vanish. Then the first equation yields

$$T_0 = \frac{QL^2}{2k}$$

which is identical to the nodeless parameter shown in Eq. (4.18b). This means the nodeless variable varies during the transient response

and provides the value required for computation of the exact temperature variation when thermal equilibrium is reached.

For other heat transfer cases such as conduction with surface convection or surface heating, the same procedure is applied. Element matrices corresponding to each heat transfer case in the form of Eq. (4.16) are given in Appendix C. Capabilities of the nodeless parameter and the nodeless variable finite elements for transient analysis are evaluated by comparisons with an exact transient conduction-convection solution and the linear conventional finite element in the first example at the end of the chapter.

4.2.2 Axisymmetric Element

Similar to the rod element, the axisymmetric element previously described in the steady-state heat transfer (Fig. 4, Case 3) is extended for the transient analysis. Radial heat conduction is combined with internal heat generation and specified surface heating or surface convection on the inner or outer cylinder surfaces are considered through the boundary conditions. The governing differential equations for the cases of pure conduction and conduction combined with internal heat generation are

$$\rho c \, \frac{\partial T}{\partial t} - \frac{k}{r} \, \frac{\partial}{\partial r} \left(r \, \frac{\partial T}{\partial r} \right) = 0 \qquad (4.21\text{a})$$

$$\rho c \, \frac{\partial T}{\partial t} - \frac{k}{r} \, \frac{\partial}{\partial r} \left(r \, \frac{\partial T}{\partial r} \right) = Q \qquad (4.21\text{b})$$

respectively, where r denotes the radial coordinate.

Element equations can be derived by the method of weighted residuals applied to the governing differential equations.

C - 2

Typical element equations are in the form of equation (4.16). The element conductance matrix and heat load vector are identical to those obtained in the steady-state analysis shown in Eqs. (3.38b) and (3.38c), respectively. The element capacitance matrix associated with the rate of change of nodal temperatures has the form

$$[C] = \int_a^b \rho c \, \{N_T\} \lfloor N_T \rfloor \, r \, dr \qquad (4.22)$$

For the element interpolation functions associated with the heat transfer cases shown in Appendix A, the corresponding capacitance matrix can be evaluated in closed form. Capacitance matrices in the form of Eq. (4.16) are given in Appendix C.

4.3 Applications

4.3.1 Transient Heat Conduction in a Rod with Surface Convection

A rod with length L subjected to surface convection and specified end temperatures is shown in Fig. 11(a). Initially the rod is convectively cooled by a surrounding temperature at 255 K and, at time t = 0⁺, the surrounding temperature is raised instantaneously to 589 K. Transient temperature distributions along the rod are computed using: (1) the exact solution [27], (2) two linear conventional finite elements, (3) two nodeless parameter finite elements, and (4) two nodeless variable finite elements. In each finite element model, the element lengths are taken to be equal (L/2) with an unknown of nodal temperature at the center of the rod. Comparisons of the temperature variations obtained from these three
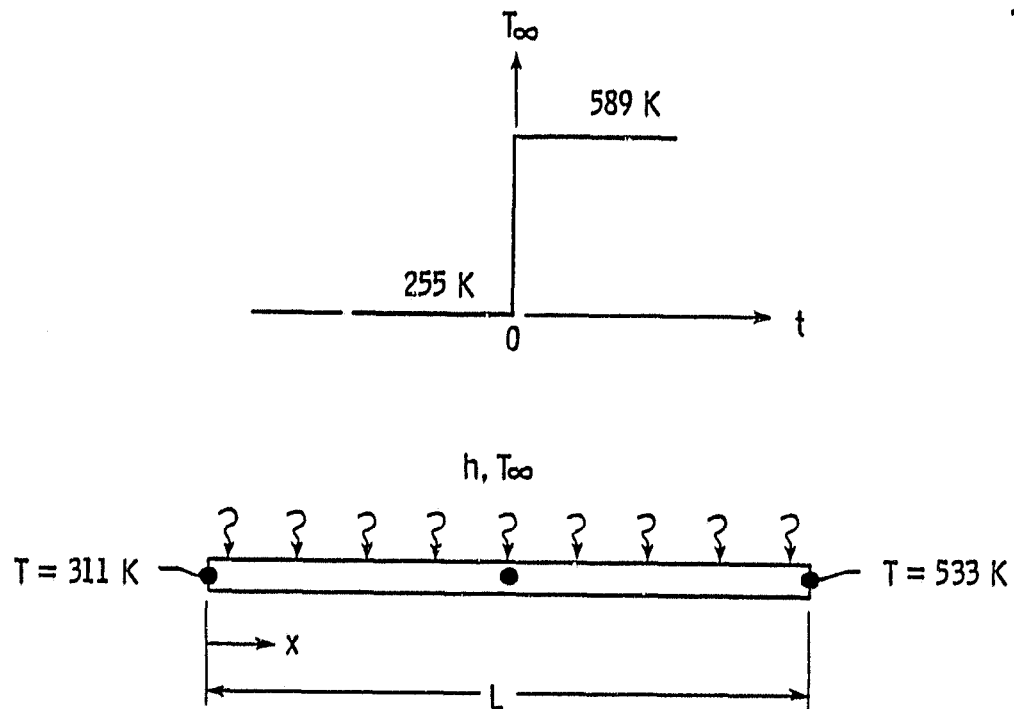
(a) Rod heated by surface convection.

Fig. 11. Conventional and nodeless variable finite element solutions for a rod with surface convection.

finite element models and the exact solution for t = 0, 0.01 and 0.3 s. are made as shown in Fig. 11(b-d).

At time t = 0 while the rod is in thermal equilibrium, two nodeless variable finite elements provide the exact steady-state temperature distribution. Two conventional finite elements are unable to provide details of the nonuniform temperature distribution due to the assumption of linear temperature distribution within the element. At time t = 0.01 s. (Fig. 11(c)) after the rod has been convectively heated, the differences in the transient response predicted by three finite element models are shown clearly. Two linear conventional finite elements predict the unknown nodal temperature at the center of the rod with fair accuracy but the element temperature distributions are overestimated from the actual temperature distribution with a relatively high error. Two nodeless parameter finite elements yield the unknown nodal temperature with the same accuracy as of two linear conventional finite elements but predict extremely poor element temperature distributions. Two nodeless variable finite elements provide the best approximation of the unknown nodal temperature with excellent temperature distributions within the elements. As the rod temperatures approach a new steady-state solution at time t = 0.3 s. (Fig. 11(d)), two linear conventional finite elements yield a fair approximation of the unknown nodal temperature but crudely approximate the temperature distribution. Both the nodeless parameter finite elements and the nodeless variable finite elements provide excellent prediction of the unknown nodal temperature and details of the nonuniform temperature distribution.
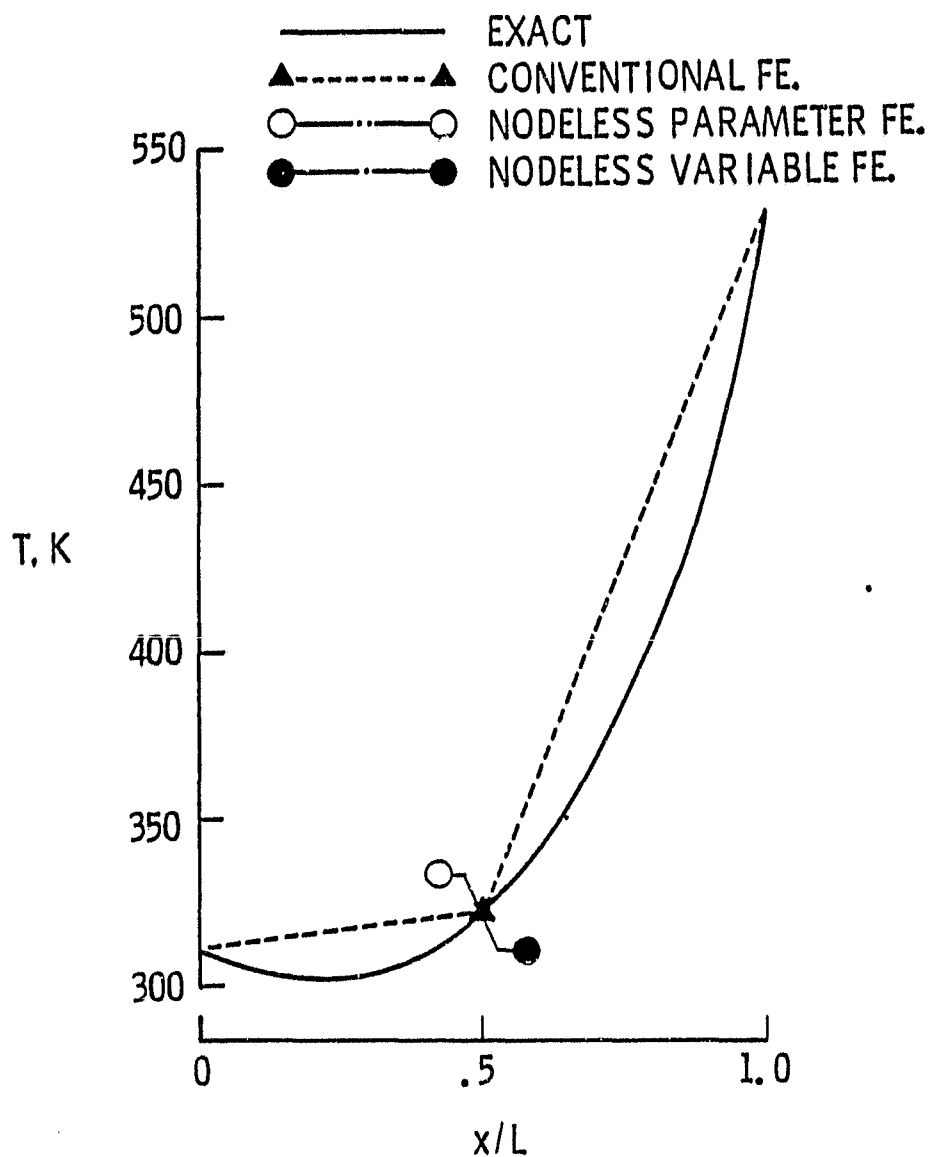
(b) Comparative temperature distributions at t = 0 s.

Fig. 11. Conventional and nodeless variable finite element
solutions for a rod with surface convection.
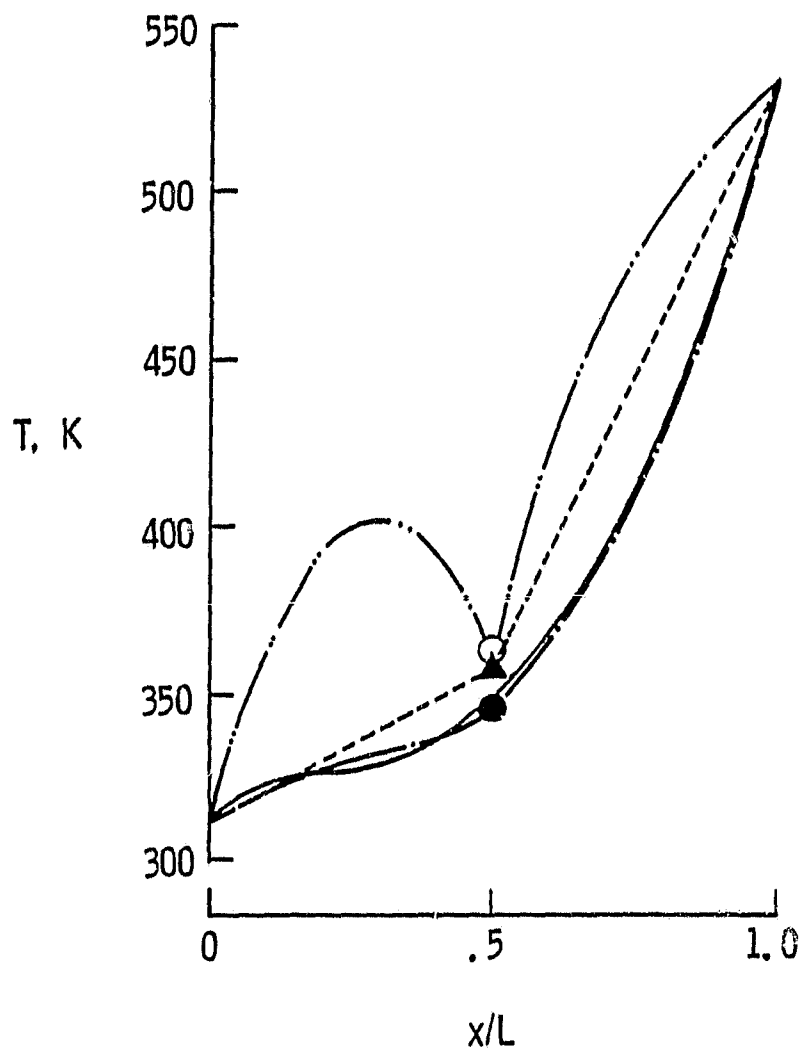
(c) Comparative temperature distributions at t = .01 s.

Fig. 11. Conventional and nodeless variable finite element
solutions for a rod with surface convection.

(d) Comparative temperature distributions at t = .30 s.

Fig. 11. Conventional and nodeless variable finite element
solutions for a rod with surface convection.
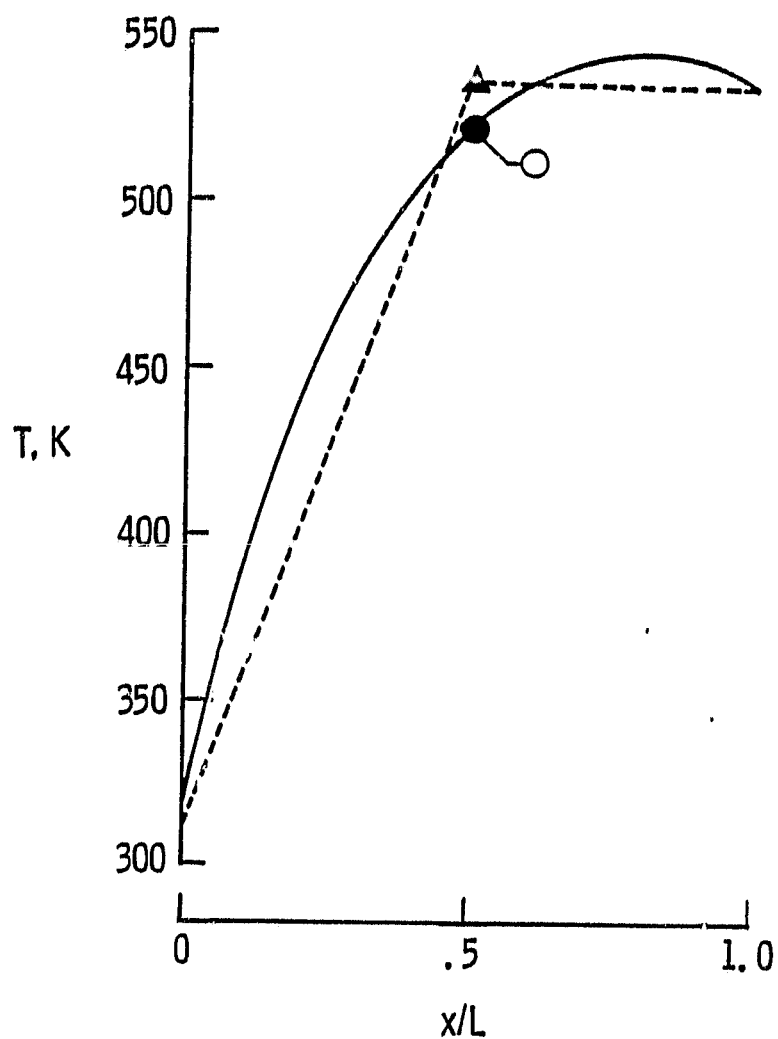
Even though the nodeless parameter approach employed in this problem yields excellent representation of the temperature distributions at the beginning (t = 0 s.) and near the end (t = 3.0 s.) of the response, the approach is unable to provide reasonable element temperature distributions during the response. As shown in Fig. 11(c) at time t = 0.01 s., temperatures obtained from the nodeless parameter finite elements are characterized by bumps within the elements. These unacceptable results are caused by using the steady-state element temperature distribution with the constant nodeless parameter for the transient analysis. Therefore, the nodeless parameter approach should not be employed for transient response predictions. Instead, the nodeless variable approach should be used since it gives accuracy superior to the linear conventional finite element throughout the response and predicts exact steady-state solutions.

4.3.2 Transient Thermal Stresses in a Rod with Internal Heat Generation

To further illustrate the use of the nodeless variable approach for one-dimensional transient problems and demonstrate additional benefits that can be achieved, an analysis of transient thermal stresses in a rod with internal heat generation is presented.

A rod with constant cross-sectional area A and length L encased between fixed walls is shown in Fig. 12(a). Both ends of the rod have the specified temperatures at 311 K and 533 K at x = 0 and x = L, respectively. Initially, the rod is subjected to a uniform internal heat generation rate Q = 358 kW/m³ and is in the thermal equilibrium. At time t = 0⁺, the internal heat
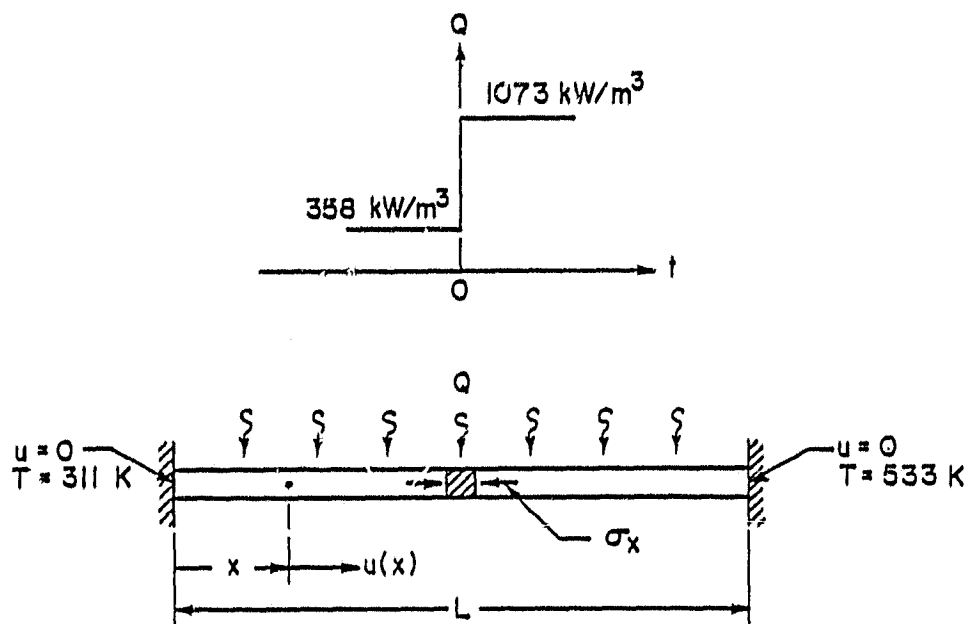
(a) ROD WITH INTERNAL HEAT GENERATION

Fig. 12. Conventional and nodeless variable finite element solutions for a fixed end rod with internal heat generation.

generation rate increases abruptly to 1073 kW/m^3 and remains constant thereafter. The rod is modeled using: (1) 20 linear conventional finite elements, (2) two linear conventional finite elements, and (3) two nodeless variable finite elements. Comparative temperature distributions at time t = 0, 0.1 and 1.0 hr. are shown in Fig. 12(b). The figure shows that two nodeless variable finite elements have the same capability in predicting transient temperatures as 20 linear conventional finite elements. Two linear conventional finite elements underestimate the temperature distributions with relatively large error throughout the transient response.

In the structural analysis, three structural finite element models with the same discretizations as for the thermal finite element models are employed. Element temperatures obtained from the thermal finite element model are transferred directly to the structural finite element model for computation of displacements and stresses. For the quasi-static analysis, the structural response are computed at times corresponding to the transient thermal solutions obtained previously. At each time, the equivalent nodal thermal forces are computed using Eq. (3.57) and the element nodal displacements are computed from Eq. (3.55). Once the element nodal displacements are obtained, element displacement distributions and element thermal stresses are computed from Eqs. (3.53) and (3.58), respectively.

Displacement distributions obtained from the three structural finite element models are shown in Fig. 12(c). The figure shows that two linear conventional finite elements are inadequate to represent the details of nonuniform displacement distributions.

——— CONVENTIONAL F.E., 20 ELEMENTS
▲—·—▲ CONVENTIONAL F.E., 2 ELEMENTS
O—––O NODELESS VARIABLE F.E., 2 ELEMENTS

$t = 0$ HR

$t = 0.1$ HR

$t = 1.0$ HR

(b) COMPARATIVE TEMPERATURE DISTRIBUTIONS

Fig. 12. Conventional and nodeless variable finite
element solutions for a fixed end rod with
internal heat generation.
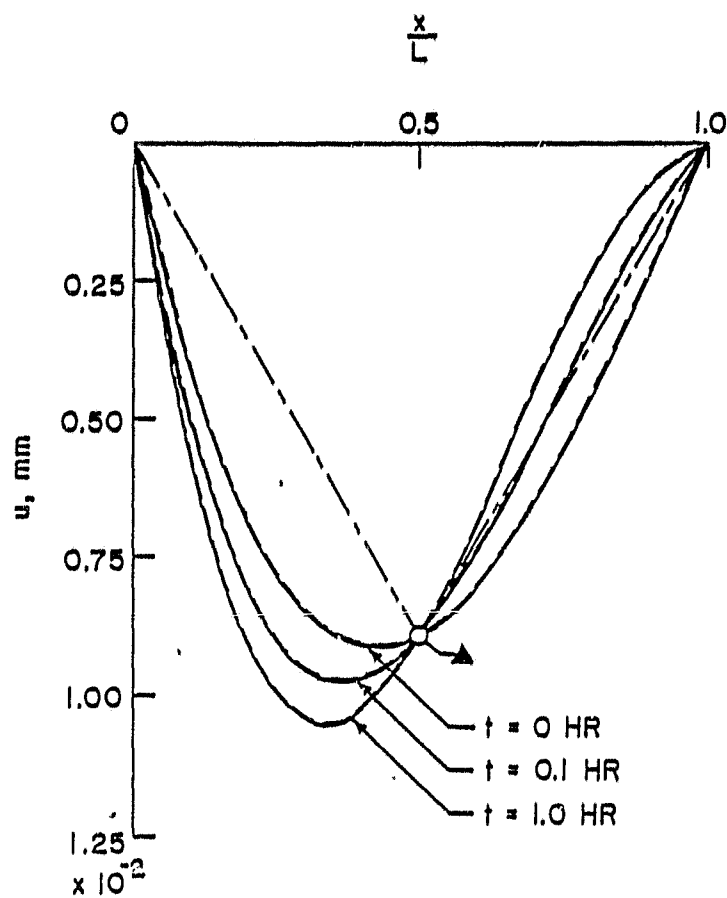
(c) COMPARATIVE DISPLACEMENT DISTRIBUTIONS
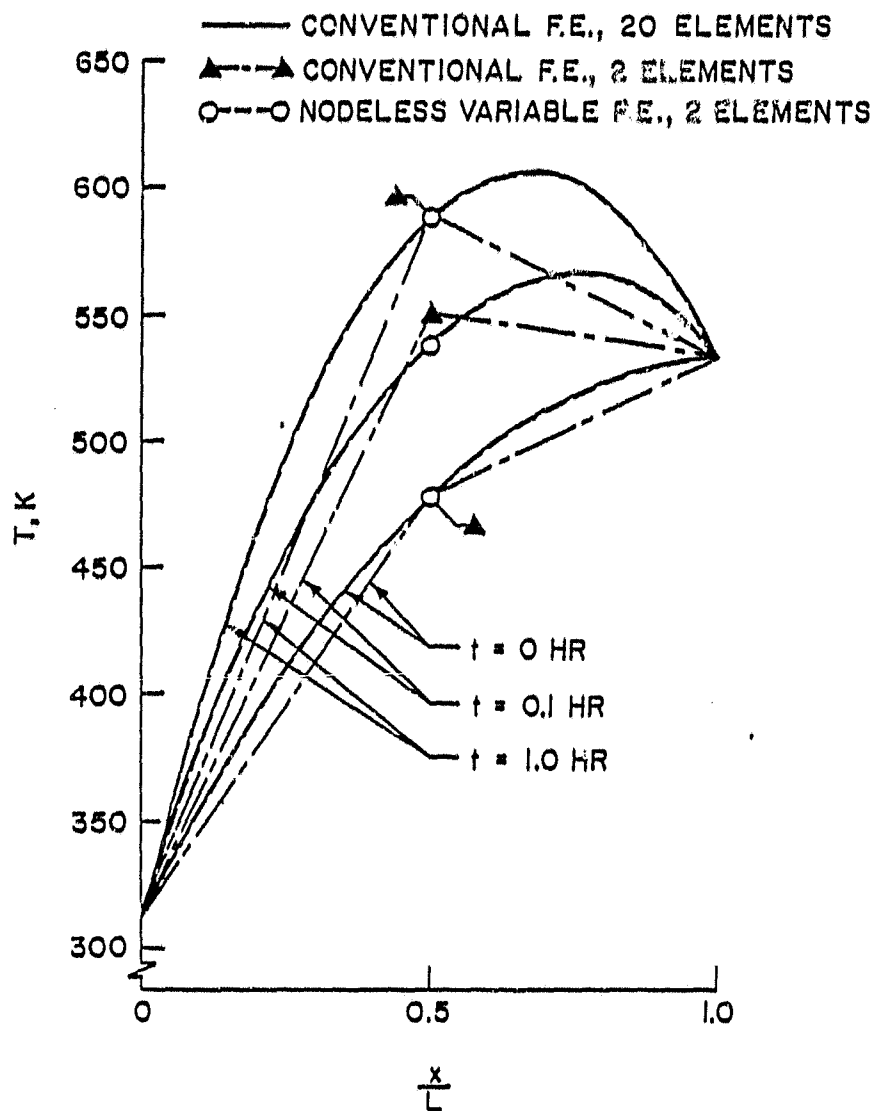
Fig. 12. Conventional and nodeless variable finite
element solutions for a fixed end rod with
internal heat generation.

Similar to the thermal analysis, displacement distributions obtained from two nodeless variable finite elements and 20 linear conventional finite elements are in excellent agreement throughout the transient response. Comparative thermal stresses obtained from these finite element models at the times mentioned above are given in Table 5. Thermal stresses computed from two nodeless variable finite elements and 20 linear conventional finite elements are equal since temperature variations of these two finite element models coincided. Two linear conventional finite elements underestimate the thermal stresses and the error increases with time with a maximum of 10% at $t = 1.0$ hr.

These two examples clearly demonstrate benefits of using the nodeless variable approach in one-dimensional transient thermal-structural problems. Further applications of the nodeless variable approach can be found in Ref. [28]. The use of the nodeless variable for improving temperature solutions in the transient thermal analysis directly improves accuracy of displacement and stress distributions in the structural analysis. The advantages of the nodeless variable approach for linear transient thermal-structural problems have been demonstrated in this chapter. The approach will be extended to nonlinear steady-state and transient thermal-structural analysis which includes radiation heat transfer in the next chapter.

Table 5

Comparative Thermal Stresses for a Rod with
Internal Heat Generation

		Stress, MPa	
Time, t Hr.	2 Conventional Elements	20 Conv. Elements 2 Nodeless Variable Elements	% Diff.
0	−507	−531	4.5%
0.1	−598	−640	6.5%
1.0	−652	−724	10.0%

Chapter 5

ONE-DIMENSIONAL THERMAL-STRUCTURAL FINITE ELEMENT ANALYSIS
WITH RADIATION HEAT TRANSFER

Due to their relatively low weight, high stiffness and ease of fabrication, trusses have high potential for use in space structures for solar collectors, antenna and space stations. Thermal analysis of these structures includes conduction heat transfer combined with significant radiation heat transfer. Radiation heat transfer introduces a strong nonlinearity in the energy equation being solved. Furthermore, a time dependent solution procedure is required for the analysis due to the changing orientation of the structure during the orbit.

In this chapter, finite element solution procedures for one-dimensional transient thermal analysis with radiation heat transfer are presented. Three finite element types are formulated: (1) an isothermal element, (2) a linear conventional element, and (3) a nodeless variable element. Accuracy and efficiency of the finite elements are evaluated using two thermal-structural examples at the end of the chapter.

5.1. Solution Procedures for One-dimensional Transient Thermal Analysis with Radiation Heat Transfer

In this section, transient thermal analysis for a one-dimensional finite element with radiation heat transfer is presented.

100

The radiation surface is assumed to be diffuse, gray and opaque which means the emitted radiation energy is uniformly distributed, independent of wave length and the material does not transmit radiation. For convenience all material thermal properties are assumed constant.

For one-dimensional transient heat conduction in a rod with surface radiation, the governing differential equation for the temperature distribution $T(x,t)$ can be derived using an energy balance on a small segment. With the assumptions mentioned above, the governing differential equation is

$$\rho c A \frac{\partial T}{\partial t} - kA \frac{\partial^2 T}{\partial x^2} + \epsilon \sigma p_s T^4 = a p_q \dot{q}_r \qquad (5.1)$$

where ρ is the density, c is the specific heat, A is the rod cross-sectional area, k is the material thermal conductivity, σ is the Stefan-Boltzmann constant, ϵ is the surface emissivity, a is the surface absorptivity, q_r is the incident surface heating rate from distance directional sources per unit area, p_s and p_q are the cross-sectional perimeters for surface emitted energy and incident energy, respectively.

Finite element equations corresponding to the governing differential equation (5.1) can be derived using the method of weighted residuals as described in section 2.3. For this case, typical element equations have the form

$$[C] \{\dot{T}\} + [[K_c] + [K_r]] \{T\} = \{Q_c\} + \{Q_r\} \qquad (5.2)$$

where $[C]$ is the element capacitance matrix; $[K_c]$ and $[K_r]$ are

the element conductance matrices corresponding to conduction and radiation, respectively, $\{Q_c\}$ is the element vector of conduction heat flux across element boundary, and $\{Q_r\}$ is the element heat load vector due to incident radiation. These matrices are expressed in the form of integrals over the element length L as follows:

$$[C] = \int_0^L \rho c A \{N_T\} \lfloor N_T \rfloor \, dx \tag{5.3a}$$

$$[K_c] = \int_0^L kA \{\frac{dN_T}{dx}\} \lfloor \frac{dN_T}{dx} \rfloor \, dx \tag{5.3b}$$

$$[K_r] \{T\} = \int_0^L \varepsilon \sigma P_s T^4 \{N_T\} \, dx \tag{5.3c}$$

$$\{Q_c\} = \left\{ \left[-kA \frac{dT}{dx} N_T \right]_0^L \right\} \tag{5.4a}$$

$$\{Q_r\} = \int_0^L a P_q q_r \{N_T\} \, dx \tag{5.4b}$$

where $\lfloor N_T \rfloor$ denotes the element temperature interpolation functions.

As shown in equation (5.3c), the conductance radiation matrix contains the element temperature within the integral. The element equations, Eq. (5.2), thus constitute a nonlinear set of equations. Since the time rate of change of the temperature vector $\{\dot{T}\}$ also

appears in the element equations, a transient nonli. _ar solution procedure is required for the analysis.

Typical techniques for transient nonlinear solutions combine a linear transient solution method and a steady-state nonlinear solution method. The solution technique here uses a time-marching scheme where temperatures are computed at the middle of the time step, the Crank-Nicolson algorithm. At each time step, Newton-Raphson iteration is used to correct for nonlinearities. Further details of these methods including other solution algorithms can be found in the finite element text, Ref. [15].

Starting from the element equations, Eq. (5.2), the time-marching scheme is first applied by approximating the time rate of change of nodal temperatures as

$$\{\dot{T}\} = \frac{1}{\Delta t} (\{T\}_{n+1} - \{T\}_n) \tag{5.5}$$

where Δt is the time interval between the time step n and $n+1$ such that $t_{n+1} = t_n + \Delta t$; $\{T\}_n$ and $\{T\}_{n+1}$ are the vectors of nodal temperatures at the time step n and $n+1$, respectively. Since the Crank-Nicolson algorithm computes temperature solutions at the middle of time steps, nodal temperatures at the middle of the step are approximated by

$$\{T\} = \frac{1}{2} (\{T\}_n + \{T\}_{n+1}) \tag{5.6}$$

where $\{T\}$ denotes the vector of nodal temperatures at the middle of the step. From this equation, the vector of nodal temperatures at the step $n+1$ is

$$\{T\}_{n+1} = 2\{T\} - \{T\}_n \qquad (5.7)$$

By combining Eqs. (5.5) and (5.7), the time rate of change of the nodal temperature vector shown in Eq. (5.5) can be expressed in terms of nodal temperatures at the middle of the step and step n as

$$\{\dot{T}\} = \frac{2}{\Delta t} (\{T\} - \{T\}_n) \qquad (5.8)$$

Substituting Eq. (5.8) into Eq. (5.2), the element equations become,

$$[\frac{2}{\Delta t} [C] + [K_c] + [K_r]] \{T\} = \{Q_c\} + \{Q_r\} + \frac{2}{\Delta t} [C] \{T\}_n \qquad (5.9)$$

In Eq. (5.9), the vector of nodal temperatures $\{T\}_n$ that appears on the right-hand side is known from the previous step. Since the unknown nodal temperatures contained in the vector $\{T\}$ are computed at the middle of time step, the heat load vectors must be evaluated at the same time. Once the unknown nodal temperature vector $\{T\}$ is obtained, the nodal temperature vector $\{T\}_{n+1}$ at the step n+1 can be computed from Eq. (5.7).

The element equations obtained by applying the Crank-Nicolson algorithm shown in Eq. (5.9) are in the form of nonlinear algebraic equations

$$[K(T)] \{T\} = \{Q\} \qquad (5.10)$$

where

$$[K(T)] \{T\} = [\frac{2}{\Delta t} [C] + [K_c] + [K_r]] \{T\} \qquad (5.11a)$$

and

$$\{Q\} = \{Q_c\} + \{Q_r\} + \frac{2}{\Delta t} [C] \{T\}_n \qquad (5.11b)$$

For any temperature vector $\{T\}$ that is not an exact solution to equations shown in Eq. (5.10) above, an unbalanced nodal heat loads exist which can be written in the form of a vector $\{\psi\}$ as

$$\{\psi\} = [K(T)] \{T\} - \{Q\} \qquad (5.12a)$$

or in tensor notations,

$$\psi_i = \sum_{j=1}^{r} K_{ij} T_j - Q_i \qquad (5.12b)$$

To develop the Newton-Raphson method a Taylor series expansion with the first order-derivative accuracy is written as

$$\psi_i(\{T\}^m) + (\frac{\partial \psi_i}{\partial T_j})^m \Delta T_j = 0 \qquad (5.13)$$

A set of algebraic equations is obtained in the form

$$[J]^m \{\Delta T\}^{m+1} = \{R\}^m \qquad (5.14)$$

where the superscript m denotes the mth iteration. The matrices $[J]^m$ and $\{R\}^m$ are the Jacobian matrix and the residual load vector, respectively, defined by

$$J_{ij} = \frac{\partial \psi_i}{\partial T_j} \qquad (5.15a)$$

$$R_i = - \psi_i \qquad (5.15b)$$

At each iteration, the vector of nodal temperature increments $\{\Delta T\}^{m+1}$ is computed using Eq. (5.14) and a new temperature vector is obtained from

$$\{T\}^{m+1} = \{T\}^m + \{\Delta T\}^{m+1} \qquad (5.16)$$

The iteration process is terminated when a convergence criteria (such as the maximum nodal temperature increment is less than a specified value) is met. For steady-state analysis, the equations shown in Eq. (5.2) do not contain the time rate of change of nodal temperatures, and only the Newton-Raphson iteration is required.

5.2 Element Formulations

In this section, three one-dimensional finite elements with surface radiation are formulated. Crank-Nicolson and Newton-Raphson methods described in the preceding section are employed for the transient and nonlinear solutions, respectively.

5.2.1 Isothermal Element

The isothermal element is a simple finite element suitable for problems with negligible conduction heat transfer. A uniform temperature variation is assumed along the element that varies only with time (Fig. 13(a)). This element is different from the finite elements mentioned in the previous chapters since element temperature is the only unknown for the isothermal element. Since the element
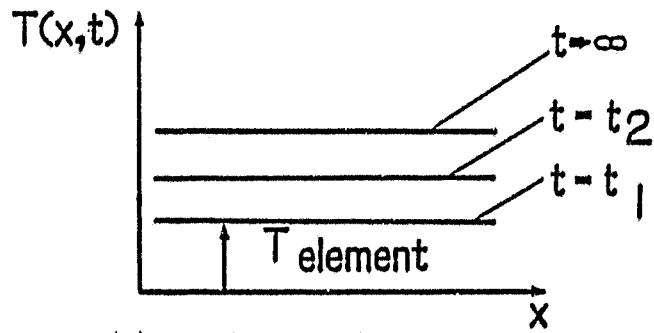
(a) Isothermal element
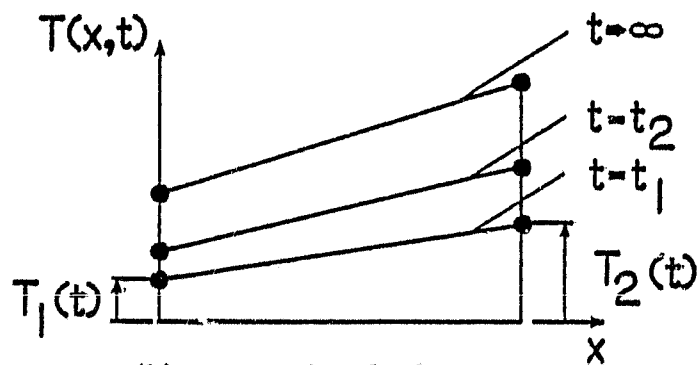
(b) Conventional element
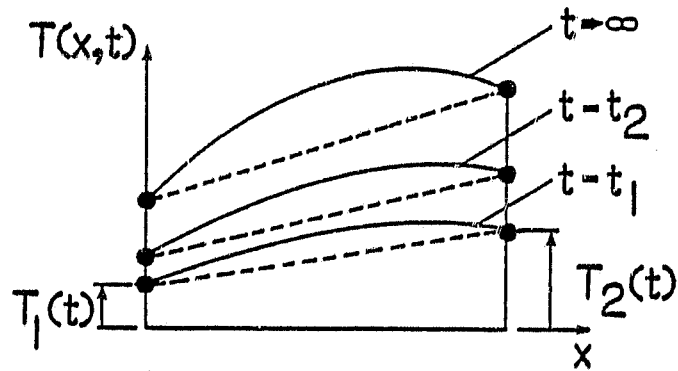
(c) Nodeless variable element

Fig. 13. One-dimensional element interpolation
functions for nonlinear transient
analysis with radiation.

neglects heat conduction, the governing differential equation shown in Eq. (5.1) becomes

$$\rho c A \frac{dT}{dt} + \varepsilon \sigma p_s T^4 = a p_q p_r \qquad (5.17)$$

where T denotes the element temperature which is a function only of time t.

The Crank-Nicolson algorithm is applied to the above differential equation by first writing the rate of change of the element temperature in the form of Eq. (5.8),

$$\frac{dT}{dt} = \dot{T} = \frac{2}{\Delta t} (T - T_n)$$

where T denotes the element temperature at the middle of the step. Substituting this equation into Eq. (5.17) yields a nonlinear algebraic equation in the form

$$(\frac{2}{\Delta t} \rho c A + \varepsilon \sigma p_s T^3) T = a p_q q_r + \frac{2}{\Delta t} \rho c A T_n \qquad (5.18)$$

After the element temperature T at the middle of the step shown in the above equation is obtained, the element temperature at the end of the step is computed from

$$T_{n+1} = 2T - T_n \qquad (5.19)$$

Next, the nonlinear algebraic equation shown in Eq. (5.18) is solved by applying the Newton-Raphson method. In this case, the unbalanced element heat load is given by (see Eq. (5.12)),

$$\psi = (\frac{2}{\Delta t} \rho cA + \epsilon \sigma p_s T^3) T - a p_q q_r - \frac{2}{\Delta t} \rho cA T_n \qquad (5.20)$$

Using Taylor series approximation, an algebraic equation is obtained in the form

$$J^m \Delta T^{m+1} = R^m \qquad (5.21)$$

where J^m and R^m are the Jacobian and the residual load at the mth iteration defined by

$$J^m = \frac{\partial \psi}{\partial T} = \frac{2}{\Delta t} \rho cA + 4 \epsilon \sigma p_s T^3 \qquad (5.22a)$$

$$R^m = -\psi = \frac{2}{\Delta t} \rho cA (T_n - T) - \epsilon \sigma p_s T^4$$
$$+ a p_q p_r \qquad (5.22b)$$

At each iteration, the element temperature increment ΔT is computed from Eq. (5.21) and a new element temperature is obtained from

$$T^{m+1} = T^m + \Delta T^{m+1} \qquad (5.23)$$

After the convergence criterion is met, the element temperature shown in Eq. (5.23) is used in Eq. (5.19) to compute the element temperature at the end of the step. The use of the isothermal element does not require a set of simultaneous equations due to the assumption of negligible heat conduction as previously mentioned. The transient response of each element, therefore, can be computed separately.

The isothermal element is useful for modeling truss members where heat conduction is negligible in comparison with the incident heating and emitted radiation. Applications of the isothermal element for transient analysis of truss-type structures with surface radiation can be found in Refs. [29,30].

5.2.2 Conventional Element

For the conventional element, a linear temperature variation is assumed between the two element nodes (Fig. 13(b)),

$$T(x,t) = \lfloor 1 - \frac{x}{L} \quad \frac{x}{L} \rfloor \left\{ \begin{array}{c} T_1(t) \\ T_2(t) \end{array} \right\} = \lfloor N_T \rfloor \ \{T\} \tag{5.24}$$

where the unknown nodal temperatures $T_1(t)$ and $T_2(t)$ are a function of time t. With the conduction-radiation differential equation shown in Eq. (5.1), element equations can be derived as shown in Eq. (5.2). The vector of unbalance nodal heat loads shown in Eq. (5.12a) is written explicitly in the form

$$\{\psi\} = \frac{2}{\Delta t} [C]\{T\} + [K_c]\{T\} + [K_r]\{T\} - \{Q_c\} - \{Q_r\}$$

$$- \frac{2}{\Delta t} [C]\{T\}_n$$

or

$$\{\psi\} = \frac{2}{\Delta t} [C]\{\{T\} - \{T\}_n\} + [K_c]\{T\} + [K_r]\{T\}$$

$$- \{Q_c\} - \{Q_r\} \tag{5.25}$$

For convenience nodal heat load vectors corresponding to each term on the right-hand side of the above equation are introduced to yield

$$\{\psi\} = \{\psi_{C_c}\} + \{\psi_{K_c}\} + \{\psi_{K_r}\} - \{\psi_{Q_c}\} - \{\psi_{Q_r}\} \tag{5.26}$$

The Jacobian matrices and the residual heat load vector can now be formulated by using the definitions (see Eq. (5.15))

$$J_{ij} = \frac{\partial \psi_i}{\partial T_j} \qquad \text{and} \qquad R_i = -\psi_i$$

For example, the first term on the right-hand side of Eq. (5.26) is the heat load vector associated with the capacitance matrix,

$$\{\psi_{C_c}\} = \frac{2}{\Delta t} [C]\{\{T\} - \{T\}_n\}$$

$$= \frac{2}{\Delta t} \int_0^L \rho c A \{N_T\} \lfloor N_T \rfloor \, dx \, \{\{T\} - \{T\}_n\}$$

With the linear element interpolation functions shown in Eq. (5.24), this term can be evaluated in closed form as

$$\{\psi_{C_c}\} = \frac{2}{\Delta t} \begin{bmatrix} \frac{1}{3} & \frac{1}{6} \\ \frac{1}{6} & \frac{1}{3} \end{bmatrix} \left\{ \begin{Bmatrix} T_1 \\ T_2 \end{Bmatrix} - \begin{Bmatrix} T_1 \\ T_2 \end{Bmatrix}_n \right\}$$

Using the definition of Jacobian $J_{ij} = \partial \psi_i / \partial T_j$, $i,j = 1,2$, the corresponding Jacobian matrix is

$$[J_{C_c}] = \frac{2}{\Delta t} \rho c A L \begin{bmatrix} \frac{1}{3} & \frac{1}{6} \\ \frac{1}{6} & \frac{1}{3} \end{bmatrix} = \frac{2}{\Delta t} [C] \qquad (5.27)$$

Similarly, the Jacobian matrix associated with the conductance conduction matrix is obtained in the form

$$[J_{K_c}] = [K_c] = \frac{kA}{L} \begin{bmatrix} 1 & -1 \\ -1 & 1 \end{bmatrix} \qquad (5.28)$$

The third term on the right-hand side of Eq. (5.26) is the heat load vector associated with the radiation matrix,

$$\{\psi_{K_r}\} = [K_r] \{T\} = \int_0^L \varepsilon \sigma p_s T^4 \{N_T\} \, dx$$

or

$$\psi_i = \int_0^L \varepsilon \sigma p_s T^4 N_i \, dx$$

Therefore, the corresponding Jacobian is

$$J_{ij} = \frac{\partial \psi_i}{\partial T_j} = 4 \int_0^L \varepsilon \sigma p_s T^3 N_i N_j \, dx$$

or

$$[J_{K_r}] = 4 \int_0^L \varepsilon \sigma p_s T^3 \{N_T\} \lfloor N_T \rfloor \, dx \qquad (5.29)$$

With the linear element interpolation functions shown in Eq. (5.24), this Jacobian matrix can be evaluated in closed form as

$$[J_{K_r}] = \frac{1}{15} \epsilon \sigma p_s L \begin{bmatrix} 10T_1^3 + 6T_1^2 T_2 + 3T_1 T_2^2 + T_2^3 & 2T_1^3 + 3T_1^2 T_2 + 3T_1 T_2^2 + 2T_2^3 \\ \\ 2T_1^3 + 3T_1^2 T_2 + 3T_1 T_2^2 + 2T_2^3 & T_1^3 + 3T_1^2 T_2 + 6T_1 T_2^2 + 10T_2^3 \end{bmatrix}$$

$$(5.30)$$

It can be seen that the Jacobian matrix associated with the radiation conductance matrix is strongly nonlinear since the unknown nodal temperatures contribute to all terms in the matrix. The matrix is sometimes [31] approximated by lumping these terms together similar to the lumped capacitance matrix given in Eq. (4.6). The lumped Jacobian matrix results in a much simpler form with zero off-diagonal terms,

$$[J_{K_r}] = 2 \epsilon \sigma p_s L \begin{bmatrix} T_1^3 & 0 \\ \\ 0 & T_2^3 \end{bmatrix}$$

$$(5.31)$$

From Eqs. (5.15) and (5.26), the total residual load vector is

$$\{R\} = - \{\psi_{C_c}\} - \{\psi_{K_c}\} - \{\psi_{K_r}\} + \{\psi_{Q_c}\} + \{\psi_{Q_r}\}$$

$$(5.32)$$

For example, the residual load vector associated with the radiation conductance matrix is

$$\{R_{K_r}\} = -\{\psi_{K_r}\} = - [K_r] \{T\}$$

$$= - \int_0^L \varepsilon \sigma p_s T^4 \{N_T\} \, dx$$

Using the linear element interpolation functions shown in Eq. (5.24), this residual load vector can be evaluated in closed form,

$$\{R_{K_r}\} = - \frac{1}{30} \varepsilon \sigma p_s L \left\{ \begin{array}{c} 5T_1^4 + 4T_1^3 T_2 + 3T_1^2 T_2^2 + 2T_1 T_2^3 + T_2^4 \\[2mm] T_1^4 + 2T_1^3 T_2 + 3T_1^2 T_2^2 + 4T_1 T_2^3 + 5T_2^4 \end{array} \right\} \quad (5.33)$$

After all Jacobian matrices and residual heat load vectors are computed, a final set of algebraic equations is obtained in the form

$$[J]^m \{\Delta T\}^{m+1} = \{R\}^m \qquad (5.34a)$$

where the superscript m denotes the mth iteration and,

$$[J] = [J_{C_c}] + [J_{K_c}] + [J_{K_r}] \qquad (5.34b)$$

$$\{R\} = \{R_{C_c}\} + \{R_{K_c}\} + \{R_{K_r}\} + \{R_{Q_c}\} + \{R_{Q_r}\} \qquad (5.34c)$$

The solution of the temperature vector at successive times proceeds as previously discussed for the isothermal element.

As shown in Eq. (5.34a), the transient and nonlinear solution procedures lead to a set of algebraic equations. The Jacobian matrices and the residual heat load vectors shown in Eqs. (5.34b-c) are thus necessary for the analysis.. With the linear element inter-polation functions shown in Eq. (5.24), these matrices can be

evaluated in closed form and are given as computer subroutines in Appendix D.

5.2.3 Nodeless Variable Element

In the preceding chapter, the nodeless variable approach was introduced for improvement of temperature solutions in one-dimensional linear transient analysis. The basic idea of the approach is the use of the steady-state element temperature interpolation function derived from the solution of a given ordinary differential equation. An element nodeless variable is employed so that exact steady-state solutions are obtained at the beginning and at the end of the transient with realistic temperature distributions prediced throughout the response. For one-dimensional conduction-radiation heat transfer, it is not possible to obtain a closed form solution to the governing differential equation, Eq. (5.1). However, the nodeless variable approach is still useful for the analysis to provide improved temperature solutions for the thermal element while maintaining the same discretization as the two node structural element. The element temperature distribution with a nodeless variable is written in the form,

$$T(x,t) = \lfloor N_0(x) \quad N_1(x) \quad N_2(x) \rfloor \left\{ \begin{array}{c} T_0(t) \\ T_1(t) \\ T_2(t) \end{array} \right\} = \lfloor N_T \rfloor \{T\} \qquad (5.35)$$

where $N_0(x)$ is the nodeless variable interpolation function, $N_i(x)$, $i = 1,2$ are typical element interpolation functions; $T_0(t)$ is the nodeless variable, and $T_i(t)$, $i = 1,2$ are the nodal temperatures.

As mentioned earlier, the nodeless variable interpolation function N_0 must vanish at nodes in order to preserve continuity of temperature between elements. There are wide choices for selecting the nodeless variable interpolation function to meet this requirement. The simplest function is in the form of polynomials with one order higher than the linear element interpolation functions used in the conventional finite element,

$$N_0(x) = \frac{x}{L}\left(1 - \frac{x}{L}\right) \qquad (5.36a)$$

$$N_1(x) = 1 - \frac{x}{L} \qquad (5.36b)$$

$$N_2(x) = \frac{x}{L} \qquad (5.36c)$$

With these element interpolation functions, the element temperature distribution, Eq. (5.35), results in a parabolic distribution over the element length as illustrated in Fig. 13(c).

The use of the nodeless variable element for transient heat conduction with surface radiation follows the same procedure described for the linear conventional element. Typical element equations derived from the method of weighted residuals shown in Eq. (5.2) contain three unknowns. These element unknowns are the nodeless variable T_0 and two nodal temperatures T_1 and T_2. For transient solutions, the Crank-Nicolson algorithm is applied, and a set of nonlinear algebraic equations is obtained. Next the Newton-Raphson method is used and a new form of simultaneous Eq. (5.34a) is obtained where the Jacobian matrices and the residual

load vectors are defined by Eqs. (3.54b-c), respectively. For example, the Jacobian matrix contributed from the radiation conductance matrix has the form

$$[J_{K_r}] = 4 \int_0^L \epsilon \sigma p_s T^3 \{N_T\} \lfloor N_T \rfloor \, dx$$

Using the element nodeless variable temperature distribution and their element interpolation functions shown in Eqs. (5.35) and (5.36), respectively, this Jacobian matrix is written explicitly as,

$$[J_{K_r}] = 4 \int_0^L \epsilon \sigma p_s (N_0 T_0 + N_1 T_1 + N_2 T_2)^3 \begin{Bmatrix} N_0 \\ N_1 \\ N_2 \end{Bmatrix} \lfloor N_0 \quad N_1 \quad N_2 \rfloor \, dx$$

Due to the complexity of the Jacobian matrix as shown above and other matrices that appear in Eq. (5.34), the computer-based symbolic manipulation language MACSYMA [32] was used to evaluate the matrices in closed form. Results of the Jacobian matrices and the residual load vectors are provided in the form of computer subroutines in Appendix D.

After the Jacobian matrices and the residual load vectors are computed, typical element equations shown in Eq. (5.34a) can be written in the form,

$$\begin{bmatrix} J_{00} & J_{01} & J_{02} \\ J_{10} & J_{11} & J_{12} \\ J_{20} & J_{21} & J_{22} \end{bmatrix}^m \begin{Bmatrix} \Delta T_0 \\ \Delta T_1 \\ \Delta T_2 \end{Bmatrix}^{m+1} = \begin{Bmatrix} R_0 \\ R_1 \\ R_2 \end{Bmatrix}^m \qquad (5.37)$$

These element equations contain unknowns in the increments of the nodeless variable and the nodal temperatures, i.e. one more unknown than those obtained from the linear conventional element. Once these unknowns are obtained, new values of the nodal temperatures and the nodeless variable are computed using Eq. (5.16). After the iteration process is terminated, the nodal temperatures and the nodeless variable at the end of time step are computed from Eq. (5.7). Finally, the temperature distribution within the element is computed by using the element nodeless variable interpolation functions shown in Eq. (5.35).

It should be noted that the nodeless variable interpolation functions, Eq. (5.36), introduced in this section are applicable when other heat transfer modes (such as surface convection) are included in the analysis. The element temperature distribution in the parabolic form can provide a more realistic temperature distribu tion than the linear conventional element. This type of the nodeless variable interpolation functions suggests that the nodeless variable approach can be generalized to other finite element types. To investigate this possibility, a two-dimensional nodeless variable thermal element is developed in the next chapter.

5.3 Applications

The effectiveness of the nodeless variable finite element described in this chapter is demonstrated for two examples of conduction and radiation heat transfer. The linear conventional finite element described in section 5.2.2 is used in these two examples for comparison of solution accuracy. Temperatures computed from the

nodeless variable and linear conventional finite elements are used
in the structural analysis for computation of displacements and
thermal stresses.

5.3.1 Thermal Stress in a Rod with Surface Radiation

A rod with constant cross-section area A and length L
encased between fixed walls is shown in Fig. 14(a). The rod has
specified end temperatures at 311 K and 533 K at x = 0 and
x = L, respectively, and is cooled along the surface by radiation
to zero medium temperature. The rod is modeled using (1) 20 conven-
tional elements with consistent Jacobian matrices (see Eq. 5.30)),
(2) two conventional elements with consistent Jacobian matrices,
(3) two conventional elements with lumped Jacobian matrices (see
Eq. (5.31)), and (4) two nodeless variable elements. The terms
consistent and lumped refer to the formulation of the Jacobian matrix
contributed by the radiation conductance matrix described in section
5.2.2.

Temperature distributions computed from these four finite
element models are compared as shown in Fig. 14(b). The figure shows
that two nodeless variable elements have the same capability in
predicting the unknown nodal temperature (at x/L = 0.5) and element
temperature distributions as 20 conventional finite elements. Two
conventional finite elements with consistent formulation underesti-
mate the unknown nodal temperature and crudely approximate temperature
distribution. Two conventional finite elements with lumped formula-
tion overestimate both the unknown nodal temperature and element
temperature distributions with relatively large error.

RADIATING HEAT

$u = 0$
$T = 311$ K

$u = 0$
$T = 533$ K

σ_x

x → $u(x)$

l
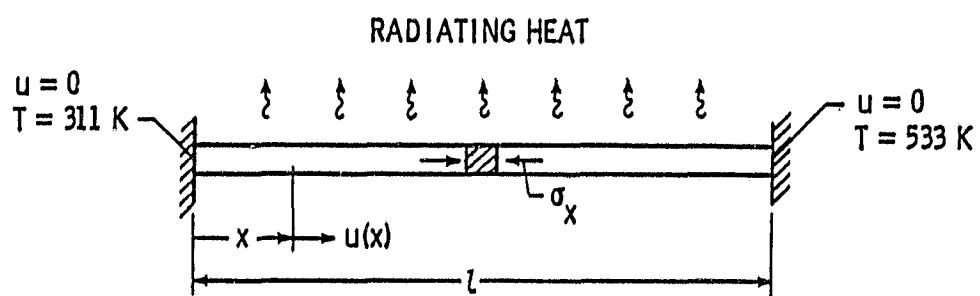
(a) ROD WITH SURFACE RADIATION

Fig. 14.   Conventional and nodeless variable finite
element solutions for a fixed end rod
radiating to space.
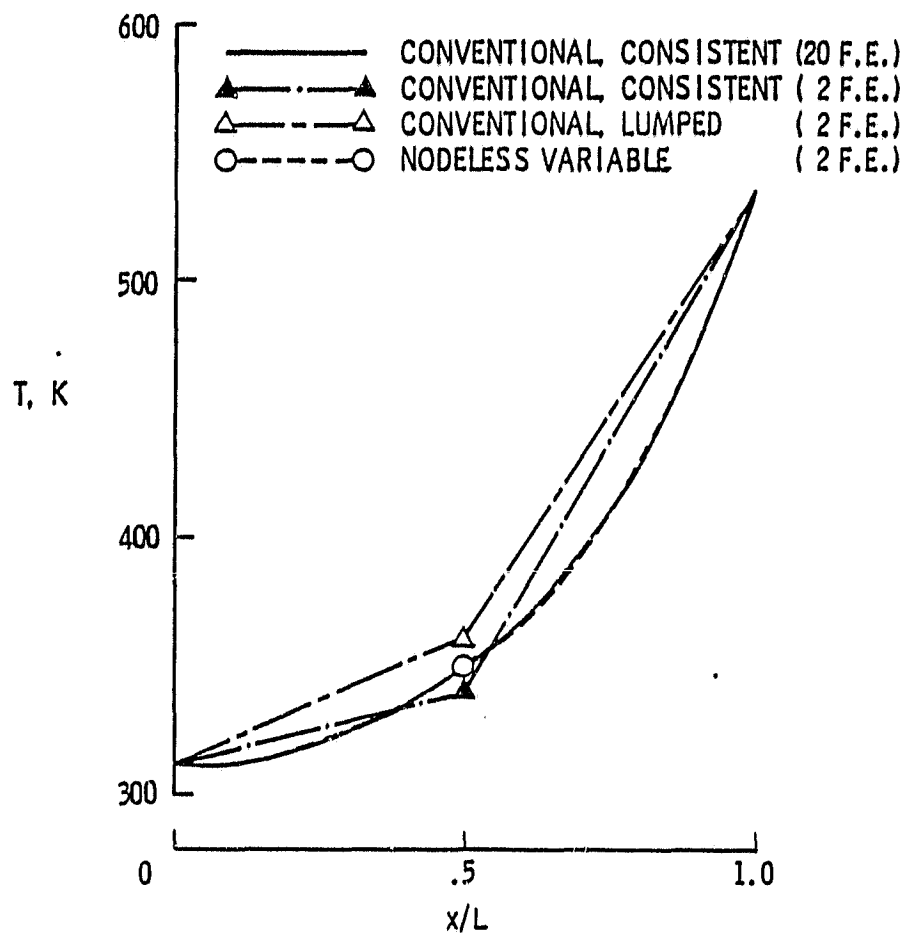
(b) COMPARATIVE TEMPERATURE DISTRIBUTIONS·

Fig. 14. Conventional nodeless variable finite element
          solutions for a fixed rod radiating to space.

In the structural analysis, four structural elements with the same discretizations as for the thermal models are employed. Element temperatures obtained from the thermal model are transferred directly to the structural finite element model for computation of displacements and stresses. The conventional structural finite elements employ linear element displacement distributions as used in typical finite element programs. The structural finite element for the nodeless variable thermal element uses the exact displacement distribution, Eq. (3.53), derived based upon the parabolic element temperature distribution shown in Eq. (5.35). Displacement distributions obtained from these structural finite element models are compared as shown in Fig. 14(c). The figure shows that two conventional finite elements are inadequate to represent the nonuniform of displacement distribution. In addition, two conventional finite elements with consistent and lumped formulations overestimate the thermal stress (not shown) by 12 and 23 percent, respectively. Displacement distributions obtained from two nodeless variable finite elements and 20 conventional finite elements are in excellent agreement where the difference in the thermal stresses is negligible (less than 0.05 percent).

5.3.2 Thermal Analysis and Structural Response of a Space Truss Module

A three member orbiting truss module shown in Fig. 15(a) is used to demonstrate the efficiency of the nodeless variable finite element. A typical truss member receives incident heating which is a combination of: (1) solar heating, (2) earth emitting heating, and (3) earth reflected solar heating. With the open-truss type
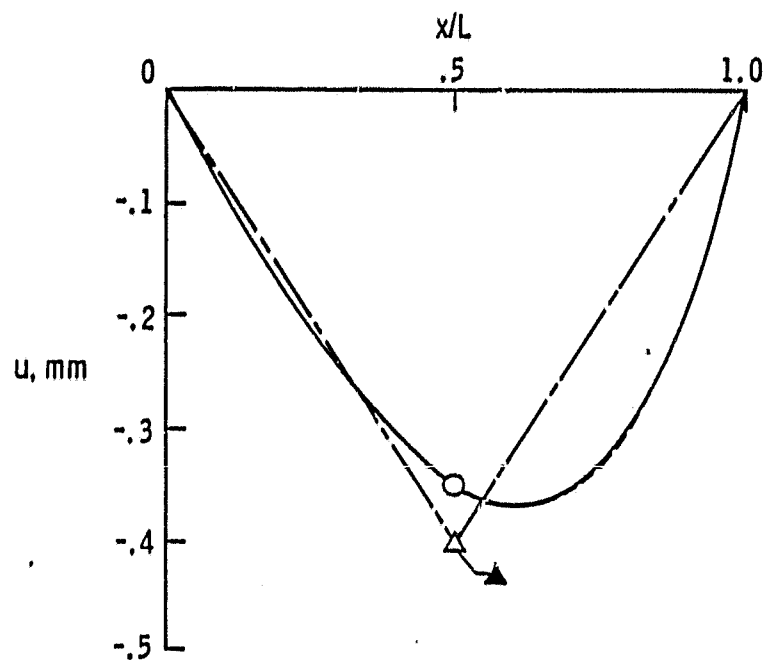
(c) COMPARATIVE DISPLACEMENT DISTRIBUTIONS

Fig. 14. Conventional and nodeless variable finite
element solutions for a fixed end rod
radiating to space.
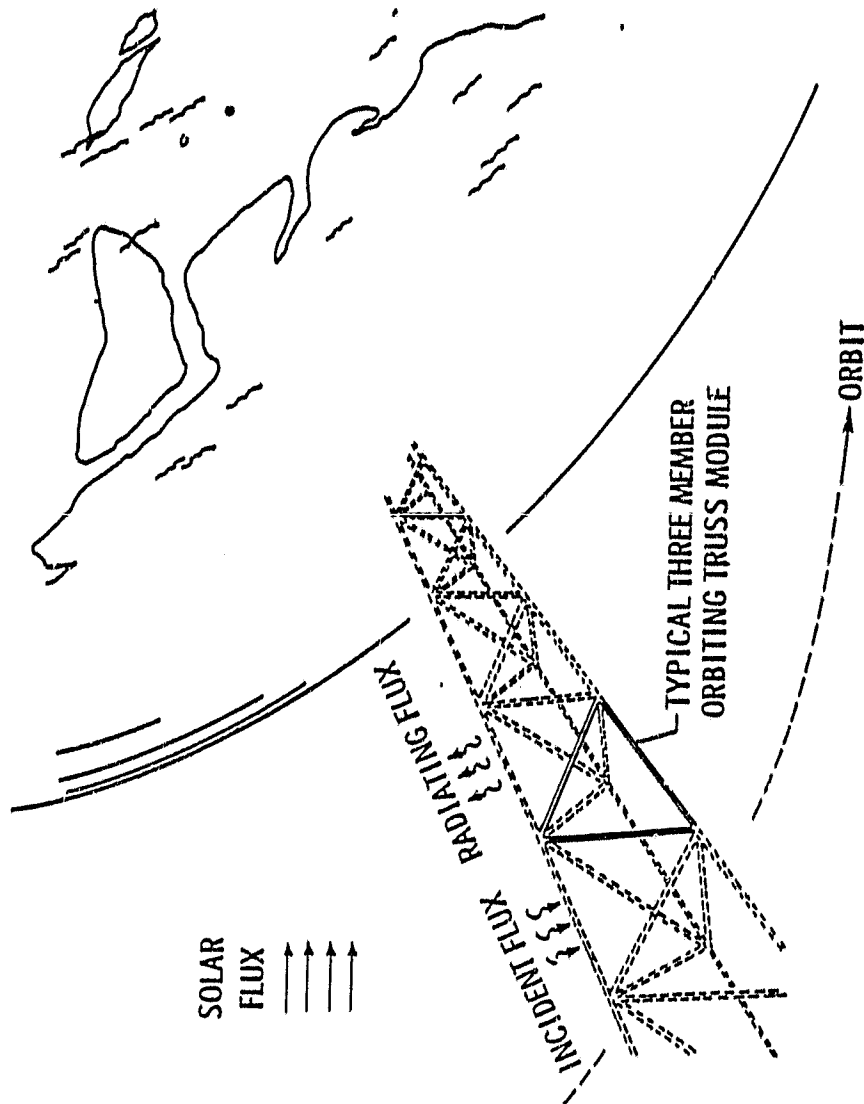
(a) Orbiting truss space structure.

Fig. 15. Thermal analysis and structural response of a space truss module.

structure as shown in the figure, member to member radiation exchanges are relatively small and are neglected. A geosynchronous orbit (period of 24 hr.) is employed where solar heating is large compared to the earth emitted heating. During the orbit, incident heating normal to a typical truss member varies continuously due to the changing orientation of the member. As the orbiting truss enters and leaves the earth's shadow, the incident heating changes rapidly. Member temperatures and structural deformations thus depend strongly on the time-dependent incident heating.

To demonstrate the use of the conventional and the nodeless variable finite elements formulated in the preceding section, the truss module with properties of aluminum is considered. Four finite element models are employed where each truss member is represented by: (1) 10 conventional elements with consistent formulation, (2) one conventional element with consistent formulation, (3) one conventional element with lumped formulation, and (4) one nodeless variable element. Temperature distributions computed from these four finite element models at a typical orbital position are shown in Fig. 15(b). The figure shows that the nodeless variable finite element model provides excellent prediction of the nodal temperatures and very good element temperature distributions compared to the refined conventional finite element model. The conventional finite elements with consistent formulation tend to average the nonuniform temperature distributions and thus cannot provide accurate nodal temperatures. The conventional finite elements with lumped formulation predict nodal temperatures very well but yield large errors for member interior temperatures. Comparative temperature distributions of
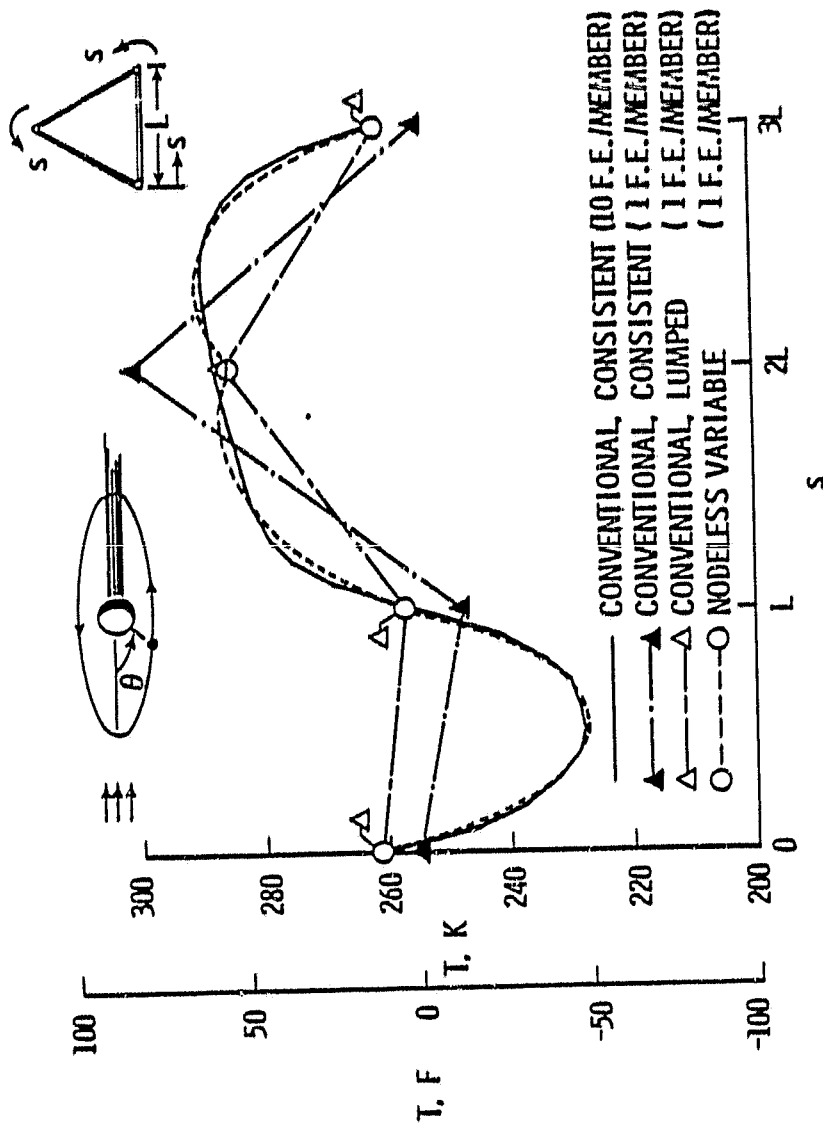
(b) Comparative temperature distribution of a three member
orbiting truss at θ = 60 degrees.

Fig. 15. Thermal analysis and structural response of a space truss module.

finite element models at other orbital positions also show a similar trend; the nodeless variable finite elements predict nodal temperatures and member temperature distributions very accurately compared to the refined conventional finite elements.

Temperature obtained from the four thermal finite element models for a complete orbit are transferred to the structural finite element models for computation of displacement histories. The quasi-static analysis described in section 2.4 is employed for the computation of the unknown nodal displacements. Fig. 15(c) shows a comparison of typical member elongation histories computed from the finite element models during the orbit. Since the temperature distributions obtained from the nodeless variable finite element model and the refined conventional finite element model are in very good agreement, member elongation histories predicted by these two finite element models almost coincide (maximum difference of 1 percent). Conventional finite element models with consistent and lumped formulations yield errors for member elongation up to 29 and 44 percent, respectively. Such large errors result from the incapability of the conventional finite element to provide realistic member temperature distributions. Since the conventional finite element with consistent formulation trends to average the member temperature as previously mentioned, accuracy of the member elongation history obtained is thus higher than the conventional finite element with lumped formulation.

These two examples clearly demonstrate the benefits of using the nodeless variable finite elements in one-dimensional radiation-conduction problems that are characterized by nonuniform temperature distributions. The elements predict member temperatures accurately
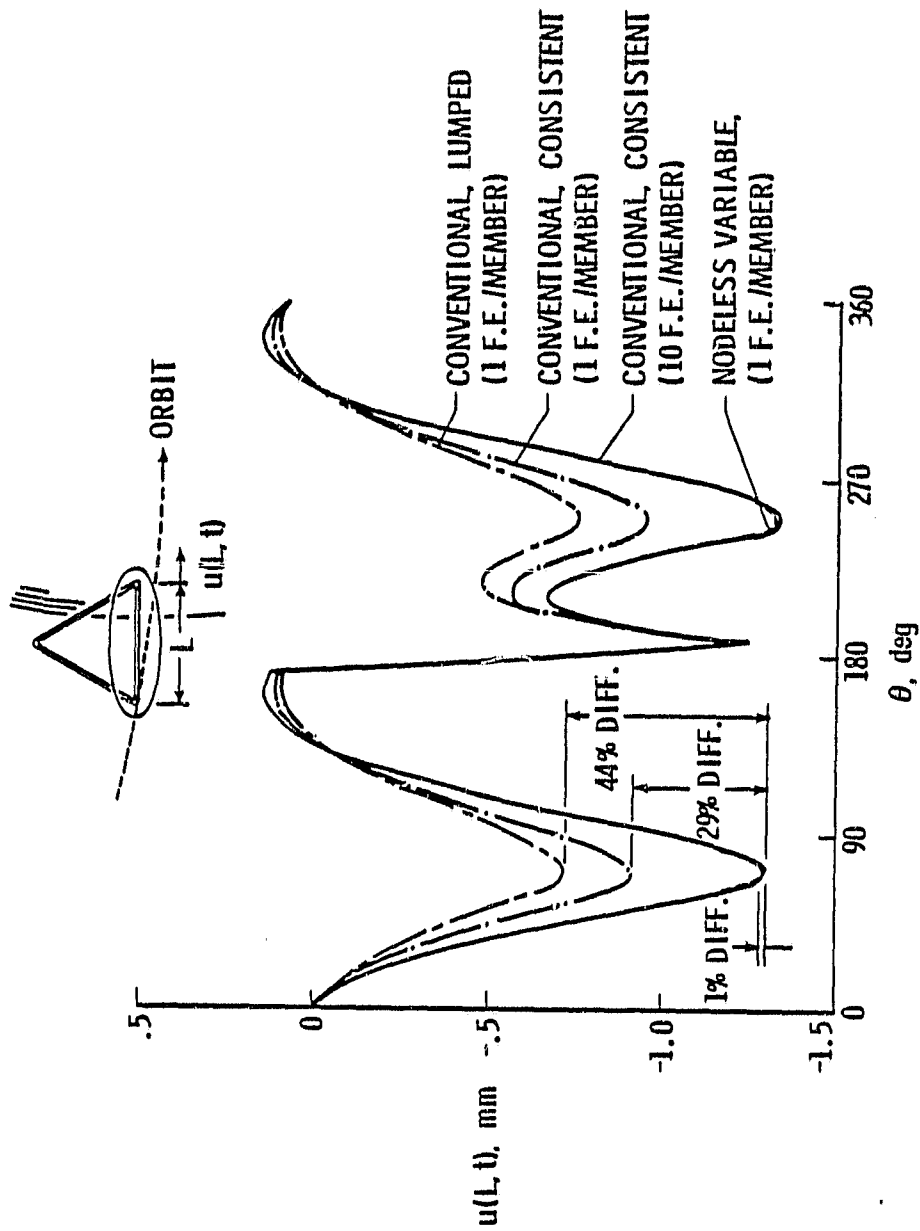
(c) Comparative displacements of a three member orbiting truss.

Fig. 15. Thermal analysis and structural response of a space truss model.

and are compatible with two-node structural elements to permit an integrated thermal-structural analysis. Additional applications of the nodeless variable finite element for one-dimensional thermal problems with conduction and radiation heat transfer appear in Ref. [33].

Chapter 6

TWO-DIMENSIONAL NODELESS VARIABLE FINITE ELEMENTS

In the two preceding chapters the nodeless variable approach
was applied to one-dimensional linear thermal-structural analysis
and to nonlinear radiation heat transfer. The unique feature of the
approach is the use of an additional nodeless variable for a thermal
finite element. Improvement of solution accuracy is achieved while
the same discretization is employed for both thermal and structural
finite element models.

In this chapter the approach is extended for development of
two-dimensional nodeless variable finite elements. Restrictions for
developing these finite elements are first discussed. Two nodeless
variable finite elements and their interpolation functions are
presented. Then the use of the nodeless finite elements for linear
thermal-structural analysis is described. Efficiency of the nodeless
variable finite elements is evaluated by comparison with the
conventional bilinear four-node finite element and exact solutions
in examples at the end of the chapter.

For simplicity in understanding characteristics of the two-
dimensional nodeless variable finite elements, a brief description
of a conventional bilinear four-node thermal finite element is
first given. The element temperature distribution for a bilinear
four-node element is expressed in the form,

$$T = \lfloor N_1 \quad N_2 \quad N_3 \quad N_4 \rfloor \left\{ \begin{array}{c} T_1 \\ T_2 \\ T_3 \\ T_4 \end{array} \right\} = \lfloor N_T \rfloor \{T\} \qquad (6.1)$$

where N_i, $i = 1,4$ are the element interpolation functions which are a function of spatial coordinates in two-dimensions, and T_i, $i = 1,4$ are the time dependent nodal temperatures.

Fig. 16(a) shows a conventional four-node element with a general quadrilateral shape. As described in section 2.3, typical finite element matrices are in the form of integrals over the element volume or along the element boundary. Such element matrices for a quadrilateral shape are difficult to evaluate. To simplify the element integrations, the quadrilateral element in the Cartesian coordinate system (x,y) is transformed to a natural coordinate system (ξ,η) as shown in Fig. 16(b). The two coordinate systems are related by

$$x = \sum_{i=1}^{4} N_i(\xi,\eta) \, x_i = \lfloor N \rfloor \{x\} \qquad (6.2a)$$

$$y = \sum_{i=1}^{4} N_i(\xi,\eta) \, y_i = \lfloor N \rfloor \{y\} \qquad (6.2b)$$

where N_i, $i = 1,4$ are the element shape functions defined by,

$$N_1 = \frac{1}{4}(1-\xi)(1-\eta) \qquad\qquad N_2 = \frac{1}{4}(1+\xi)(1-\eta)$$

$$(6.3a)$$

$$N_3 = \frac{1}{4}(1+\xi)(1+\eta) \qquad\qquad N_4 = \frac{1}{4}(1-\xi)(1+\eta)$$
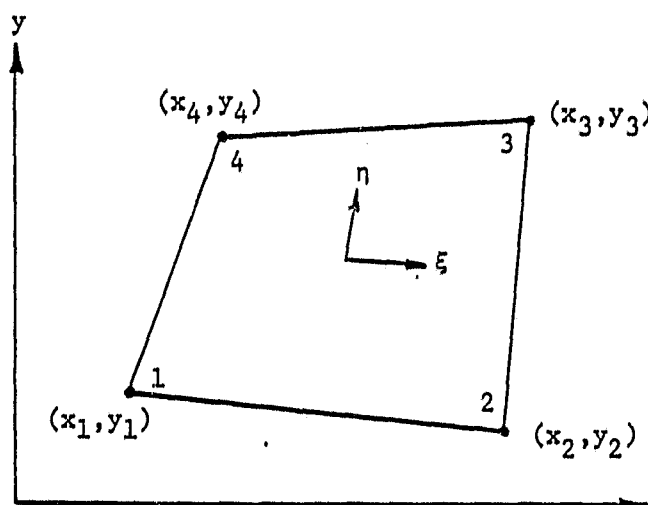
(a) Global coordinates
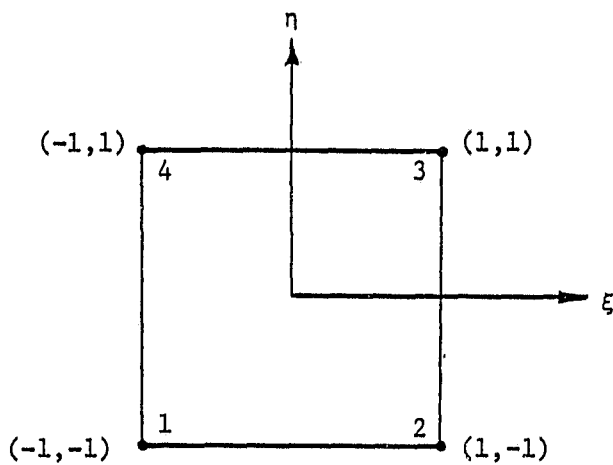
(b) Natural coordinates

Fig. 16. Four node isoparametric finite element in global and natural coordinates.

or in compact form,

$$N_i = \frac{1}{4}(1 + \xi\xi_i)(1 + \eta\eta_i) \qquad i = 1,4 \qquad (6.3b)$$

where ξ_i and η_i, $i = 1,4$ are the nodal coordinates in the natural coordinate system. For example, $\xi_1 = \eta_1 = -1$, $\xi_2 = 1$, $\eta_2 = -1$, etc.

When the shape functions N_i shown in Eq. (6.3) are used as the element temperature interpolation functions in Eq. (6.1), this conventional element is called an isoparametric quadrilateral element because the same interpolation functions are used to interpolate temperature and spatial coordinates.

Note that an element temperature interpolation function shown in Eq. (6.3) has a value of unity at the node to which it pertains and a value of zero at the other nodes. Along the element edge ($\xi = \pm 1$, $\eta = \pm 1$), these element interpolation functions are linear. Therefore, the temperature distribution along a typical element edge varies linearly where the magnitude depends on the temperatures of the two corner nodes located at that edge. When elements are connected, the conventional quadrilateral element preserves continuity of temperature along the element interfaces. The continuity of the element interface temperatures is a basic requirement to assure convergence of the temperature solution as element size decreases. This continuity requirement must be met when a new thermal finite element is constructed. Further details of requirements for a typical finite element to meet convergence criteria can be found in Ref. [15].

6.1 Two-Dimensional Nodeless Variable Thermal Finite Elements

In several thermal-structural applications, a more detailed finite element thermal model is required than the finite element structural model. To maintain the same discretization for thermal and structural models, new thermal finite elements are required. In this section, two type of two-dimensional nodeless variable thermal finite elements for improved temperature solutions are presented. These elements predict more realistic temperature distributions than the conventional finite element previously described. The basic objectives for developing the new finite elements are: (1) the elements should provide a nonlinear temperature distribution but maintain four element nodes to be congruent with the four node structural element, and (2) compatibility of temperature along element interfaces must be preserved. The nodeless variable concept previously described for one-dimensional element is extended to two-dimensions to meet these objectives.

6.1.1 "Bubble" Nodeless Variable

One approach [34] for constructing nodeless variable finite elements is to add a "bubble" function which vanishes along the element boundaries. The element temperature distribution is written in the form,

$$T = \lfloor N_1 \quad N_2 \quad N_3 \quad N_4 \rfloor \left\{ \begin{array}{c} T_1 \\ T_2 \\ T_3 \\ T_4 \end{array} \right\} + N_0 T_0 \qquad (6.4)$$

where N_0 is the nodeless interpolation (bubble) function defined by

$$N_0 = (1 - \xi^2)(1 - \eta^2) \qquad (6.5)$$

and T_0 is the nodeless variable.

Along the element boundary ($\xi = \pm 1$, $\eta = \pm 1$), the bubble function, Eq. (6.5), is identically zero. Therefore, the element boundary temperature reduces to a linear variation as for the conventional finite element and continuity of temperature along element interfaces is preserved. Within the bubble nodeless variable element, the temperature distribution is a combination of the conventional element temperature distribution and a bubble function where its magnitude is measured by the nodeless varaible T_0. The combination thus permits a quadratic temperature distribution over the element.

It should be noted that even though the bubble nodeless variable finite element can provide a quadratic temperature distribution within the element, the temperature along the element boundary is linear. To achieve further improvement of the temperature solution, the temperature distribution should vary nonlinearly along the element boundary. With the idea of the bubble function, a nodeless variable finite element with this behavior can be constructed. This type of nodeless variable finite element is presented in the next section.

6.1.2 Boundary Nodeless Variable

In order to establish a nonlinear temperature distribution along the four element edges as well as within the element interior, the following four nodeless variable interpolation functions (see Fig. 17) are employed

$$N_5 = \frac{1}{2} (1 - \xi^2)(1 - \eta) \tag{6.6a}$$

$$N_6 = \frac{1}{2} (1 + \xi)(1 - \eta^2) \tag{6.6b}$$

$$N_7 = \frac{1}{2} (1 - \xi^2)(1 + \eta) \tag{6.6c}$$

$$N_8 = \frac{1}{2} (1 - \xi)(1 - \eta^2) \tag{6.6d}$$

where each interpolation function varies quadratically along one edge and vanishes on the other edges. For example, the nodeless variable interpolation function N_5 varies as $1 - \xi^2$ along the edge $\eta = -1$ and is identically zero on the other three edges.

As mentioned earlier, continuity of the temperature along the element interfaces must be assured for convergence of the solution. This restriction can be met by providing a nodeless variable for each element edge. With a nodeless variable for each element edge, element interpolation functions for a quadrilateral element can be written in the form,

$$T = \lfloor N_1 \quad N_2 \quad N_3 \quad N_4 \rfloor \begin{Bmatrix} T_1 \\ T_2 \\ T_3 \\ T_4 \end{Bmatrix} + \lfloor N_5 \quad N_6 \quad N_7 \quad N_8 \rfloor \begin{Bmatrix} T_5 \\ T_6 \\ T_7 \\ T_8 \end{Bmatrix} \tag{6.7}$$
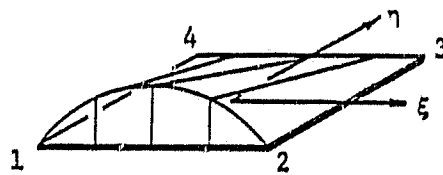
$$N_5 = \frac{1}{2}(1-\xi^2)(1-\eta)$$
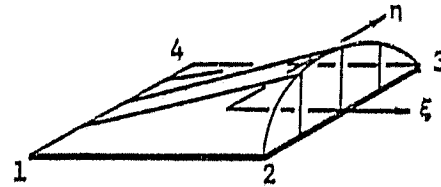
$$N_6 = \frac{1}{2}(1+\xi)(1-\eta^2)$$
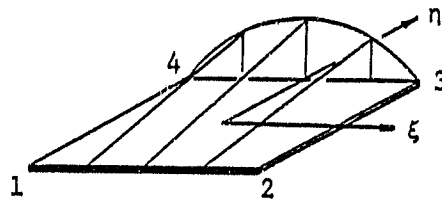
$$N_7 = \frac{1}{2}(1-\xi^2)(1+\eta)$$
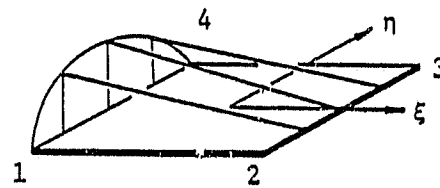
$$N_8 = \frac{1}{2}(1-\xi)(1-\eta^2)$$

Fig. 17. Nodeless variable interpolation functions for two-dimensional quadrilateral finite element.

where T_i, $i = 1,4$ and $i = 5,8$ are the nodal temperatures and the nodeless variables, respectively. Element interpolation functions N_i, $i = 1,4$ are the same as for the conventional bilinear four node element given in Eq. (6.3), and N_i, $i = 5,8$ are the nodeless variable interpolation functions given in Eq. (6.6).

The combination of the conventional and nodeless variable interpolation functions, Eq. (6.7), provides a quadratic temperature distribution over the element but with only four element nodes. Interelement' compatibility is preserved since adjacent elements have a common nodeless variable on adjoining edges. The magnitude of the nonlinear variation on an element edge is measured by the corresponding nodeless variable. Temperature distributions for the conventional bilinear element and the nodeless variable element are compared in Fig. 18.

6.2 Nodeless Variable Finite Element Formulation for Thermal-Structural Analysis

In this section, the thermal finite element formulation for two-dimensional linear transient analysis is described. The formulation is valid for both the conventional element and the nodeless variable element. A four node structural element which will be used in junction with the thermal element for computation of thermal stresses is also presented.

6.2.1 Linear Thermal Analysis

In two-dimensional transient heat conduction, the governing differential equation for the temperature distribution $T(x,y,t)$ may be expressed in the form of
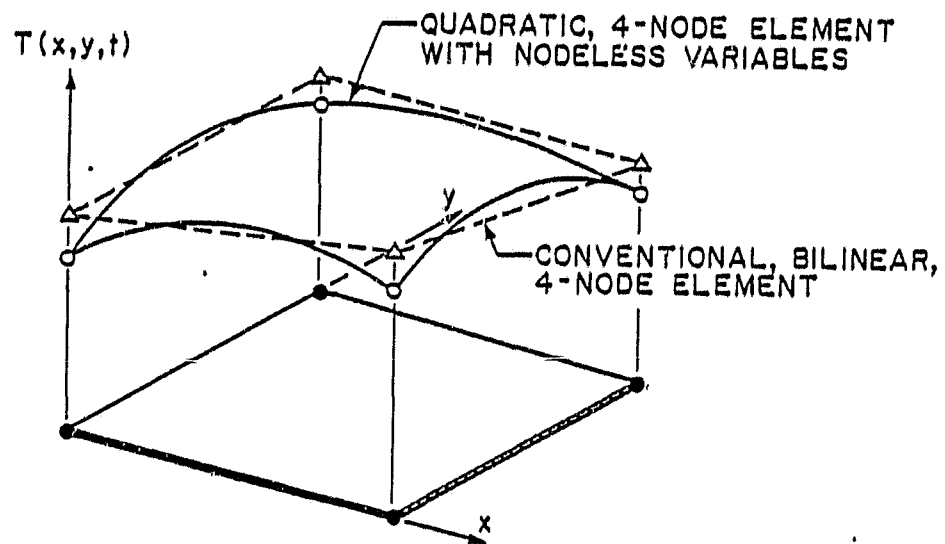
Fig. 18.   Two-dimensional element interpolation
functions.

$$\frac{\partial}{\partial x}\left(k_x \frac{\partial T}{\partial x}\right) + \frac{\partial}{\partial y}\left(k_y \frac{\partial T}{\partial y}\right) + Q = \rho c \frac{\partial T}{\partial t} \qquad (6.8)$$

where k_x and k_y are the thermal conductivities in x and y directions, respectively, Q is the internal heat generation rate per unit volume, ρ is the density, and c is the specific heat.

To derive the element equations and element matrices, the method of weighted residuals (see section 2.3) is applied to the governing differential equation (6.8). With the boundary conditions of specified temperatures, surface heating and surface convection as shown in Eqs. (2.5a-c), typical element equations have the form

$$[C]\,\{\dot{T}\} + [K_c + K_h]\,\{T\} = \{Q_c\} + \{Q_Q\} + \{Q_q\} + \{Q_h\} \qquad (6.9)$$

where [C] is the element capacitance matrix; $[K_c]$ and $[K_h]$ are element conductance matrices corresponding to conduction and convection, respectively. These matrices are expressed in the form of integrals over the surface area A of an element with the thickness t as follows:

$$[C] = t \int_A \rho c \,\{N_T\}\,\lfloor N_T \rfloor \, dx \, dy \qquad (6.10a)$$

$$[K_c] = t \int_A [B_T]^T \,[k]\,[B_T]\, dx \, dy \qquad (6.10b)$$

$$[K_h] = \int_A h \{N_T\}\,\lfloor N_T \rfloor \, dx \, dy \qquad (6.10c)$$

where $[B_T]$ denotes the temperature gradient interpolation matrix, and h is the convection coefficient. The right-hand side of the

discretized equation (6.9) contains heat load vectors due to specified nodal temperatures, internal heat generation, surface heating, and surface convection. These vectors are defined by

$$\{Q_c\} = -\int_{S_1} (\vec{q} \cdot \hat{n}) \, \{N_T\} \, ds \tag{6.11a}$$

$$\{Q_Q\} = t \int_A Q \{N_T\} \, dx \, dy \tag{6.11b}$$

$$\{Q_q\} = \int_A q \{N_T\} \, dx \, dy \tag{6.11c}$$

$$\{Q_h\} = \int_A h \, T_\infty \, \{N_T\} \, dx \, dy \tag{6.11d}$$

where $\vec{q}$ is the vector of conduction heat flux across boundary S_1 that is required to maintain the specified nodal temperatures, q is the surface heating rate per unit area, and T_∞ is the convective medium temperature.

As mentioned earlier, a typical quadrilateral element in Cartesian coordinates (x,y) is transformed to the natural coordinates (ξ, η) to perform the element matrix integration. In computation of the conduction conductance matrix (Eq. (6.10b)), for example, the chain rule is first applied to relate the temperature gradients in both coordinate systems,

$$\begin{Bmatrix} \dfrac{\partial T}{\partial \xi} \\[2mm] \dfrac{\partial T}{\partial \eta} \end{Bmatrix} = \begin{bmatrix} \dfrac{\partial x}{\partial \xi} & \dfrac{\partial y}{\partial \xi} \\[2mm] \dfrac{\partial x}{\partial \eta} & \dfrac{\partial y}{\partial \eta} \end{bmatrix} \begin{Bmatrix} \dfrac{\partial T}{\partial x} \\[2mm] \dfrac{\partial T}{\partial y} \end{Bmatrix} \tag{6.12}$$

Using the coordinate trasnformation shown in Eq. (6.2), the above
relations become

$$\left\{ \begin{array}{c} \dfrac{\partial T}{\partial \xi} \\[2ex] \dfrac{\partial T}{\partial \eta} \end{array} \right\} = [J] \left\{ \begin{array}{c} \dfrac{\partial T}{\partial x} \\[2ex] \dfrac{\partial T}{\partial y} \end{array} \right\}$$

or

$$\left\{ \begin{array}{c} \dfrac{\partial T}{\partial x} \\[2ex] \dfrac{\partial T}{\partial y} \end{array} \right\} = [J]^{-1} \left\{ \begin{array}{c} \dfrac{\partial T}{\partial \xi} \\[2ex] \dfrac{\partial T}{\partial \eta} \end{array} \right\} \tag{6.13}$$

where $[J]$ is the Jacobian matrix defined by

$$[J] = \begin{bmatrix} \displaystyle\sum_{i=1}^{4} \dfrac{\partial N_i}{\partial \xi} x_i & \displaystyle\sum_{i=1}^{4} \dfrac{\partial N_i}{\partial \xi} y_i \\[4ex] \displaystyle\sum_{i=1}^{4} \dfrac{\partial N_i}{\partial \eta} x_i & \displaystyle\sum_{i=1}^{4} \dfrac{\partial N_i}{\partial \eta} y_i \end{bmatrix} \tag{6.14}$$

Substituting the element temperature, Eq. (6.1) or (6.7), into the
right-hand side of Eq. (6.13) yields

$$\left\{ \begin{array}{c} \dfrac{\partial T}{\partial x} \\[2ex] \dfrac{\partial T}{\partial y} \end{array} \right\} = \left[B_T(\xi,\eta) \right] \left\{ \begin{array}{c} T_1 \\ T_2 \\ \vdots \\ T_r \end{array} \right\} \tag{6.15}$$

where r is the number of the element unknowns; $r = 4$ and 8 for
the conventional bilinear element and the nodeless variable

element, respectively. The temperature gradient interpolation matrix in the above equation is given by

$$[B_T(\xi,\eta)] = [J]^{-1} \begin{bmatrix} \dfrac{\partial N_1}{\partial \xi} & \dfrac{\partial N_2}{\partial \xi} & \cdots\cdots & \dfrac{\partial N_r}{\partial \xi} \\ & & \bullet & \\ \dfrac{\partial N_1}{\partial \eta} & \dfrac{\partial N_2}{\partial \eta} & \cdots\cdots & \dfrac{\partial N_r}{\partial \eta} \end{bmatrix} \qquad (6.16)$$

Using $dx\,dy = |J|\,d\xi\,d\eta$ where $|J|$ is the determinant of $[J]$, the conduction conductance matrix terms of the natural coordinates is

$$[K_c] = t \int_{-1}^{1}\int_{-1}^{1} [B_T(\xi,\eta)]^T [k] [B_T(\xi,\eta)] |J|\,d\xi\,d\eta \qquad (6.17)$$

Next, the coefficients in the conduction conductance matrix are computed by numerical integration; the Lagendre-Gauss method is used where the above conduction conductance matrix is written in the form,

$$[K_c] = \sum_{i=1}^{NG}\sum_{j=1}^{NG} W_i\,W_j\,[B_T(\xi_i,\eta_j)]^T [k] [B_T(\xi_i,\eta_j)] |J(\xi_i,\eta_j)| \qquad (6.18)$$

where W_i, W_j denote Gauss weight factors, ξ_i, η_j denote gauss integration points and NG is the number of Gauss points in each

coordinate direction. Gauss weight factors and Gauss integration point coordinates can be found in Ref. [15].

Other element matrices shown in Eqs. (6.10 - 6.11) can be formulated in the same manner. For example, the conductance matrix and the heat load vector associated with surface convection are expressed as

$$[K_h] = h \sum_{i=1}^{NG} \sum_{j=1}^{NG} W_i W_j [N_T(\xi_i, \eta_j)]^T [N_T(\xi_i, \eta_j)] |J(\xi_i, \eta_j)| \qquad (6.19a)$$

$$\{Q_h\} = hT_\infty \sum_{i=1}^{NG} \sum_{j=1}^{NG} W_i W_j [N_T(\xi_i, \eta_j)]^T |J(\xi_i, \eta_j)| \qquad (6.19b)$$

In performing the numerical integration, the accuracy of the matrices depends on the number of Gauss points used. In general, the use of n Gauss points provides exact integration when the integrand contains polynomials of order up to $2n - 1$. For the conventional bilinear finite element, two Gauss points (NG = 2) in each coordinate direction are normally used. Since the nodeless temperature interpolation functions contain higher order of polynomials than those for the conventional bilinear element, more Gauss points should be used. For the linear thermal analysis presented herein, three Gauss points in each coordinate direction

was found by numerical tests to be appropriate for accurate node-less variable element matrices.

After element matrices are computed, typical element equations can be written in the form

$$[C] \{\dot{T}\} + [K] \{T\} = \{Q\} \tag{6.20}$$

The conventional bilinear element has four nodal temperatures as the unknowns, thus the above element equations contain four unknowns. The nodeless variable element has four nodal temperatures and four nodeless variables as the element unknowns, therefore, the element equations contain eight unknowns. In transient analysis, these eight equations must be solved simultaneously similar to the one-dimensional nodeless variable described in the preceding chapter. In steady-state analysis, the four nodeless variable unknowns can be eliminated from the element equations using the matrix condensation technique [35]. The final number of element equations thus reduces to be the same as of the conventional bilinear element.

6.2.2 Structural Element

In this section, the congruent structural element is briefly described. The element contains four nodes and permits the same discretization with the conventional and nodeless variable thermal elements described in the preceding sections. The element stiffness matrix is the same as used in conventional four node structural elements. However, the improved element temperature distributions,

Eq. (6.7), are incorporately consistently in the thermal force vector computation to yield an integrated thermal structural element.

The structural element at each node has two in-plane displacement unknowns u and v which may vary with the element local coordinates x, y and time t. Element displacement distributions are assumed in the form (see Eq. (2.23)),

$$\left\{ \begin{array}{c} u(x,y,t) \\ v(x,y,t) \end{array} \right\} = \left[\begin{array}{cccccccc} N_1 & 0 & N_2 & 0 & N_3 & 0 & N_4 & 0 \\ 0 & N_1 & 0 & N_2 & 0 & N_3 & 0 & N_4 \end{array} \right] \left\{ \begin{array}{c} u_1 \\ v_1 \\ u_2 \\ v_2 \\ u_3 \\ v_3 \\ u_4 \\ v_4 \end{array} \right\} = [N_s]\{\bar{\delta}\} \tag{6.21}$$

where N_i, $i = 1,4$ are the element displacement interpolation functions which have the same form as for the conventional finite element temperature interpolation functions shown in Eq. (6.3).

For the quasi-static analysis, typical element equations shown in Eq. (2.26) reduce to

$$[K_s] \{\delta\} = \{F_T\} \tag{6.22}$$

where $[K_s]$ is the element stiffness matrix, and $\{F_T\}$ is the

equivalent nodal thermal load vector. These matrices are expressed in the form of integrals over the element volume V as

$$[K_s] = \int_V [B_s]^T [D] [B_s] \, dv \qquad (6.23a)$$

$$\{F_T\} = \int_V [B_s]^T [D] \{\alpha\}(T(x,y,t) - T_{ref}) \, dV \qquad (6.23b)$$

where $[B_s]$ is the strain-displacement interpolation matrix obtained from the strain-displacement relations,

$$\begin{Bmatrix} \varepsilon_x \\ \varepsilon_y \\ \gamma_{xy} \end{Bmatrix} = \begin{Bmatrix} \dfrac{\partial u}{\partial x} \\ \dfrac{\partial v}{\partial y} \\ \dfrac{\partial u}{\partial y} + \dfrac{\partial v}{\partial x} \end{Bmatrix} = [B_s] \{\bar{\delta}\} \qquad (6.24)$$

[D] is the elasticity matrix defined by (plane stress),

$$[D] = \frac{E}{1-\nu^2} \begin{bmatrix} 1 & \nu & 0 \\ \nu & 1 & 0 \\ 0 & 0 & \dfrac{1-\nu}{2} \end{bmatrix} \qquad (6.25)$$

where ν is Poisson's ratio. The vector $\{\alpha\}$ contains the thermal expansion coefficients given by (plane stress)

$$\{\alpha\} = \begin{Bmatrix} \alpha \\ \alpha \\ 0 \end{Bmatrix} \qquad (6.26)$$

$T(x,y,t)$ is the element temperature computed using the conventional or the nodeless variable thermal element and T_{ref} is the reference temperature for zero stress. The elasticity matrix $[D]$ and the vector of thermal expansion coefficients shown in the above equations can be used for plane strain by replacing $E/(1-\nu^2)$ for E, $\nu(1-\nu)$ for ν, and $(1+\nu)\alpha$ for α.

Similar to the quadrilateral thermal element, numerical integration is required for computing the element matrices. Using the Lagendre-Gauss method, the element stiffness matrix and the equivalent thermal load vector shown in Eqs. (6.23a-b) are written in the form,

$$[K_s] = t \sum_{i=1}^{NG} \sum_{j=1}^{NG} W_i W_j [B_s(\xi_i, \eta_j)]^T [D] [B_s(\xi_i, \eta_j)] |J(\xi_i, \eta_j)| \quad (6.27a)$$

$$\{F_T\} = t \sum_{i=1}^{NG} \sum_{j=1}^{NG} W_i W_j [B_s(\xi_i, \eta_j)]^T [D] \{\alpha\} (T(\xi_i, \eta_j) - T_{ref}) |J(\xi_i, \eta_j)|$$
$$(6.27)$$

where $T(\xi_i, \eta_j)$ is the temperature at the element Gauss integration point ξ_i and η_j.

Unlike the thermal finite element previously described, the nodal displacement unknowns of the structural element are the vector quantities. Transformation of the element matrices from the local coordinates (x,y) to the global coordinates (X,Y,Z) is required. In three-dimensions, the element stiffness matrix becomes a 12 by 12 matrix and similarly with the nodal force vector. Thus the element equations contain a total of 12 equations with 12 nodal displacement unkonwns in the global coordinates. After the global element matrices are assembled and the nodal displacements are computed, element nodal

displacements in the local coordinates can be obtained. Then the element stresses can be computed from

$$
\left\{
\begin{array}{c}
\sigma_x \\
\sigma_y \\
\tau_{xy}
\end{array}
\right\}
= [D] \left\{ [B_s] \{\bar{\delta}\} - \{\alpha\} \, (T(x,y,t) - T_{ref}) \right\}
\qquad (6.28)
$$

6.3 Applications

To illustrate the performance of the two-dimensional nodeless finite element presented in section 6.1.2, two examples are analyzed: (1) a rectangular plate with surface convection, and (2) a simplified wing section with aerodynamic heating. In each example, benefits of the nodeless variable finite element are demonstrated by comparison with results from conventional finite element and analytical solutions.

6.3.1 Steady-State Heat Conduction in a Plate with Surface Convection

A rectangular plate (Fig. 19(a)) has a specified temperature T_0 along the boundaries. The plate is cooled by surface convection to a zero medium temperature, $T_\infty = 0$. Using symmetry, a quarter of the plate is first modeled by: (1) one conventional element, and (2) one nodeless variable element.

Fig. 19(b) shows·the comparative temperature distributions at $y = b/2$ for an analytical solution [27], the conventional element and the nodeless variable element solutions. For these models, the conventional element gives a relatively high error compared to the nodeless variable element. The largest error for both finite element models occurs at the center of the plate (16% and 3% for the
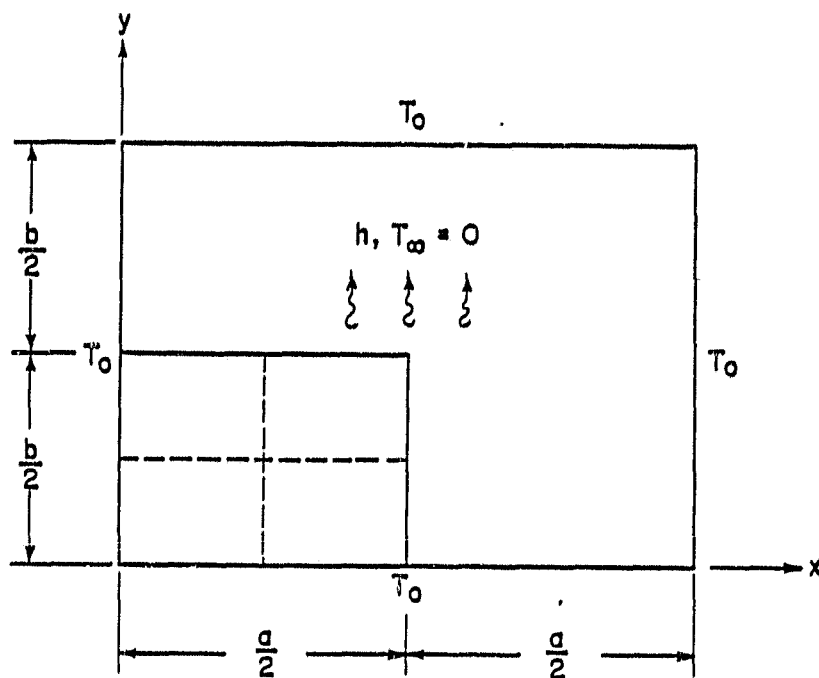
(a) PLATE COOLED BY SURFACE CONVECTION

Fig. 19.   Conventional and nodeless variable finite
element solutions for a plate with surface
convection.
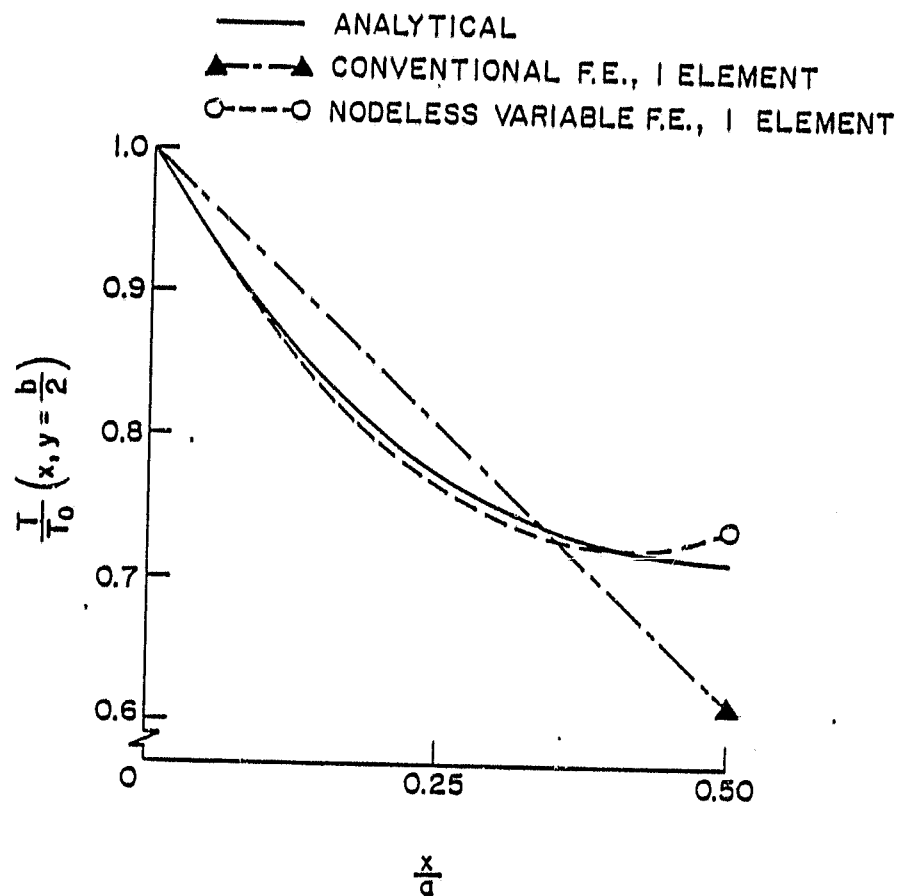
(b) COMPARATIVE TEMPERATURE DISTRIBUTIONS ALONG $y = \frac{b}{2}$.

Fig. 19. Conventional and nodeless variable finite element
solutions for a plate with surface convection.

conventional element and the nodeless variable element, respectively).
At the center of the plate, both elements show a discontinuity of
conduction heat flux indicating a need for mesh refinement. Next,
the plate is modeled by using four finite elements shown by the dotted
lines in Fig. 19(a); comparative temperature distributions are shown
in Fig. 19(c). Four conventional elements provide a fair estimate
of the temperature variation, but four nodeless variable elements
yield excellent predictions for both nodal and element temperatures.
Comparisons of temperatures at other sections of the plate (not shown)
demonstrate that four nodeless variable elements provide excellent
agreement with the analytical solution for the entire plate.

6.3.2 Simplified Wing Section with Aerodynamic Heating

To demonstrate the usefulness of the two-dimensional nodeless
variable elements in aerospace thermal-structural analysis, a simpli-
fied wing section is analyzed (Fig. 20(a)). Top and bottom skins
of the wing section are connected by three corrugated spars and are
subjected to symmetrical, nonuniform time-dependent aerodynamic
heating.

Three finite element models are employed to computed temperatures.
For a unit depth in the spanwise direction, the first model consists
of seven conventional elements; two elements each for the top and
bottom skins and one element for each spar. The second model is
identical to the first model except nodeless variable elements are
used. The third model uses a refined mesh (not shown) with 35 conven-
tional elements.

(c) COMPARATIVE TEMPERATURE DISTRIBUTIONS ALONG $y = \frac{b}{2}$.

Fig. 19. Conventional and nodeless variable finite element
solutions for a plate with surface convection.

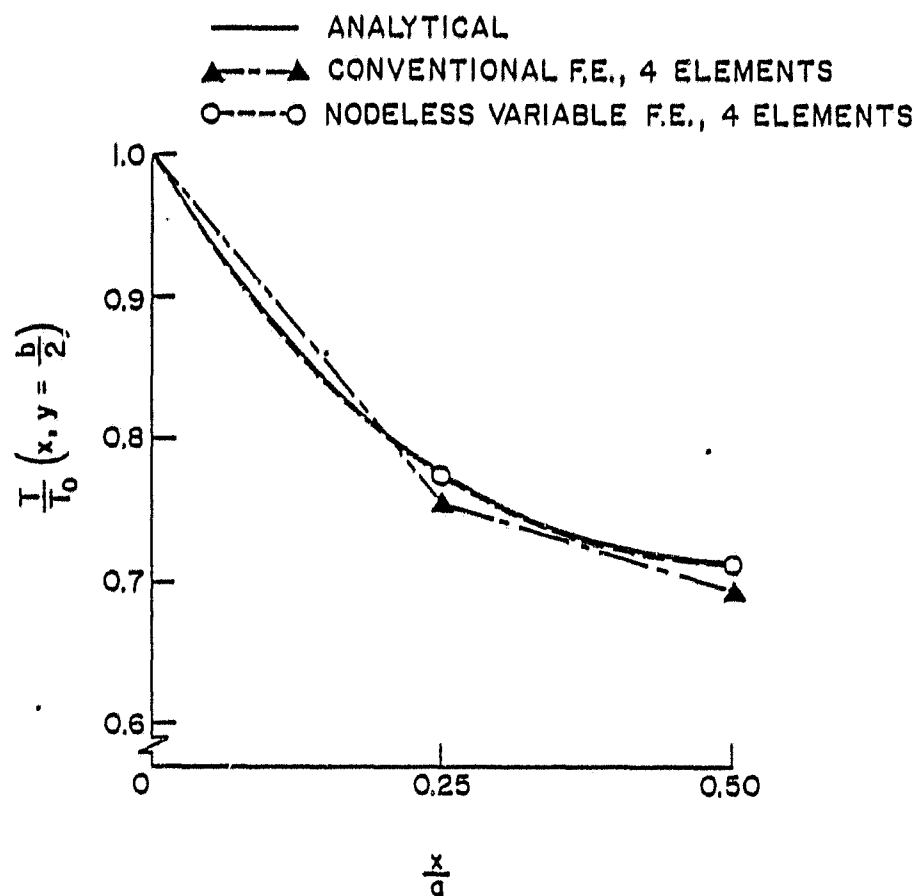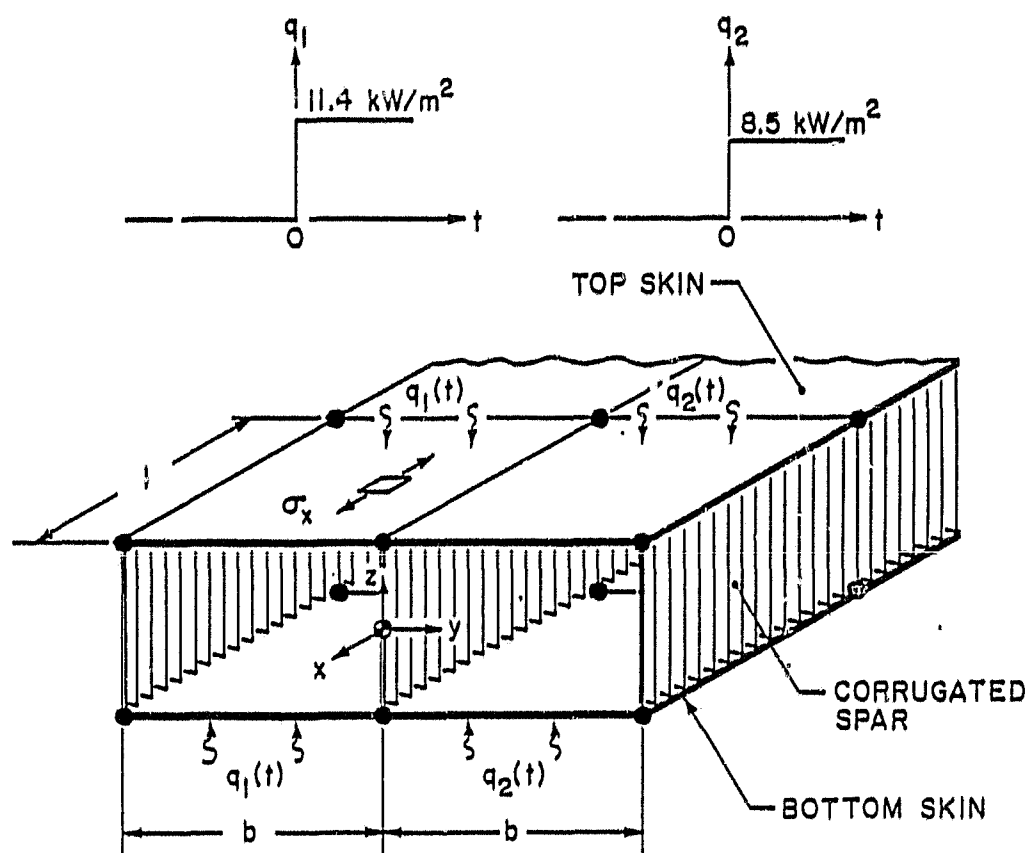(a) SIMPLIFIED WING SECTION WITH AERODYNAMIC HEATING

Fig. 19. Conventional and nodeless variable finite element
solutions for a simplified wing section with
aerodynamic heating.

Comparative skin temperature distributions at t = 150 s. are shown in Fig. 20(b); the number of elements cited is for the skin only. The nodeless variable finite element model predicts a realistic temperature distribution and gives very good agreement with the result from the refined conventional finite element model. The crude conventional finite element model underestimates the average skin temperature and is unable to provide details of the nonuniform temperature distribution.

In computation of the skin thermal stress, classical beam theory [16] is employed for comparison with two finite element stress analyses. Detailed temperature distributions from the refined conventional finite element thermal model are used to compute the stress σ_x from beam theory. Temperature distributions from the crude conventional thermal finite element model and the nodeless variable thermal finite element model are transferred to a structural finite element model with the same discretization for the stress computations. Comparative stress distributions at t = 150 s. are presented in Fig. 20(c). The advantage of using the improved temperature distributions from the nodeless variable finite element model in computing stresses is clearly demonstrated. These stress distributions are in excellent agreement with the result from beam theory with both the critical stress and its location accurately predicted. Using the temperature distribution from the crude conventional finite element model yields significant errors in the stress distribution and is unaccetable for this problem.

These two examples clearly demonstrate the benefits of the two-dimensional nodeless variable finite element that can be obtained
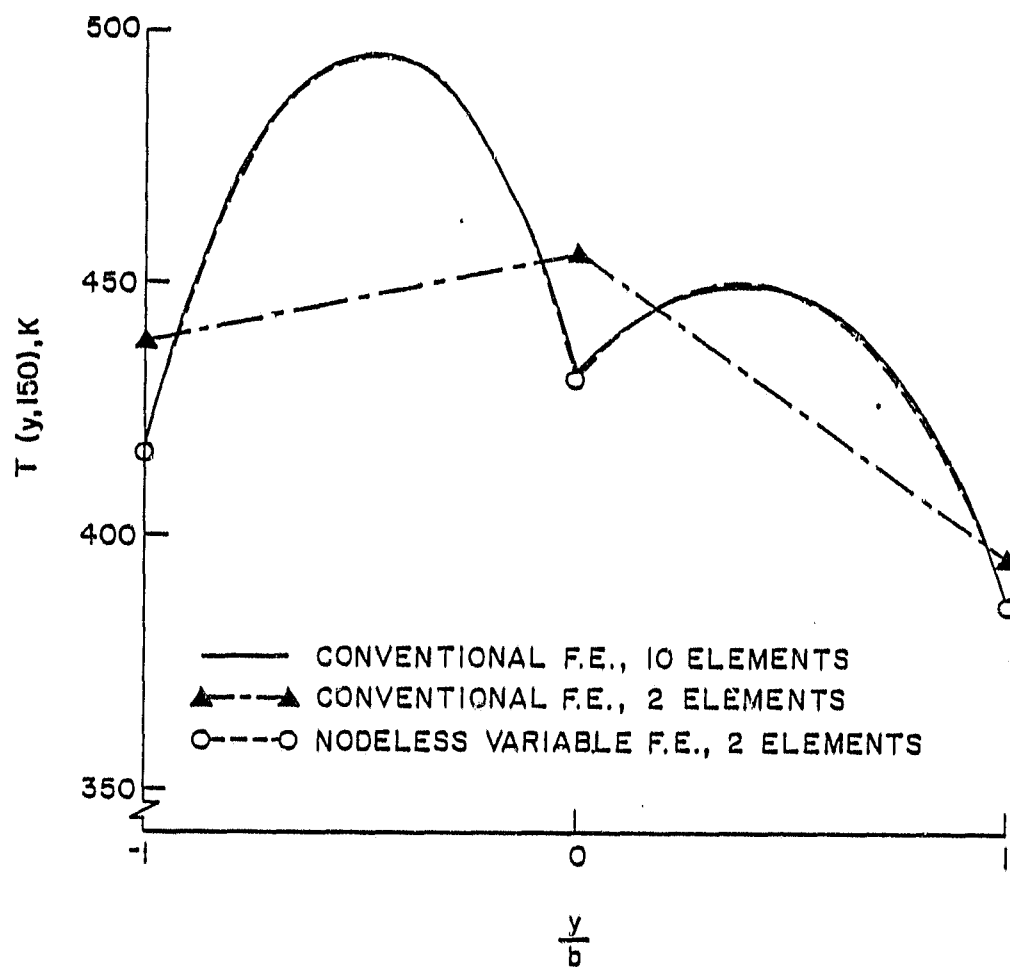
(b) COMPARATIVE TEMPERATURE DISTRIBUTIONS
ALONG CHORDWISE DIRECTION, t = 150 s.

Fig. 20. Conventional and nodeless variable finite element
solutions for a simplified wing section with
aerodynamic heating.
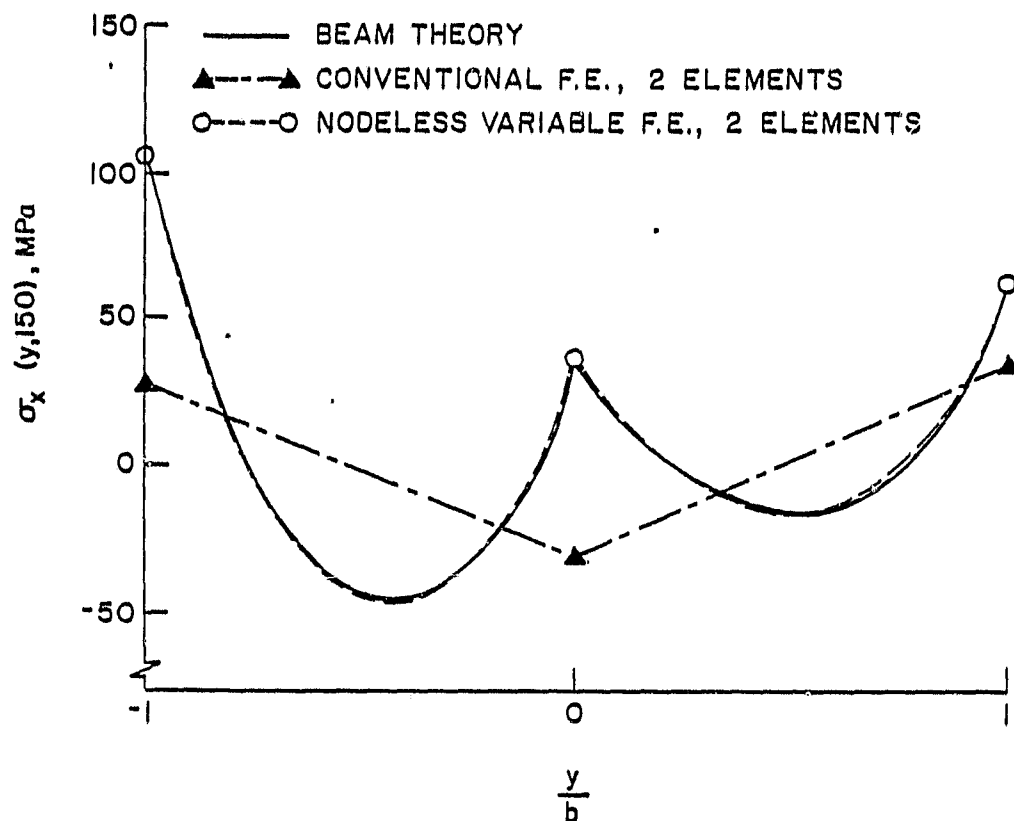
(c) COMPARATIVE THERMAL STRESS DISTRIBUTIONS ALONG CHORDWISE DIRECTION, t = 150 s.

Fig. 20. Conventional and nodeless variable finite element solutions for a simplified wing section with aerodynamic heating.

for thermal-structural analysis. Additional applications, a summary of the nodeless variable approach and the thermal-structural finite element formulation presented in this chapter appear in Ref. [36].

Chapter 7

CONCLUDING REMARKS

An integrated approach for improved thermal-structural finite element analysis is presented. The approach was motivated by aerospace applications to improve thermal-structural finite element analysis capabilities. An important goal is to eliminate the incompatibility between thermal-structural analyses where a more detailed finite element model is required for the thermal analysis than for the structural analysis. The integrated approach is characterized by: (1) thermal and structural finite elements formulated with common geometric discretization for full compatibility during the coupling of the analyses, (2) accurate nodal and element temperatures provided by improved thermal finite elements, and (3) accurate thermal loads for the structural finite element analysis to further improve accuracy of the structural response.

Basic concepts and procedures of the integrated thermal-structural finite element analysis are described. New thermal finite elements for improved thermal analysis accuracy are developed. Thermal finite elements which yield exact nodal and element temperatures for one-dimensional linear steady-state heat transfer problems are presented. These thermal finite elements are formulated based upon using closed-form solutions of the governing differential equations. For general heat transfer problems where closed-form solutions are not available,

159

improved thermal finite elements are developed by employing the nodeless variable formulation. The nodeless variable finite element uses extra unknowns as element variables to permit higher order element temperature interpolation functions. Detailed element temperature distributions are obtained without using additional element nodes while a common discretization with lower order congruent structural finite elements are maintained.

Nodeless variable finite elements are formulated for the following heat transfer cases: (1) one-dimensional linear transient analysis, (2) one-dimensional nonlinear transient analysis with radiation, and (3) two-dimensional linear transient analysis. General formulations of the nodeless variable finite elements for each heat transfer case are described in detail. For comparison, conventional finite elements customarily used in typical finite element programs are also presented. Results of temperatures obtained from the thermal analysis are transferred directly to the structural analysis to compute displacements and stresses.

To demonstrate the capabilities and efficiency of the integrated finite element approach, several examples in academic and more realistic problems are employed. The accuracy of the approach is evaluated by comparisons with analytical solutions and conventional thermal-structural analyses. Results indicate that the integrated finite element approach provides a significant improvement in the accuracy and efficiency of thermal-structural analysis and offers potential for applications to other coupled problems.

LIST OF REFERENCES

1. Turner, M. J., Clough, R. W., Martin, H. C., and Topp, L. J., "Stiffness and Deflection Analysis of Complex Structures," Journal of Aerospace Science, Vol. 23, July 1956, pp. 805-823.

2. Zienkiewicz, O. C. and Cheung, Y. K., "Finite Elements in the Solution of Field Problems," The Engineer, September 1965, pp. 507-510.

3. Wilson, E. L. and Nickell, R. E., "Application of the Finite Element Method to Heat Conduction Analysis," Nuclear Engineering Design, Vol. 4, October 1966, pp. 276-286.

4. Emergy, A. F. and Carson, W. W., "An Evaluation of the Use of the Finite Element Method in the Computation of Temperature," Journal of Heat Transfer, Vol. 93, May 1971, pp. 136-153.

5. Wilson, E. L., Bathe, K. J., and Peterson, F. E., "Finite Element Analysis of Linear and Nonlinear Heat Transfer," Nuclear Engineering and Design, Vol. 29, November 1974, pp. 110-124.

6. Bruch, J. C. Jr. and Zyvolosky, G., "Transient Two-Dimensional Heat Conduction Problems Solved by the Finite Element Method," International Journal for Numerical Methods in Engineering, Vol. 8, August 1974, pp. 481-494.

7. Tay, A. O. and Davis, G. De V., "Application of the Finite Element Method to Convection Heat Transfer Between Parallel Planes," International Journal of Heat and Mass Transfer, Vol. 14, August 1971, pp. 1057-1070.

8. Gallagher, R. H. and Mallett, R. H., "Efficient Solution Processes for Finite Element Analysis of Transient Heat Conduction," Journal of Heat Transfer, Vol. 93, August 1971, pp. 257-263.

9. Lee, H. P., "Application of Finite Element Method in the Computation of Temperature with Emphasis on Radiative Exchanges," AIAA Progress in Astronautics and Aeronautics, Thermal Control and Radiation, Vol. 31, Edited by Tien, C. L., The MIT Press, Cambridge, Mass., April 1973, pp. 497-520.

10. Beckett, R. E. and Chu, S. C., "Finite Element Method Applied to Heat Conduction with Nonlinear Boundary Conditions," Journal of Heat Transfer, Vol. 95, February 1973, pp. 126-129.

11. Lee, H. P. and Jackson, C. E. Jr., "Finite Element Solution for Radiative Conductive Analyses with Mixed Diffuse-Specular Surfaces," AIAA Progress in Astronautics and Aeronautics, Radiative Transfer and Thermal Control, Vol. 49, Edited by Smith, A. M., AIAA, New York, May 1976, pp. 25-46.

12. Thornton, E. A. and Wieting, A. R., "A Finite Element Thermal Analysis Procedure for Several Temperature-Dependent Parameters," Journal of Heat Transfer, Vol. 100, August 1978, pp. 551-553.

13. Wieting, A. R., "Application of Numerical Methods to Heat Transfer and Thermal Stress Analysis of Aerospace Vehicles," Numerical Methods in Thermal Problems, Proceedings of the First International Conference held at University College, Swansea, Wales, July 2-6, 1977, Pineridge Press, pp. 634-643.

14. Thornton, E. A. and Wieting, A. R., "Evaluation of Finite-Element Formulations of Transient Conduction Force-Convection Analysis," Numerical Heat Transfer, Vol. 3, March 1980, pp. 281-285.

15. Huebner, K. and Thornton, E. A., The Finite Element Method for Engineers, Second Edition, John Wiley, 1982.

16. Boley, B. A. and Weiner, J. H., Theory of Thermal Stresses, John Wiley, 1960.

17. Conner, J., "A Survey of Finite Element Method in Continuum Mechanics," Variational Methods in Engineering, Department of Civil Engineering, University of Southampton (Eds.), The Gresham Press, Old Working, Surrey, Vol. I, April 1973, pp. 4/1-4/32.

18. Desai, C. S. and Abel, J. F., Introduction to the Finite Element Method, Van Nostrand Reinhold, New York, 1972.

19. Thornton, E. A. and Murray, K. H., "Fundamentals of the Finite Element Method," Notes for a Short Course on Finite Element Analysis, School of Engineering, Old Dominion University, Norfolk, Virginia, July 1973.

20. Zienkiewicz, O. C., The Finite Element Method, Third Edition, McGraw-Hill, 1977.

21. Christie, I., Griffiths, D. F., Mitchell, A. R., and Zienkiewicz, O. C., "Finite Element Methods for Second Order Differential Equations with Significant First Derivatives," International Journal for Numerical Methods in Engineering, Vol. 10, November 1976, pp. 1389-1396.

22. Timoshenko, S. and Goodier, J. N., *Theory of Elasticity*, McGraw-Hill, 1951.

23. Thornton, E. A., "TAP2: A Finite Element Program for Thermal Analysis of Convectively Cooled Structures," NASA CR 159038, April 1980.

24. Bathe, K. J. and Wilson, E. L., *Numerical Methods in Finite Element Analysis*, Prentice-Hall, 1976.

25. Arpaci, V. S., *Conduction Heat Transfer*, Addison-Wesley, 1966, p. 173.

26. Adelman, H. M., Walsh, J. L., and Narayanaswami, R., "An Improved Method for Optimum Design of Mechanically and Thermally Loaded Structure," NASA TN D-7965, August 1975.

27. Carslaw, H. S. and Jaeger, J. C., *Conduction of Heat in Solids*, Second Edition, Oxford University Press, 1959.

28. Thornton, E. A., Dechaumphai, P., Wieting, A. R., and Tamma, K. K., "Integrated Transient Thermal-Structural Finite Element Analysis," Proceedings of the AIAA/ASME/ASCE/AHS 22nd Structures, Structural Dynamics and Materials Conference, Atlanta, Georgia, AIAA Paper No. 81-0480, April 6-8, 1981.

29. Mahaney, J., Thornton, E. A., and Dechaumphai, P., "Integrated Thermal-Structural Analysis of Large Space Structures," Computational Aspects of Heat Transfer in Structures Symposium Held at NASA Langley Research Center, Hampton, VA., November 3-6, 1981, NASA CP-2216, pp. 179-198.

30. Thornton, E. A., Mahaney, J., and Dechaumphai, P., "Finite Element Thermal-Structural Modeling of Orbiting Truss Structures," Third Annual Technical Review Large Space Systems Technology held at NASA Langley Research Center, Hampton, Va., November 17-20, 1981, NASA CP-2215, Part 1, pp. 93-108.

31. Marlowe, M. B., Moore, R. A., and Whetstone, W. D., *SPAR Thermal Analysis Processors Reference Manual*, System Level 16, NASA CR-159162, June 1979.

32. Bogen, R., *MACSYMA Reference Manual*, The Mathlab Group, Laboratory for Computer Science, Massachusetts Institute of Technology, Cambridge, Massachusetts, Version 9, December 1977.

33. Thornton, E. A., Dechaumphai, P., and Wieting, A. R., "Integrated Finite Element Thermal-Structural Analysis with Radiation Heat Transfer," Proceedings of the AIAA/ASME/ASCE/AHS 23rd Structures, Structural Dynamics and Materials Conference, New Orleans, Louisiana, AIAA Paper No. 82-0703, May 10-12, 1982.

34. Sander, G. and Beckers, P., "Improvements of Finite Element Solutions for Structural and Nonstructural Applications," Air Force Flight Dynamics Laboratory, Wright-Patterson Air Force Base, Ohio, Technical Report AFFDL-TR-72-94, December 1972.

35. Wilson, E. L., "The Static Condensation Algorithm," _International Journal for Numerical Methods in Engineering_, Vol. 8, No. 1, March 1974, pp. 198-203.

36. Dechaumphai, P. and Thornton, E. A., "Nodeless Variable Finite Elements for Improved Thermal-Structural Analysis," Proceedings of the International Conference of Finite Element Methods, Shanghai, China, August 2-6, 1982.

37. Adelman, H. M. and Catherines, D. S., "Calculation of Temperature Distributions in Thin Shells of Revolution by the Finite-Element Method," NASA TN D-6100, February 1971.

APPENDICES

APPENDIX A

FXACT FINITE ELEMENT INTERPOLATION FUNCTIONS

Exact element interpolation functions in the form of equation (3.14) for the thermal finite element Cases 1-8 (Figure 4 and Table 1, pp. 39 and 40) are presented. Nodeless parameters are shown in Table 2 (p. 41). The lower case letters in parentheses denote heat load cases defined in Table 1. General solutions to the differential equations for Cases 6 and 7 appear in reference [37].

Rod (Case 1)

$$N_1 = 1 - \frac{x}{L} \qquad N_2 = \frac{x}{L} \qquad (a,c,d)$$

$$N_0 = \frac{x}{L}(1 - \frac{x}{L})$$

$$N_1 = \frac{\sinh m(L-x)}{\sinh mL} \qquad N_2 = \frac{\sinh mx}{\sinh mx} \qquad (b)$$

$$N_0 = 1 - N_1 - N_2$$

where $m = \sqrt{hp/kA}$.

Slab (Case 2)

$$N_1 = 1 - \frac{x}{L} \qquad N_2 = \frac{x}{L} \qquad (a,c)$$

$$N_0 = \frac{x}{L}(1 - \frac{x}{L})$$

Hollow Cylinder (Case 3)

$$N_1 = \frac{1}{w} \ln\left(\frac{b}{r}\right) \qquad N_2 = \frac{1}{w} \ln\left(\frac{r}{a}\right) \qquad \text{(a,c)}$$

$$N_0 = \ln\left(\frac{r}{a}\right) + \frac{a^2}{b^2} \ln\left(\frac{b}{r}\right) - \frac{r^2}{b^2} w \qquad \text{(a,c)}$$

where $w = \ln\left(\frac{b}{a}\right)$.

Hollow Sphere (Case 4)

$$N_1 = \frac{a(b-r)}{r(b-a)} \qquad N_2 = \frac{b(r-a)}{r(b-a)} \qquad \text{(a,c)}$$

$$N_0 = \frac{1}{r}(r-a)(b-r)(r+a+b)$$

Cylindrical Shell (Case 5)

$$N_1 = 1 - \frac{s}{L} \qquad N_2 = \frac{s}{L} \qquad \text{(a,c,d)}$$

$$N_0 = \frac{s}{L}\left(1 - \frac{s}{L}\right)$$

$$N_1 = \frac{\sinh m(L-s)}{\sinh mL} \qquad N_2 = \frac{\sinh ms}{\sinh mL} \qquad \text{(b)}$$

$$N_0 = 1 - N_1 - N_2$$

where $m = \sqrt{h/kt}$.

Conical Shell (Case 6)

$$N_1 = \frac{1}{w}\ln(\tfrac{b}{s}) \qquad N_2 = \frac{1}{w}\ln(\tfrac{s}{a}) \qquad\qquad (a,c,d)$$

$$N_0 = \ln(\tfrac{2}{a}) + \frac{a^2}{b^2}\ln(\tfrac{b}{s}) - \frac{s^2}{b^2}w$$

$$\bar{N}_1 = \frac{I_0(ms)\,K_0(mb) - I_0(mb)\,K_0(ms)}{I_0(ma)\,K_0(mb) - I_0(mb)\,K_0(ma)} \qquad\qquad (b)$$

$$\bar{N}_2 = \frac{I_0(ma)\,K_0(ms) - I_0(ms)\,K_0(ma)}{I_0(ma)\,K_0(mb) - I_0(mb)\,K_0(ma)}$$

$$\bar{N}_0 = 1 - \bar{N}_1 - \bar{N}_2$$

where $w = \ln(\tfrac{b}{a})$, $m = \sqrt{h/kt}$; I_0 and K_0 are modified Bessel functions of the first and second kind of order zero, respectively.

Spherical Shell (Case 7)

$$N_1 = 1 - N_2 \qquad N_2 = \frac{\ln\frac{1+\sin(s/a)}{1-\sin(s/a)}}{\ln\frac{1+\sin(L/a)}{1-\sin(L/a)}} \qquad (a,c,d)$$

$$N_0 = \ln[\cos(s/a)] - N_2\,\ln[\cos(L/a)]$$

Flow Passage (Case 8)

$$N_1 = 1 - \frac{1 - e^{2\alpha x}}{1 - e^{2\alpha L}} \qquad N_2 = \frac{1 - e^{2\alpha x}}{1 - e^{2\alpha L}} \qquad (a,d)$$

$$N_0 = \frac{x}{L} - N_2$$

$$N_1 = e^{\alpha x} \frac{\sinh \beta(L-x)}{\sinh \beta L} \qquad N_2 = e^{\alpha(x-L)} \frac{\sinh \beta x}{\sinh \beta L} \qquad (b)$$

$$N_0 = 1 - N_1 - N_2$$

where $\alpha = \dot{m}c/2kA$, $\beta = \sqrt{\alpha^2 + m^2}$, and $n = \sqrt{hp/kA}$.

APPENDIX B

FINITE ELEMENT MATRICES FOR ONE-DIMENSIONAL
LINEAR STEADY-STATE PROBLEMS

Exact finite element matrices for the thermal and structural finite elements described in Chapter 3 are presented. Thermal conductance matrices and heat load vectors are given in the form of equation (3.27) for Cases 1-6 and equation (3.17) for Case 8 (Figure 4 and Table 1, pp. 39 and 40). These finite element matrices are derived using the exact element interpolation functions shown in Appendix A. Similarly, structural stiffness matrices and equivalent nodal forces due to thermal loads are derived using the element displacement interpolation functions shown in Tables 3 and 4 (pp. 61 and 67). The lower case letters in parentheses denote heat load cases defined in Table 1.

THERMAL FINITE ELEMENT MATRICES

Rod (Case 1)

Conductance Matrices:

$$\bar{K}_{11} = \bar{K}_{22} = kA/L \qquad\qquad (a,c,d)$$

$$\bar{K}_{12} = - kA/L$$

$$\bar{K}_{11} = \bar{K}_{22} = (hp \cosh mL)/(m \sinh mL) \qquad\qquad (b)$$

$$\bar{K}_{12} = - hp/(m \sinh mL)$$

Heat Load Vectors:

$$\bar{Q}_1 = \bar{Q}_2 = QAL/2 \qquad\qquad (c)$$

$$\bar{Q}_1 = \bar{Q}_2 = qpL/2 \qquad\qquad (d)$$

where $m = \sqrt{hp/kA}$.

Slab (Case 2)

Conductance Matrices:

$$\bar{K}_{11} = \bar{K}_{22} = k/L \qquad\qquad (a,c)$$

$$\bar{K}_{12} = - k/L$$

Heat Load Vector

$$\bar{Q}_1 = \bar{Q}_2 = QL/2 \qquad\qquad (c)$$

Hollow Cylinder (Case 3)

Conductance Matrices

$$\bar{K}_{11} = \bar{K}_{22} = k/w \qquad\qquad (a,c)$$

$$\bar{K}_{12} = - k/w$$

Heat Load Vector

$$\bar{Q}_1 = Q \left(- a^2/2 + (b^2 - a^2) / 4w \right) \qquad\qquad (c)$$

$$\bar{Q}_2 = Q \left(b^2/2 - (b^2 - a^2) / 4w \right)$$

where $w = \ln(b/a)$

Hollow Sphere (Case 4)

Conductance Matrices

$$\bar{K}_{11} = \bar{K}_{22} = kab/(b-a) \qquad\qquad (a,c)$$

$$\bar{K}_{12} = - kab/(b-a)$$

Heat Load Vector

$$\bar{Q}_1 = Qa(2a^3 + b^3 - 3a^2 b) / (6(b-a)) \qquad\qquad (c)$$

$$\bar{Q}_2 = Qb(a^3 + 2b^3 - 3ab^2) / (6(b-a))$$

Cylindrical Shell (Case 5)

Conductance Matrices

$$\bar{K}_{11} = \bar{K}_{22} = k/L \qquad\qquad\qquad (a,c,d)$$

$$\bar{K}_{12} = - k/L$$

$$\bar{K}_{11} = \bar{K}_{22} = (h \cosh mL) / (mt \sinh mL) \qquad (b)$$

$$\bar{K}_{12} = - h/(mt \sinh mL)$$

Heat Load Vectors

$$\bar{Q}_1 = \bar{Q}_2 = QL/2 \qquad\qquad\qquad (c)$$

$$\bar{Q}_1 = \bar{Q}_2 = qL/2t \qquad\qquad\qquad (d)$$

$$\bar{Q}_1 = \bar{Q}_2 = hT_\infty (\cosh mL - 1) / (mt \sinh mL) \qquad (b)$$

where $m = \sqrt{h/kt}$.

Conical Shell (Case 6)

Conductance Matrices

$$\bar{K}_{11} = \bar{K}_{22} = k/w \qquad\qquad\qquad (a,c,d)$$

$$\bar{K}_{12} = - k/w$$

Heat Load Vectors

$$\bar{Q}_1 = Q(-a^2/2 + (b^2-a^2)/4w) \qquad \text{(c)}$$

$$\bar{Q}_2 = Q(b^2/2 - (b^2-a^2)/4w)$$

$$\bar{Q}_1 = q(-a^2/2t + (b^2-a^2)/4wt) \qquad \text{(d)}$$

$$\bar{Q}_2 = a(b^2/2t - (b^2-a^2)/4wt)$$

where $w = \ln(b/a)$

Flow Passage (Case 8)

Conductance Matrices

$$K_{c_{11}} = K_{c_{22}} = ka\alpha(e^{2\alpha L} + 1)/(e^{2\alpha L} - 1) \qquad \text{(a,d)}$$

$$K_{c_{12}} = K_{c_{21}} = -K_{c_{11}}$$

$$K_{c_{11}} = kA((\beta H/2G) - (\alpha/2) - (\beta^2 E(E+F)/2\alpha G^2)) \qquad \text{(b)}$$

$$K_{c_{22}} = kA((\beta H/2G) + (\alpha/2) - (\beta^2 E(E-F)/2\alpha G^2))$$

$$K_{c_{12}} = K_{c_{21}} = kA(-(\beta^2 EH/2\alpha G^2) - (\beta F/2G))$$

$$K_{v_{11}} = K_{v_{12}} = -\dot{m}c/2 \qquad \text{(a,d)}$$

$$K_{v_{21}} = K_{v_{22}} = \dot{m}c/2$$

$$K_{v_{11}} = - K_{v_{22}} = - \dot{m}c/2 \tag{b}$$

$$K_{v_{12}} = - K_{v_{21}} = \beta E/\alpha G$$

$$K_{h_{11}} = hp((\beta H/G) + (\alpha) - (\beta^2 E(F+E)/\alpha G^2)) / 2(\beta^2 - \alpha^2) \tag{b}$$

$$K_{h_{22}} = hp((\beta H/G) - (\alpha) - (\beta^2 E(F-E)/\alpha G^2)) / 2(\beta^2 - \alpha^2)$$

$$K_{h_{12}} = K_{h_{21}} = hp((\beta^2 EF/\alpha G^2) - (\beta F/G)) / 2(\beta^2 - \alpha^2)$$

Heat Load Vectors

$$Q_1 = qp(1 - e^{2\alpha L} + 2\alpha L) / 2\alpha(1 - e^{2\alpha L}) \tag{d}$$

$$Q_2 = qp(-1 + e^{2\alpha L} - 2\alpha L\, e^{2\alpha L}) / 2\alpha(1 - e^{2\alpha L})$$

$$Q_1^{*} = hpT_{\infty}(\beta(H+E-F) - \alpha G) / G(\beta^2 - \alpha^2) \tag{b}$$

$$Q_2 = hpT_{\infty}(\beta(H-E-F) + \alpha G) / G(\beta^2 - \alpha^2)$$

where $\alpha = \dot{m}c/2kA$, $\beta = \sqrt{\alpha^2 + m^2}$, $m = \sqrt{hp/kA}$, $E = \sinh \alpha L$,
$F = \cosh \alpha L$, $G = \sinh \beta L$, $H = \cosh \beta L$.

STRUCTURAL FINITE ELEMENT MATRICES

Truss Element (Case 1)

Stiffness Matrices

$$K_{11} = K_{22} = AE/L \qquad\qquad (a,b,c,d)$$

$$K_{12} = K_{22} = -\ AE/L$$

Force Vectors

$$F_1 = -\ F_2 = -\ \alpha EA(T_0/6 + (T_1+T_2)/2) \qquad (a,c,d)$$

$$F_1 = -\ F_2 = -\ \alpha EA(C_1 T_0 + C_2(T_1+T_2)) \qquad (b)$$

where $C_1 = 1 - (2(\cosh mL - 1)/mL \sinh mL)$.

$$C_2 = (\cosh mL - 1)/mL \sinh mL$$

Axisymmetric Element (Case 3, Plane Stress)

Stiffness Matrices

$$K_{11} = E((b^2 + a^2) - \nu(b^2 - a^2))/(1 - \nu^2)(b^2 - a^2) \qquad (a,c)$$

$$K_{22} = E((b^2 - a^2) + \nu(b^2 - a^2))/(1 - \nu^2)(b^2 - a^2)$$

$$K_{12} = E(-2ab)/(1 - \nu^2)(b^2 - a^2)$$

Force Vectors

$$F_1 = - aE\alpha P/2w(1 - \nu)(b^2 - a^2) \qquad (a,c)$$

$$F_2 = bE\alpha P/2w(1 - \nu)(b^2 - a^2)$$

where $P = (-2a^2 w + b^2 - a^2)(T_1 + a^2 w T_0 / b^2)$

$$+ (2b^2 w - b^2 + a^2)(T_2 + w T_0)$$

$$- (b^4 - a^4) w^2 T_0 / b^2 - 2(b^2 - a^2) wT_{ref}$$

APPENDIX C

FINITE ELEMENT MATRICES FOR ONE-DIMENSIONAL
LINEAR TRANSIENT PROBLEMS

Finite element capacitance matrices for the thermal rod and
axisymmetric elements described in Chapter 4 are presented. The
conductance matrix coefficients K_{00}, and heat load vector
components Q_0 are presented; the coefficients K_{ij} and Q_i,
$i,j = 1,2$ appear in Appendix B, Cases 1 and 3. The lower case
letters in the parentheses denote heat load cases defined in Table 1.

Rod Element

Capacitance Matrices

$$C_{00} = \rho c A L/30 \qquad\qquad\qquad (a,c,d)$$

$$C_{01} = C_{02} = \rho c A L/12$$

$$C_{11} = C_{22} = \rho c A L/3$$

$$C_{12} = \rho c A L/6$$

$$C_{00} = \rho c A(((\cosh mL - 1)/\sinh mL)(L/\sinh mL - 3/m) + L) \qquad (b)$$

$$C_{01} = C_{02} = \rho c A((1 - \cosh mL)(mL - \sinh mL)/2m \sinh^2 mL)$$

$$C_{11} = C_{22} = \rho c A((\sinh mL \cosh mL - mL)/2m \sinh^2 mL)$$

$$C_{12} = \rho c A((mL \cosh mL - \sinh mL)/2m \sinh^2 mL)$$

Conductance Matrices

$$K_{00} = kA/3L \qquad\qquad\qquad (a,c,d)$$

$$K_{00} = (hp/m)(mL - 2(\cosh mL - 1)/\sinh mL) \qquad (b)$$

Heat Load Vectors

$$Q_0 = QAL/6 \qquad\qquad\qquad (c)$$

$$Q_0 = qpL/6 \qquad\qquad\qquad (d)$$

$$Q_0 = hpT_\infty (L - 2(\cosh mL - 1)/m \sinh mL) \tag{b}$$

where $m = \sqrt{hp/kA}$

Axisymmetric Element

Capacitance Matrices

$$C_{00} = \rho c(b^2-a^2)(4w^2(a^4 + a^2b^2 + b^4) + 9w(a^4-b^4) \tag{a,c}$$

$$+ 6(a^2-b^2)^2)/24b^4$$

$$C_{01} = -\rho c(4a^4w^2 + w(7a^2+3b^2)(a^2-b^2) + 4(a^2-b^2)^2)/16wb^2$$

$$C_{02} = \rho c(4b^4w^2 + w(7b^2+3a^2)(a^2-b^2) + 4(a^2-b^2)^2)/16wb^2$$

$$C_{11} = \rho c(b^2-a^2(1+2w+2w^2))/4w^2$$

$$C_{12} = \rho c(a^2-b^2 + w(a^2-b^2))/4w^2$$

$$C_{22} = \rho c(b^2(1-2w+2w^2) - a^2)/4w^2$$

Conductance Matrices

$$K_{00} = kw(w(1-(a/b)^4) - (1-(a/b)^2)^2) \tag{a,c}$$

Heat Load Vector

$$Q_0 = (Qb^2/4)(w(1-a^4/b^4) - (1-a^2/b^2)^2) \tag{c}$$

APPENDIX D

FINITE ELEMENT MATRICES FOR ONE-DIMENSIONAL NONLINEAR TRANSIENT ANALYSIS WITH RADIATION HEAT TRANSFER

Jacobian matrices and residual heat load vectors for the conventional finite element and the nodeless variable finite element described in Chapter 5 are presented. These element matrices which appear in Eq. (5.34) are given in the form of computer subroutines. The subroutines are written in FORTRAN IV where the definitions of variables used are provided.

```
C    * * * * * * * * * * * * * * * * * * * * * * * * * * * * * * * * *
C
C            VARIABLES USED IN THE FOLLOWING SUBROUTINES ARE DEFINED
C
C    AS FOLLOWS:
C
C    TK          MATERIAL THERMAL CONDUCTIVITY
C    RHO         DENSITY
C    CP          SPECIFIC HEAT
C    AREA        ROD CROSS-SECTIONAL AREA
C    XL          ELEMENT LENGTH
C    PS          CROSS-SECTIONAL PERIMETER FOR EMITTED ENERGY
C    PQ          CROSS-SECTIONAL PERIMETER FOR INCIDENT ENERGY
C    EMIS        SURFACE EMISSIVITY
C    ABSORP      SURFACE ABSORPTIVITY
C    STEFAN      STEFAN-BOLTZMANN CONSTANT
C    QDOT        INCIDENT HEATING RATE PER UNIT AREA
C    TM( )       ELEMENT NODAL TEMPERATURES AT THE M ITERATION
C    TN( )       ELEMENT NODAL TEMPERATURES AT THE N TIME STEP
C    DELTA       TIME INCREMENT USED IN CRANK-NICOLSON ALGORITHM
C    ICONS       .EQ.1  CONSISTENT FORMULATION
C                .NE.1  LUMPED    FORMULATION
C
C
C    ALL JACOBIAN MATRICES ARE REPRESENTED BY VARIABLES BEGIN WITH
C    AJ__(_,_)  E.G.  AJRAD REPRESENTS JACOBIAN MATRIX CONTRIBUTED
C    FROM CONDUCTANCE RADIATION MATRIX.
C
C    ALL RESIDUAL LOAD VECTORS ARE REPRESENTED BY VARIABLES BEGIN
C    WITH R___(_)  E.G.  RRAD REPRESENTS RESIDUAL HEAT LOAD VECTOR
C    FROM CONDUCTANCE RADIATION MATRIX.
C
```

```
C ****************************************************************
C
      SUBROUTINE JRCOND(TK,AREA,XL,TH,AJCOND,RCOND)
C
C     SET UP JACOBIAN CONDUCTION MATRIX AND CONDUCTION
C     RESIDUAL LOAD VECTOR FOR CONVENTIONAL ROD ELEMENT
C
      DIMENSION AJCOND(2,2),RCOND(2),TH(2)
C
      XX = TK*AREA/XL
      AJCOND(1,1) = XX
      AJCOND(1,2) = -XX
      AJCOND(2,1) = -XX
      AJCOND(2,2) = XX
C
      RCOND(1) = -XX*(TH(1)-TH(2))
      RCOND(2) = - RCOND(1)
C
      RETURN
      END
C ****************************************************************
C
      SUBROUTINE JRRAD(EMIS,STEFAN,PS,XL,TH,ICONS,AJRAD,RRAD)
C
C     SET UP RADIATION JACOBIAN MATRIX AND RADIATION RESIDUAL
C     LOAD VECTOR FOR CONVENTIONAL ROD ELEMENT
C
      DIMENSION AJRAD(2,2),RRAD(2),TH(2)
C
      IF(ICONS.NE.1) GO TO 10
      XX = EMIS*STEFAN*PS*XL/15.
      T1 = TM(1)
```

```
      T2 = TH(2)
      T1S = T1*T1
      T2S = T2*T2
      T1C = T1S*T1
      T2C = T2S*T2
C
      T1ST2 = T1S*T2
      T1T2S = T1*T2S
      AJRAD(1,1) = XX*(10.*T1C + 6.*T1ST2 + 3.*T1T2S +     T2C)
      AJRAD(1,2) = XX*( 2.*T1C + 3.*T1ST2 + 3.*T1T2S +  2.*T2C)
      AJRAD(2,1) = AJRAD(1,2)
      AJRAD(2,2) = XX*(    T1C + 3.*T1ST2 + 6.*T1T2S + 10.*T2C)
C
      T1F = T1C*T1
      T2F = T2C*T2
C
      T1CT2 = T1C*T2
      T1ST2S= T1S*T2S
      T1T2C = T1*T2C
      YY = -XX/2.
      RRAD(1) = YY*(5.*T1F + 4.*T1CT2 + 3.*T1ST2S + 2.*T1T2C +    T2F)
      RRAD(2) = YY*(    T1F + 2.*T1CT2 + 3.*T1ST2S + 4.*T1T2C + 5.*T2F)
C
      RETURN
C
   10 CONTINUE
      XX = 2.*EMIS*STEFAN*PS*XL
      AJRAD(1,1) = XX*(TH(1)**3.)
      AJRAD(1,2) = 0.
      AJRAD(2,1) = 0.
      AJRAD(2,2) = XX*(TH(2)**3.)
C
      YY = -XX/4.
      RRAD(1) = YY*(TH(1)**4.)
      RRAD(2) = YY*(TH(2)**4.)
C
```

```
      RETURN
      END
C
C ************************************************
C
      SUBROUTINE RQDOT(QDOT,ABSORP,PQ,XL,RQ)
C
C     SET UP INCIDENT RESIDUAL LOAD VECTOR FOR
C     CONVENTIONAL ROD ELEMENT
C
      DIMENSION  RQ(2)
C
      XX = QDOT*ABSORP*PQ*XL/2.
      RQ(1) = XX
      RQ(2) = XX
C
      RETURN
      END
C
C ************************************************
C
      SUBROUTINE JRCAP(RHO,CP,AREA,XL,DELTA,TH,TN,ICONS,AJCAP,RCAP)
C
C     SET UP CAPACITANCE JACOBIAN MATRIX AND CAPACITANCE RESIDUAL
C     LOAD VECTOR FOR CONVENTIONAL ROD ELEMENT
C
      DIMENSION AJCAP(2,2),RCAP(2),TH(2),TN(2)
C
      IF(ICONS.NE.1)  GO TO 10
      XX = RHO*CP*AREA*XL/(3.*DELTA)
      AJCAP(1,1) = 2.*XX
      AJCAP(1,2) =   XX
```

```
C
      AJCAP(2,1) = AJCAP(1,2)
      AJCAP(2,2) = AJCAP(1,1)
C
      RCAP(1) = XX*(2.*TN(1) - 2.*TH(1)) +     TN(2) -    TH(2))
      RCAP(2) = XX*(    TN(1) -    TH(1)) + 2.*TN(2) - 2.*TH(2))
C
      RETURN
C
   10 CONTINUE
      YY = RHO*CP*AREA*XL/DELTA
      AJCAP(1,1) = YY
      AJCAP(1,2) = 0.
      AJCAP(2,1) = 0.
      AJCAP(2,2) = YY
C
      RCAP(1) = YY*(TN(1)-TH(1))
      RCAP(2) = YY*(TN(2)-TH(2))
C
      RETURN
      END
C
C****************************************
C
C
      SUBROUTINE IJRCOND(TK,AREA,XL,TH,AJCOND,RCOND)
C
C   SET UP JACOBIAN CONDUCTION MATRIX AND CONDUCTION
C   RESIDUAL LOAD VECTOR FOR NODELESS VARIABLE ROD ELEMENT
C
      DIMENSION AJCOND(3,3),RCOND(3),TH(3)
C
      XX = TK*AREA/XL
      AJCOND(1,1) =  XX
      AJCOND(1,2) = -XX
      AJCOND(1,3) = 0.
```

```
      AJCOND(2,1) = -XX
      AJCOND(2,2) = XX
      AJCOND(2,3) = 0.
      AJCOND(3,1) = 0.
      AJCOND(3,2) = 0.
      AJCOND(3,3) = XX/3.

      RCOND(1) = -XX*(TM(1)-TM(2))
      RCOND(2) = -RCOND(1)
      RCOND(3) = -XX*TM(3)/3.

      RETURN
      END.

C
C
C     *************************************************************
C
C
      SUBROUTINE IJRRAD(EMIS,STEFAN,PS,XL,TM,AJRAD,RRAD)
C
C     SET UP RADIATION JACOBIAN MATRIX AND RADIATION RESIDUAL
C     LOAD VECTOR FOR NODELESS VARIABLE ROD ELEMENT
C
      DIMENSION AJRAD(3,3),RRAD(3),TM(3)
C
      XX = EMIS*STEFAN*PS*XL/630.
      T1 = TM(1)
      T2 = TM(2)
      TO = TM(3)
      T1S = T1*T1
      T2S = T2*T2
      TOS = TO*TO
      T1C = T1S*T1
      T2C = T2S*T2
      TOC = TOS*TO
C
```

```
      TOT1 = TO*T1
      TOT1S = TO*T1S
      TOST1 = TOS*T1
      AJRAD(1,1) = XX*(42.*T2C + (126.*T1 + 54.*TO)*T2S
     1           + (252.*T1S + 144.*TOT1 + 27.*TOS)*T2
     1           + 420.*T1C + 180.*TOT1S + 45.*TOST1
     1           + 5.*TOC                                 )

      AJRAD(1,2) = XX*(84.*T2C + (126.*T1 + 72.*TO)*T2S
     1           + (126.*T1S + 108.*TOT1 + 27.*TOS)*T2
     1           + 84.*T1C + 72.*TOT1S + 27.*TOST1
     1           + 4.*TOC                                 )

      AJRAD(1,3) = XX*(24.*T2C + (54.*T1 + 27.*TO)*T2S
     1           + (72.*T1S + 54.*TOT1 + 12.*TOS)*T2
     1           + 60.*T1C + 45.*TOT1S + 15.*TOST1
     1           + 2.*TOC                                 )

      AJRAD(2,1) = AJRAD(1,2)
      AJRAD(2,2) = XX*(420.*T2C + (252.*T1 + 180.*TO)*T2S
     1           + (126.*T1S + 144.*TOT1 + 45.*TOS)*T2
     1           + 42.*T1C + 54.*TOT1S + 27.*TOST1
     1           + 5.*TOC                                 )

      AJRAD(2,3) = XX*(60.*T2C + (72.*T1 + 45.*TO)*T2S
     1           + (54.*T1S + 54.*TOT1 + 15.*TOS)*T2
     1           + 24.*T1C + 27.*TOT1S + 12.*TOST1
     1           + 2.*TOC                                 )

      AJRAD(3,1) = AJRAD(1,3)
      AJRAD(3,2) = AJRAD(2,3)
      AJRAD(3,3) = XX*(15.*T2C + (27.*T1 + 15.*TO)*T2S
     1           + (27.*T1S + 24.*TOT1 + 6.*TOS)*T2
     1           + 15.*T1C + 15.*TOT1S + 6.*TOST1
     1           + 10.*TOC/11.

      T1F = T1C*T1
      T2F = T2C*T2
      TOF = TOC*TO
      TOT1C = TO*T1C
      TOST1S = TOS*T1S

C
```

```
      TOCT1 = TOC*T1
C
      YY = -XX/2.
      RRAD(1) = YY*(42.*T2F + (84.*T1 + 48.*TO)*T2C
     1 + (126.*TIS + 108.*TOT1 + 27.*TOS)*T2S
     1 + (168.*TIC + 144.*TOT1S + 54.*TOST1 + 8.*TOC)*T2
     1 + 210.*T1F + 120.*TOT1C + 45.*TOST1S + 10.*TOCT1 + TOF )
      RRAD(2) = YY*(210.*T2F + (168.*T1 + 120.*TO)*T2C
     1 + (126.*TIS + 144.*TOT1 + 45.*TOS)*T2S
     1 + (84.*TIC + 108.*TOT1S + 54.*TOST1 + 10.*TOC)*T2
     1 + 42.*T1F + 48.*TOT1C + 27.*TOST1S + 8.*TOCT1 + TOF  )
      RRAD(3) = YY*(30.*T2F + (36.*T1 + 30.*TO)*T2C
     1 + (54.*TIS + 54.*TOT1 + 15.*TOS)*T2S
     1 + (48.*TIC + 54.*TOT1S + 24.*TOST1 + 4.*TOC)*T2
     1 + 30.*T1F + 30.*TOT1C + 15.*TOST1S + 4.*TOCT1 + 5.*TOF/11.)
C
      RETURN
      END
C
C
C
C
C ************************************************************
C
      SUBROUTINE IRQDOT(QDOT,ABSORP,PQ,XL,RQ)
C
C     SET UP INCIDENT RESIDUAL LOAD VECTOR FOR
C     NODELESS VARIABLE ROD ELEMENT
C
      DIMENSION RQ(3)
C
      XX = QDOT*ABSORP*PQ*XL
      RQ(1) = XX/2.
      RQ(2) = RQ(1)
      RQ(3) = XX/6.
C
      RETURN
```

```
      END

C
C     ************************************************************
C
      SUBROUTINE IJRCAP(RHO,CP,AREA,XL,DELTA,TH,TN,AJCAP,RCAP)
C
C     SET UP CAPACITANCE JACOBIAN MATRIX AND CAPACITANCE RESIDUAL
C     LOAD VECTOR FOR NODELESS VARIABLE ROD ELEMENT
C
      DIMENSION  AJCAP(3,3),RCAP(3),TH(3),TN(3)
C
      XX = 2.*RHO*CP*AREA*XL/DELTA
      AJCAP(1,1) = XX/3.
      AJCAP(1,2) = XX/6.
      AJCAP(1,3) = XX/12.
      AJCAP(2,1) = AJCAP(1,2)
      AJCAP(2,2) = AJCAP(1,1)
      AJCAP(2,3) = AJCAP(1,3)
      AJCAP(3,1) = AJCAP(1,3)
      AJCAP(3,2) = AJCAP(2,3)
      AJCAP(3,3) = XX/30.
C
      DT0 = TN(3)-TH(3)
      DT1 = TN(1)-TH(1)
      DT2 = TN(2)-TH(2)
      RCAP(1) = XX*(DT0/12. + DT1/3.  + DT2/6.  )
      RCAP(2) = XX*(DT0/12. + DT1/6.  + DT2/3.  )
      RCAP(3) = XX*(DT0/30. + DT1/12. + DT2/12.)
C
      RETURN
      END
C
C     ************************************************************
```